Development of Defined Biological Models for Complex Radiation-Induced DNA Lesions Using Homing Endonucleases and Transposon Technology: Feasibility and Initial Characterization

Inaugural-Dissertation

zur

Erlangung des Doktorgrades

Dr. rer. nat.

der Fakultät

Biologie und Geografie

an der

Universität Duisburg-Essen

Standort Essen, Germany

vorgelegt von

Janapriya Saha

aus

Bhopal, Madhya Pradesh, Indien

September 2010

Die der vorliegenden Arbeit zugrunde liegenden Experimente wurden am Institut für Medizinische Strahlenbiologie an der Universität Duisburg-Essen, Standort Essen, durchgeführt.

1. Gutachter: **Prof. Dr. George Iliakis**

2. Gutachter: **Prof. Dr. Süleyman Ergün**

Vorsitzender des Prüfungsausschusses: **Prof. Dr. Ann Ehrenhofer-Murray**

Tag der mündlichen Prüfung: **January 11, 2011**

There are seven sins in the world: Wealth without work; pleasure without conscience; knowledge without character; commerce without morality; science without humanity; worship without sacrifice; politics without principle.

~Mahatma Gandhi

If you shut the door to all errors, truth will be shut out.

~ Rabindranath Tagore

Dedicated to

My Dearest Parents

Table of Contents

Abbreviation

°C	Degree Celsius
%	percent
Approx.	Approximately
γ-H2AX	Phosphorylated form of Histone H2AX at Ser-139
53BP1	p53 binding protein
µm	Micrometer
Ab	Antibody
ATM	Ataxia-telangiectasia-mutated
ATR	Ataxia-telangiectasia and rad3 related
B-NHEJ	Backup pathway of nonhomologous end-joining
bp	Base pair
BRCA1	Breast cancer susceptibility protein 1
BRCA2	Breast cancer susceptibility protein 2
BRCT	Breast cancer C-terminal
BSA	Bovine Serum Albumin
CE	Cytoplasmic extract
CSR	Class switch recombination
CtIP	C-terminal binding protein interacting protein
DDR	DNA damage response
D-MEM	Dulbecco's Modified Eagle's Medium
DNA	Deoxyribonucleic acid
DNA-PK	DNA dependent protein kinase
DNA-PKcs	Catalytic subunit of the protein DNA-PK
D-NHEJ	DNA-PK dependent nonhomologous end-joining
dd	Double distilled
ds	Double stranded
DSB	DNA double strand break
ECL	Enhanced Chemiluminescence
EDTA	Ethylene Diamine Tetraacetic Acid
e.g.	exempli gratia

et al.	et alii (and others)
EtBr	Ethidium Bromide
eV	Electron Volt
FACS	Fluorescence activated cell sorting
FBS	Fetal bovine serum
FITC	Fluorescein isothiocyanate
G1	Cell cycle phase Gap 1
G2	Cell cycle phase Gap 2
EGFP	Enhanced green fluorescent protein
FHA	Fork head-associated
FPLC	Fast Protein Liquid Chromatography
Gy	Gray
h	Hour
HEPES	4-(2-hydroxyl)-1-Piperazineethanesulfonic Acid
HDR	Homology directed repair
HRR	Homologous recombination repair
H3pS10	Histone H3 phosphorylated at serine 10
HST	Histogram
ICLs	Interstrand crosslinks
IR	Ionizing radiation
k	Kilo
kDa	Kilodalton
keV	Kilo electron volt
KV	Kilo Volt
LET	Linear Energy Transfer
Lig4	Ligase4
LIF	Leica image format
LSB	Low salt buffer
LMDS	Locally multiplied damage sites
MEF	Mouse embryo fibroblast
MEM	Minimal Essential Medium
Min	Minute
mAb	Monoclonal antibody

MI	Mitotic index
mm	Millimeter
M-phase	Cell cycle phase Mitosis
MPF	Mitosis promoting factor
MMEJ	Microhomology-mediated end-joining
MRN complex	Mre11-Rad50-Nbs1 complex
MQ	Milli-Q
MW	Molecular weight
NBS	Nijmegen Breakage Syndrome
NE	Nuclear extract
ng	Nanogram
nm	Nanometer
NLS	Nuclear localization signal
pAb	Polyclonal antibody
PAGE	Polyacrylamide Gel Electrophoresis
PARP-1	Poly (ADP-ribose) polymerase 1
PBS	Phosphate buffer saline
PBST	PBS with Tween 20
PCV	Packed column volume
PCC	Premature chromosome condensation
PFGE	Pulsed field gel electrophoresis
PI	Propidium iodide
PIKK	Phosphoinositide-3-kinase-related protein kinase
PMSF	Phenylmethylsulfonylfluoride
PMT	Photomultipliers
RMDS	Regionally Multiply Damaged Sites
ROS	Reactive Oxygen Species
RNAase	Ribonuclease
RPA	Replication protein factor A
RPM	Revolution per minute
RT	Room temperature
SB	Sleeping Beauty
SDS	Sodium Dodecyl Sulfate

Sec	Seconds
ss	Single stranded
SSA	Single strand annealing
Ser	Serine
S-Phase	Cell cycle Synthesis phase
SSB	Single strand breaks
TEMED	N’ N’ N’ N’-Tetramethylethylenediamine
Tris	Tris-(hydroxymethyl)-aminomethane
Thr	Threonine
Tyr	Tyrosine
UV	Ultraviolet light
V(D)J	Variable (diversity) joining
Wt	Wild type
WCE	Whole Cell extract
XRCC	X-ray cross complementation group

Abstract

Sparsely ionizing radiation (IR) deposits energy in spurs and blobs where multiple ionizations occur in a small volume. If generated close to DNA, such events induce multiple lesions within few base pairs (complex lesions) and damage both base and sugar moieties. These energy deposition events are closely confined to the paths of the constituent ionizing particles. The distances between subsequent ionization events vary randomly along the particle path, and decrease as the particle slows down and comes to a halt. Thus, at all ends of electron tracks, where X-ray energy is mainly deposited, excessive local accumulation of ionizations will generate complex DNA damage that is thought to be primarily responsible for the observed adverse cellular effects.

The DNA double strand break (DSB) is the simplest form of a complex lesion, generated when two ionizations, or radiation-induced radicals, in close proximity disrupt the sugar phosphate backbone of the two DNA strands. Further complexity, and thus also increased risk for biological consequences, is generated when additional lesions occur near the DSB. Such complex damage is presently intensively studied and is implicated in the biological effects of high LET radiation. Another dimension of complexity and a particularly high risk for biological consequences is generated when two (or more) DSBs are induced in close proximity, as they may completely destabilize chromatin and may cause DNA losses that cannot be dealt by available DNA repair pathways. Although this form of complex DNA lesion has been considered in the past, mechanistic studies able to analyze its biological consequences are lacking.

In vitro manipulation of the plasmid DNA allows the generation of DSBs with different but well-defined ends, usually generated by treatment with appropriate combinations of restriction endonucleases. While these assays recapitulate important aspects of D-NHEJ, several reports show that they fail to reproduce the marked reduction in DNA end joining efficiency of genomic DSBs observed in a variety of D-NHEJ mutants, suggesting that they mainly reflect the function of B-NHEJ. In preparation for the above mentioned studies on complex lesions we also examined the effect of the transfection method on repair pathways selection. We discovered that while electroporation generates plasmid end joining results in the different mutants closely reflecting rejoining of genomic DSBs, plasmid lipofection-generated results showing a nearly wild type plasmid end joining

efficiency in D-NHEJ mutants. We show that the subcellular localization of the transfected plasmid underlies these differences.

With this information at hand, we began studies to test the hypothesis that clustering of DSBs at distances affecting nucleosomal or local chromatin stability is highly lethal for the cell. Rather than mathematically modeling energy deposition and the general features of clustered damage induction and fitting the model to the biological effects measured, here we model the biological lesion in a highly specific way by narrowing down on the candidate lesion and testing for key biological consequences. This approach has the advantage that it allows the characterization of the general properties of radiation lesions causing mutations and cell lethality.

We describe model systems in which DSB clusters are induced in the genome of human tumor A549 cells through enzymatic restriction of I-*Sce*I sites integrated at different combinations and at multiple sites using transposon technology. To address complexity, we generated transposon-based constructs harboring a single and two I-*Sce*I sites in compatible and incompatible orientations separated by 200bp. The vector used also contains the neo^R gene as a selectable marker. The integration of the plasmid at multiple sites is facilitated by co-expression of a hyperactive transposase artificially reactivated from the “Sleeping Beauty” transposon. The number of integration sites is measured in randomly selected G418 resistant clones using Southern blotting and sets are generated with clones harboring 3-12 integration sites for each DSB arrangement.

Using these sets of clones, cell survival by colony formation, as well as chromosomal aberration formation along with other techniques like mitotic index/G2-checkpoint activation, and induction of EGFP-53BP1 foci are studied. The results obtained as part of this thesis show a correlation between lesion complexity and cell killing. Evidence for checkpoint activation and chromosome aberration formation is also obtained, but analysis of these endpoints is hampered by the apoptotic response of the generated system. More work will be necessary to define and improve the potential of this model system for radiation damage.

Key words: **Ionizing radiation, Transposon, Complex lesion, LET, Nucleofection, Lipofection, Chromatin, D-NHEJ and B-NHEJ**.

1 Introduction

1.1. DNA double strand break repair pathways

The DNA double strand break is the single most lethal lesion known for a proliferating cell and also a major cause of mutagenesis leading to a carcinogenic outcome [1]. DSBs are known to be the most biological dangerous lesions induced by ionizing radiation like x- and γ rays (IR) [2]. DNA DSBs can also be induced by radiomimetic chemical agents like bleomycin [3], neocarzinostatin [4], and calicheamycin [5], among others. DSBs are also created as secondary lesions by chemicals like methyl methane sulphonate (MMS)[6], which modifies DNA structure by methylating its bases and thus forms DSB upon replication fork collapse. DSBs are also induced indirectly by topoisomerase I inhibitors like camptothecin [7]. Topoisomerase II inhibitors like etoposide induce DSBs both directly and through the formation of stabilized cleavage complex (SCC) [8, 9].

Double strand breaks are an unavoidable evil for the cells, as they are inadvertently generated during replication, and are required during meiosis [10] and V(D)J recombination. Yet, they are also a major cause of viability loss. V(D)J recombination [11, 12] is utilized in developing B and T lymphocytes in the vertebrate immune system to generate antigen diversity by randomly recombining of a large pool of germline V, D, and J gene segments. Accidental introduction of a DSB takes place in a cell when a SSB encounters an active replication fork during the S-phase of the cell cycle or as a consequence of abortive function of Topoisomerases I and II [13].

The double strand breaks created by ionizing radiation pose a paramount risk and challenge for the cell. Each Gy of radiation is conservatively estimated to induce at least 30-60 DSBs, approx. 1500 single strand breaks and 4500 base or other damages[14]. The single strand break repair pathway is well characterized in mammalian cells and also in lower eukaryotes and prokaryotes. Mammalian cells utilize two major pathways for repairing DSBs, namely the DNA-PK-dependent non homologous end joining and Homologous recombination [15, 16] see Figure 1, although the presence of other pathways like single strand annealing [17] and Backup-NHEJ [18-20] are also known. HRR utilizes the products of genes of the Rad52 epistasis group and restores the DNA

sequence around the break with the help of a homologous sequence predominantly found in the sister chromatid but occasionally also in the homologous chromosome. It is the predominant DSB repair mechanism in yeast. In higher eukaryotes, HRR appears restricted to the G2 and S-phase of the cell cycle where it utilizes the sister chromatid, but its relative contribution to the repair of accidental DSBs remains uncharacterized.

NHEJ appears to be the dominant DSB repair pathway in higher eukaryotes. During NHEJ, the two DNA ends are enzymatically captured and rejoined after end processing that enables ligation. End processing causes nucleotide gains or losses that can at times be extensive. As a result, NHEJ restores DNA integrity without achieving the restoration of DNA sequence. It should therefore be regarded as a repair pathway with a restricted task. The classical form of NHEJ comprises DNA-PKCS, Ku70, Ku80, XRCC4, DNA Ligase4, and XLF/Cernunnos; it will be referred to here as D-NHEJ, to indicate its dependence on DNA-PK. Recent work indicates the function of an alternative pathway of NHEJ that operates as a backup (B-NHEJ) whenever D-NHEJ is compromised – chemically or genetically. B-NHEJ utilizes PARP-1, XRCC1, and DNA Ligase III and may benefit from additional DNA repair and signaling factors such as NBS1 and CtIP [21-23].

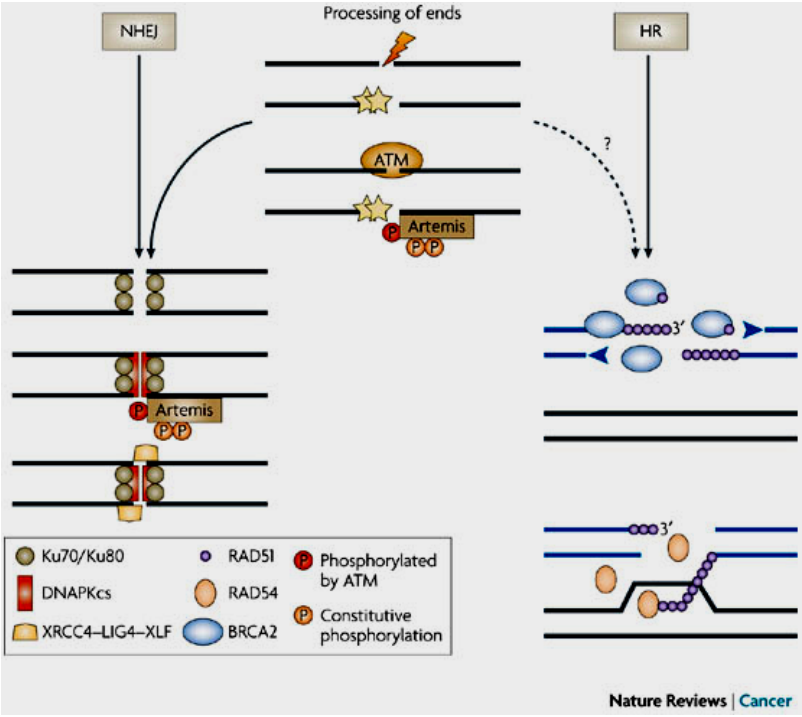

Fig. 1: Schematic representations of NHEJ and HRR mechanisms [24].

1.1.1 DNA damage response (DDR)

The utilization of ionizing radiation in medical diagnostics and therapy makes it imperative to study and characterize the pathways of DNA DSB repair to have an in depth understanding of how a cell recognizes, responds and ultimately eliminates these lesions, also called as DNA damage response or DDR, Figure 2.

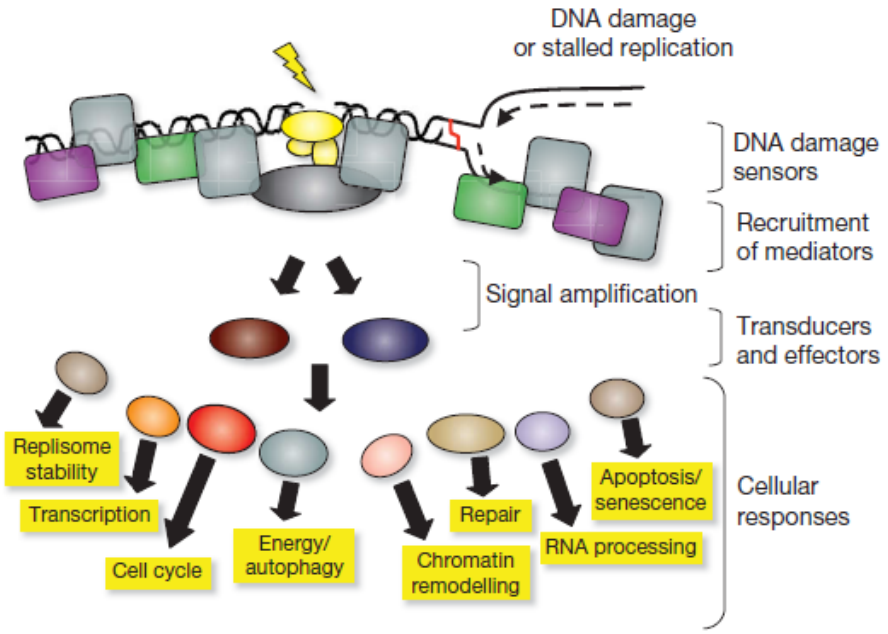

Fig. 2: Model for DDR. The presence of a lesion in the DNA, which can lead to replication stalling, is recognized by various sensor proteins. These sensors initiate signaling pathways that have an impact on a wide variety of cellular processes [13].

To prevent these cytotoxic lesions from progressing to chromosomal breaks and genomic instability, cells have devised efficient and cooperative DNA break repair pathways, which are known to have (and also being actively investigated) for overlapping functions. These repair proteins can be classified into sensors, like the Mre11, Rad50, NBS1 complex [25-31] and Ku70/80 dimer [32, 33], signal amplifiers like γ-H2AX [34-36], 53BP1 [37-39] and ATM/ATR [27, 40], and actual effectors of ligation of the ends like the *Lig4*/XRCC4/XLF [41-46] and Ligase III/XRCC1 [19, 20, 47] complexes.

1.1.2 Induction of DNA damage by ionizing radiation

The character of a DSB created by IR is one of the hotly pursued areas of radiation biology and DNA repair. Initial knowledge on DNA behavior upon irradiation came from studies of radiolytic reactions of DNA either in dry state (by electron-spin-resonance spectroscopy/ESR), or irradiated aqueous solutions of biomolecules in vitro to understand their effects in vivo. Induction of DSBs by IR takes place primarily by two mechanisms. First, by direct ionization in both DNA strands can induce DSBs. Second, hydroxyl radicals formed from the interaction of IR with water molecules can induce DSBs indirectly if the attack both DNA strands, Figure 3. Sparsely ionizing radiations like the x- and γ-rays cause more indirect damage to the DNA, in contrast to high LET radiations, which primarily damage DNA directly [48-51], Figure 4A and B.

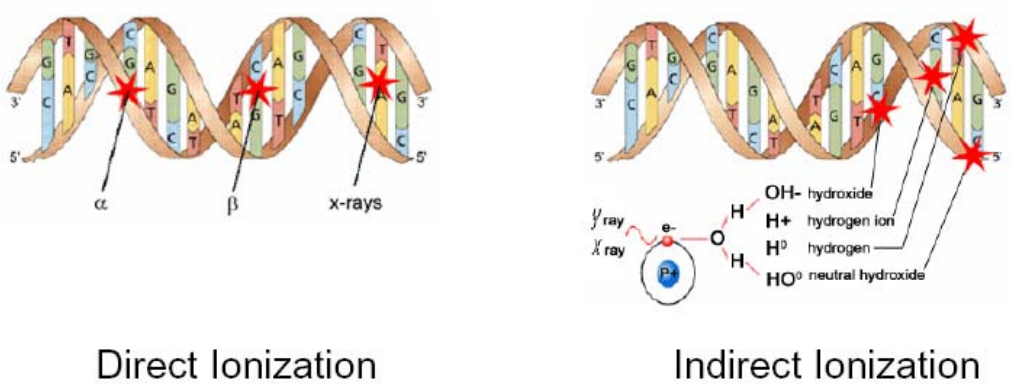

Fig. 3: Schematic representation of direct and indirect action of IR. Illustration courtesy: Canadian Nuclear Association website.

Other than DNA double and single strand breaks, ionizing radiation also induces a vast array of lesions, like the alkali labile lesions [52] (ALL; this damage on DNA bases and sugars rises linearly with dose and is sensitive to alkylating agents leading to a DSB), heat labile sites (sensitive to heat and may get converted to a DSB) [53, 54], base lesions (oxybases; oxypurines and oxypyrimidines, like FaPy Adenine, FaPy Guanine, C8-oxoGuanine, C8-oxoAdenine are examples of oxypurines; Thymine residues damaged by ring saturation, fragmentation, or ring contraction including thymine glycol and uracil residues are examples of oxypyrimidines) [55, 56] and regular and oxidized AP sites (apurinic and apyrimidinic sites with abasic sites modified with alkoxyamines and DNA containing urea residues) [57, 58], single interruptions on the sugar-phosphate

backbone, fragile sites on DNA, S1-sites and DNA-protein cross-links (formed due to the close association and interaction of DNA and proteins (histones) in chromatin, preferentially under hypoxic conditions). Comparison of radiosensitivities of bases of irradiated DNA has shown increasing radiosensitivities from Guanine (G) to Adenine (A) to Cytosine (C) and then to Thymine (T), which is in agreement with the formation and prevalence of best known radiation products thymine glycol and thymine hydroxyhydroperoxide on the C5-C6-double bond upon irradiation, which are the oxidation products of thymine [59].

Chemical alteration due to direct ionization of the molecules and free radical attack leads to degradation of biomolecules and induction of cross-linking, inter-cross-linking of the DNAs, proteins, lipids etc. All these forms of damage alter the structural conformation of the biomolecules, resulting in genetic and cell structure alterations and lead to metabolic changes in the cell. These alterations can ultimately cause mutation, transformation and cell death. The mechanisms leading to the observable cellular effects are complex, but there is evidence that they are mediated by the formation of chromosomal aberrations.

1.1.3 Introduction to LET in relation to DNA damage

Linear Energy Transfer (LET) is defined as the energy, which an ionizing particle deposits per unit distance as it traverses matter. It is the quotient dE/dl, where dE is the average energy locally imparted to the medium by a charged particle of specified energy in traversing a distance of dl.

$$L.E.T = dE/dl$$

LET is used to quantify the effects of ionizing radiation on biological specimens or electronic devices. Medical X-rays are low LET radiation, while, alpha particles and other heavier nuclei have a much higher LET. LET varies enormously depending on the speed and charge of the particle involved. The biological effects of high LET radiations are in general much higher than those of low LET radiations at the same dose [60, 61]. This is because high LET radiation can deposit most of its energy within a small volume and to produce in this way highly accumulated damage, see Figures 4A and B [62]. Each particle has a unique track structure and the distances between ionizations vary randomly on a track but decreases on the average as particles lose energy along their paths [63] [50, 64-67]. Electrons display large increases in the density of ionizations at the ends of their tracks. It has also been proposed that a break created by high LET radiation remains unrepaired over a substantial period of time [68].

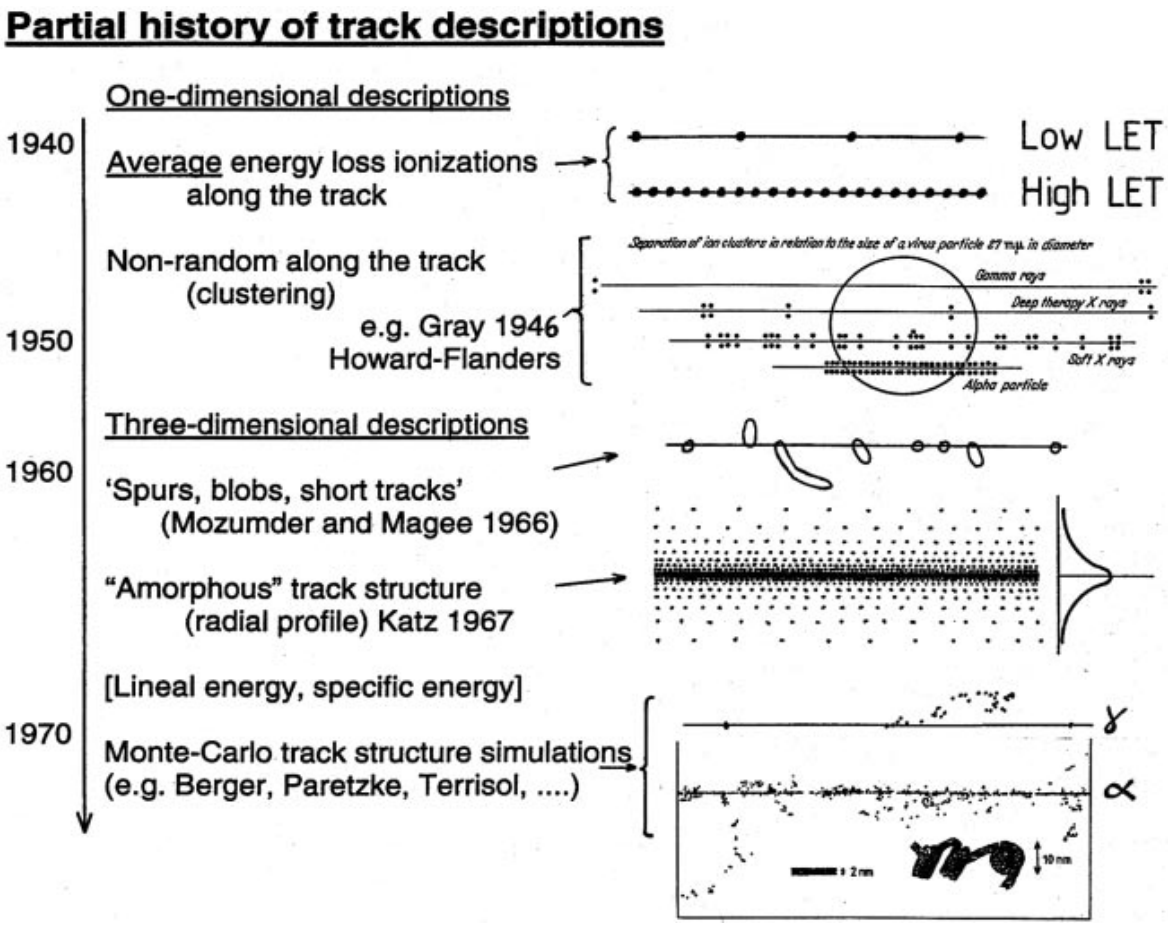

Fig. 4A: Illustration of historical development of descriptions of radiation tracks [64].

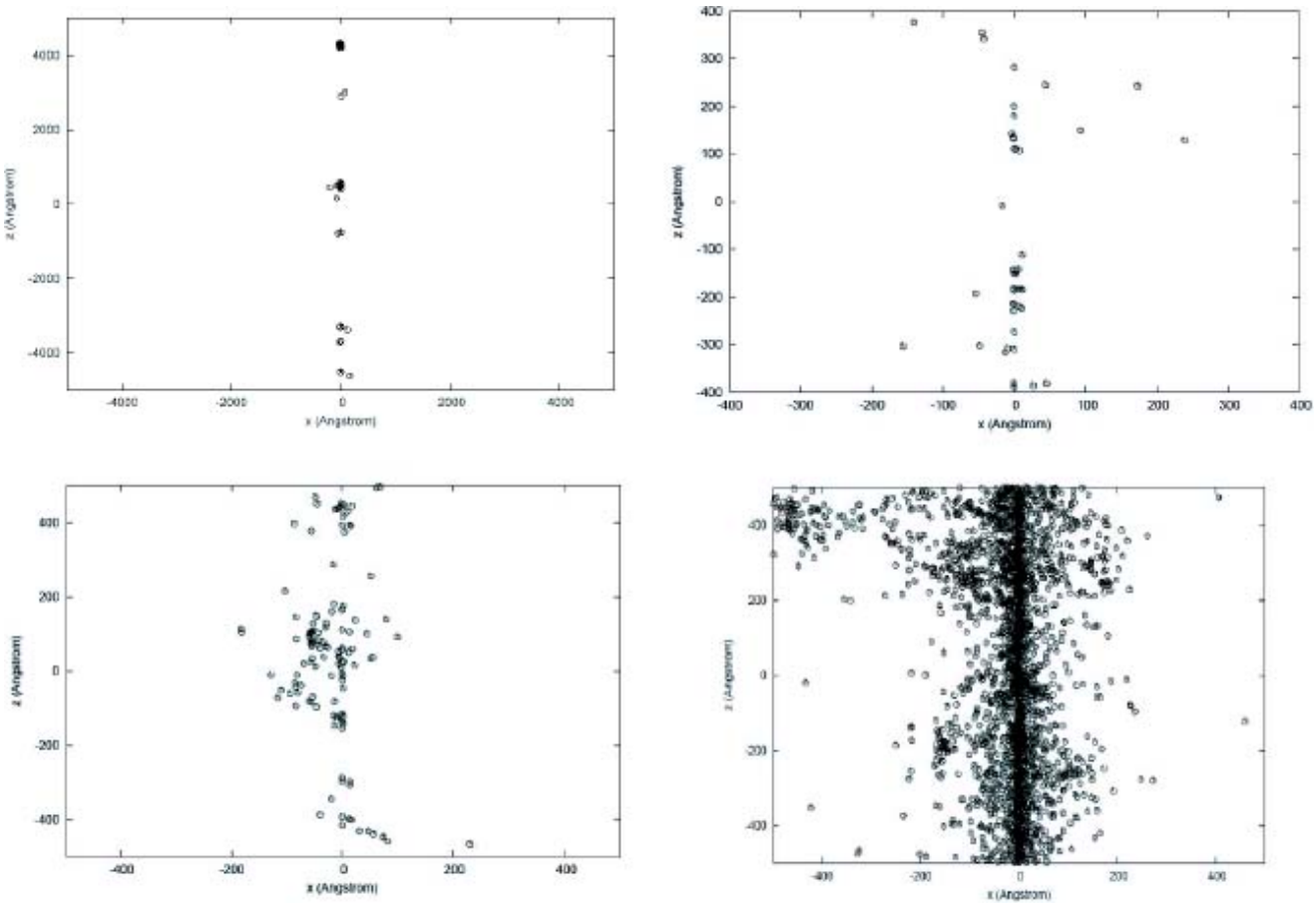

Fig. 4B: 2D projection of track-structure segments in liquid water for different ions with the same velocity (115 MeV nucleon–1) as calculated with the PARTRAC code (from top to bottom and from left to right: H, He, C and Fe; note the different scale for the proton track). (Ballarini F. et al. New J. Phys.10 (2008))

The increased effectiveness of high LET radiations can be inferred from the fact that their survival curves are linear on a semi-logarithmic plot, whereas they curvilinear ("shouldered") for low LET radiation, see Figure 5.

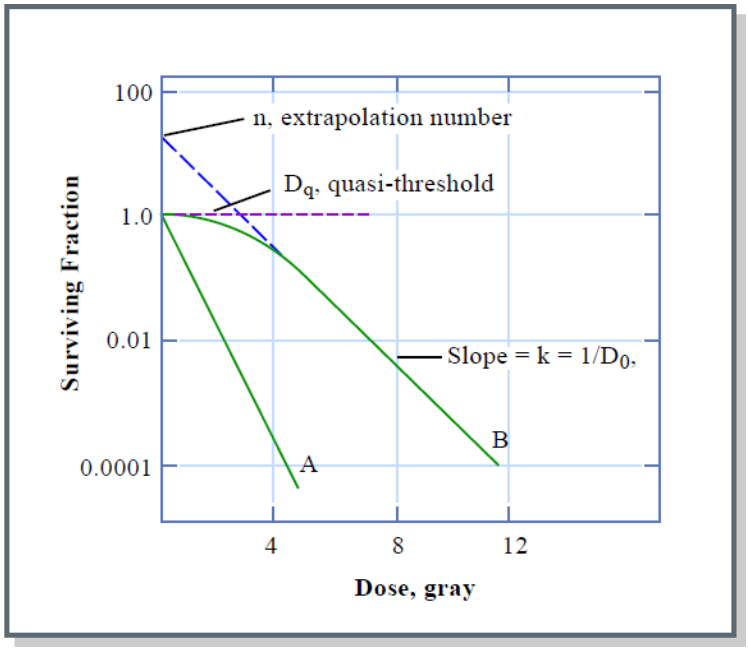

Fig. 5: Survival curve plot obtained with high (A) and low LET radiation (B).

Illustration Courtesy: http://ocw.mit.edu/terms

1.2. Introduction to complex lesions

Since the effects of radiation are stochastic, the breaks and other forms of damage created by IR are not in distinct and definite regions of the genome, but random (in broader terms) and extremely diverse. This gives rise to the possibility of induction of a complex lesion. A cluster of closely-spaced DNA lesions of same or different nature including single strand breaks, oxidized base lesions (oxybases; oxypurines and oxypyrimidines) [58] and regular and oxidized AP sites, which are produced in close proximity to each other, generally within 1 - 2 helical turns of DNA molecule and on opposite strands (bistranded lesions) has traditionally been accepted as the description of a complex lesion, a hallmark of high LET radiations, like neutrons and α-particles. Complex or clustered lesions constitute nearly 50-80% of the damage induced by IR [55]. Clustered lesions are resistant to processing by glycosylases and endonucleases and remain persistent in the genome for a significant amount of time after irradiation and are considered to be highly mutagenic [48].

1.2.1 Complex lesions induced by low and high LET radiations

Clustering of DNA lesions depends on chromatin structure and LET of the radiation, see Figure 6. For low LET radiations, the clustering occurs on the small scales of DNA molecules and nucleosomes, whereas for high LET radiations, the clustering of lesions is also seen on a much larger scale with chromatin state dependency.

There are various theories put forth for the same over the years by radiation chemists, like the theory of Locally Multiply Damaged Sites (LMDS) [69] and Regionally Multiply Damaged Sites (RMDS) [70]. LMDS theory explains that energy from ionizing radiation tends to localize along the tracks of charged particles and is not absorbed uniformly. This energy is deposited in the form of spurs and blobs, which contain a number of ion pairs (blobs more than spurs) and have a similar dimension as the DNA double helix. With the increase of LET or in high LET radiations like neutrons and α-particles, the number of blobs created is greatly enhanced, thus resulting in increased lethality. Theory of RMDS highlights the 30-nm chromatin fiber as the target for ionizing particles. Experiments showed that DNA fragments in the size range of 0.1-2 kb were formed linearly with dose with an efficiency that increased with LET. A comparison of the yield of such fragments with the yield of total DNA double-strand breaks suggests that for the high- LET ions a substantial proportion (20-90%) of DNA double-strand breaks are accompanied within 0.1-2 kb by at least one additional DNA double-strand break[70].

The crucial features of association of damage could be at any one or more of the following levels of structures: clustering of damage at the level of the DNA helix, or in higher-order DNA structures such as nucleosomes (theory of Multiple damaged sites or MDS) [14]; spatial association of separate points of damage such as across a chromatin fiber, or between adjacent chromatids [71]; in other target molecules or structures; or the simultaneity (in <10 -12 s) of the overall burden to the cell nucleus, such as the ~200 DNA single-strand breaks (SSB) and ~20 DSB from the traversal of a single α-particle. Attempts have been made also to evaluate the yields of SSB and DSB for various radiation types, either from direct ionizations in the DNA, indirect effects from nearby hydroxyl radicals or combinations of both [50, 72], which revealed that a high proportion of the DSBs have additional associated damage, such as base damage and additional strand breaks within the same very short segment of DNA [73, 74]. This clustered

damage at the DNA level appears to be a feature of virtually all ionizing radiations, although its frequency and severity depend on the radiation quality.

1.2.2 Cell lethality in relation to complex lesions

A combination of the complexity or distribution of lesions, repair enzyme levels and access to damage are major factors which influence DNA repair. The distribution of damage within higher-order chromatin structures and the position of double-strand breaks (DSBs) relative to other breaks have been suggested to play critical roles in the repair of DNA damage, the formation of chromosomal aberrations and the clonogenic survival of cells. One of the suggested models for reproductive cell killing involves a "paired" DSB mechanism, where it has been hypothesized that potentially lethal damage (PLD) might result from two DSBs produced by a single track that are separated by relatively large distances [75]. This model was proposed to be consistent with the dependence of cell lethality on linear energy transfer (LET) and inferred that packaging of DNA within the nucleus might play a role, not only in the numbers of induced DSBs but also in their distribution within the chromatin. Another Poisson-based model of induction of DSBs and elution of DNA from residual nuclear structures was proposed, which speculated that elution of DNA from nucleoids could occur only if two or more DSBs were induced within a single looped domain. Multiple DSBs within these structures released the segment of non-matrix-bound DNA delineated by two DSBs, thus allowing its elution [75-77] [78].

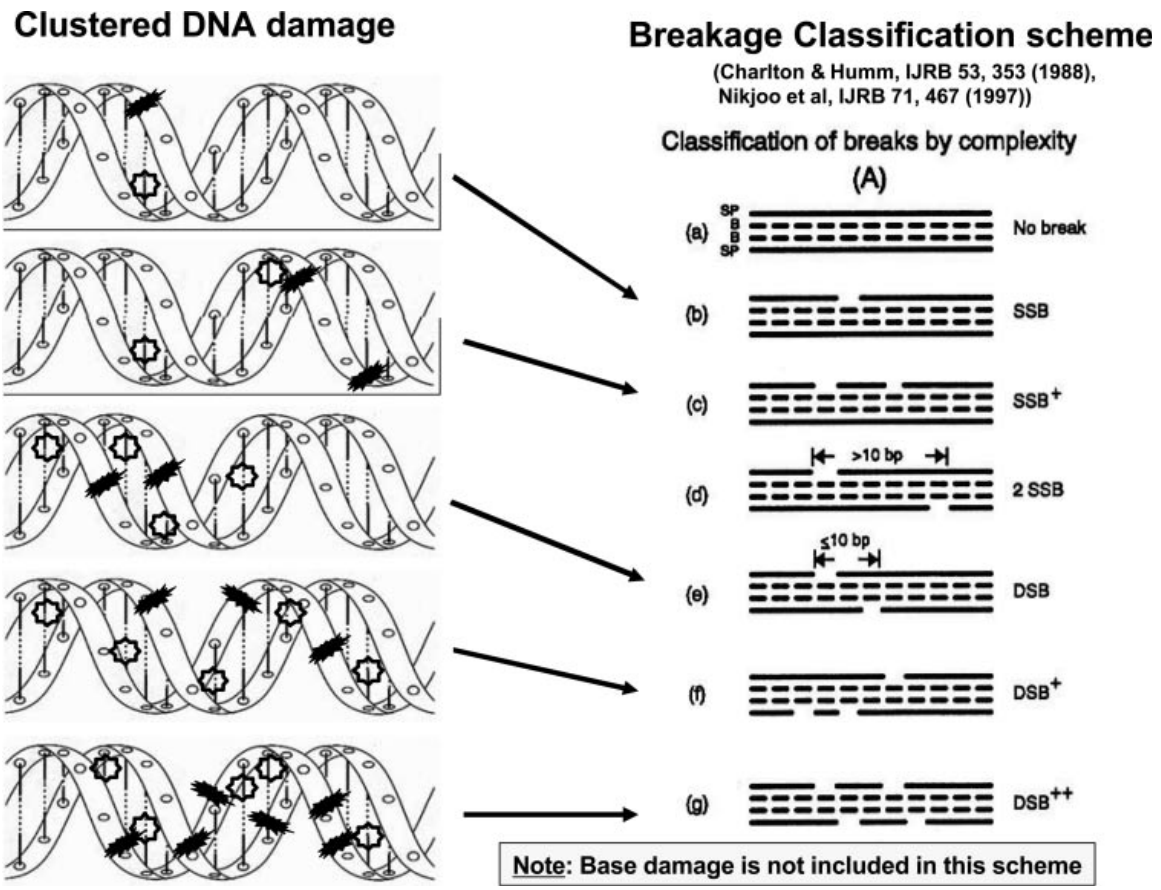

Fig. 6: Classification scheme (right hand side) used for scoring clustered damage in DNA due to multiple strand breaks. Schematic diagrams on the left illustrate typical examples of strand breakage (solid symbols), but also include examples of associated base damage (open symbols) [64].

1.3. Induction of DNA double strand breaks without utilizing IR or radiomimetic compounds

As discussed earlier, due to the stochastic nature of its effects, IR is not an optimum tool for the study of the effects elicited to only DNA double strand breaks as it also induces a multitude of other types of lesions adding new dimensions of complexity. IR-induced DSBs also cannot be placed in a controlled manner and their location, type and number varies stochastically from one cell to another. Hence, the effect of repair or misrepair of a single type of lesion can never be studied as all methods currently used take into account the collective response of all cells, thus masking or losing the fine details for the types of radiation induced damages which are most lethal to the cell.

One of the approaches to characterize the pathways of DSB repair is to monitor the repair of site-specific DSBs generated by rare-cutting endonucleases, such as I-*Sce*I [79-81]. Utilizing a single I-*Sce*I site, a study demonstrated that broken ends are positionally stable and unable to roam the cell nucleus and require the DNA end binding protein Ku80. Repair was independent of DNA repair factors, γ-H2AX, the MRN complex and the cohesion complex. In this study, a single DSB could be induced at a defined genomic site and the fate of each of the two damaged DNA ends could be tracked in real time [82]. Another study [83] utilized the presence of nearly 200-300 endogenous I-PpoI sites in the human genome for induction of DSBs and used the system to detect protein recruitment and loss at and around these breaks by chromatin immunoprecipitation (ChIP). DSB formation led to the localized disruption of nucleosomes, a process that depended on both functional NBS1 and ATM, which were also required for the efficient recruitment of the repair factor XRCC4 to DSBs and for efficient DSB repair. A study with two I-*Sce*I sites, in correct or reverse orientation [84], separated by the H2-KD and CD8 genes, showed that I-*Sce*I sites in correct orientation were rejoined either accurately or caused extended deletions. On the other hand, I-*Sce*I sites in reverse orientation generated non-fully complementary ends for CD4 expression. DSB repair under these conditions either led to extended deletion or used the annealing of two of the four protruding nucleotides. Another study utilized a NHEJ reporter construct based on two I-*Sce*I sites in reverse orientation for determining the importance of Ku and XRCC4 proteins in non-homologous end joining pathway [85]. Two I-*Sce*I site constructs were also used to study the contribution of various repair factors like Ku, CtIP, Rad51, Rad52 and ERCC1 in alternative non-homologous end joining (alt-NHEJ), HDR and SSA. [86]. The same constructs are utilized to decipher the roles of ERCC1, Msh2, Nbs1, XRCC4, and BRCA1 in the above mentioned pathways [87]. Another study involving two I-*Sce*I sites dealt with the choice of repair pathway for a type of DSB and demonstrated that non-RAG mediated DSBs are forced into the NHEJ repair pathway by physical association with RAG endonuclease [88].

Most studies involving homing endonucleases have focused on targeted integration at a specific location in the genome in tandem with various read-out systems for determining both cleaved and uncleaved status of the break. One study utilized a chromosomally integrated I-*Sce*I site besides a Tet operator array that was visualized by binding of a

Tet repressor-GFP fusion to study the recruitment of various repair factors at the site of DSB utilizing light microscopy in various mutant cell lines. A single I-*Sce*I site integrated by chance close to an endogenous dhfr locus was studied, which showed that I-*Sce*I-induced homogenously stained region (HSR) breakdown leads to formation of double minutes and induction of various types of chromosomal rearrangements [89]. A study utilizing genetically modified mouse embryonic stem cells carrying two I-*Sce*I sites in cis and non-repetitive region of the same chromosome separated by 9 kbp showed that in spite of a functional NHEJ machinery, some unusual joining intermediates are formed that severely affect the repair efficiency of these two distant DSBs, leading to a large spectra of mutagenic events [90]. Utilizing a similar approach, another group studied the effect of single and 2 DSBs induced by I-*Sce*I to determine the junctional characteristics after the breaks induced were rejoined, inferring that NHEJ for repairing I-*Sce*I-induced DSBs mainly results in small or no deletions[91]. Numerous other studies have utilized I-*Sce*I and other homing endonucleases for characterization of DNA repair pathways over the years[79-81, 92-94].

1.3.1 Homing Endonucleases

Homing Endonucleases are proteins of < 40 kDa. The word “Homing” means the lateral transfer of an intervening sequence (either an intron or intein) to a homologous allele that lacks the sequence. This process is catalyzed by double stranded DNases that recognize and cleave the target allele, which itself is coded by an open reading frame (ORF) embedded within the mobile intervening sequence.

They recognize long DNA target sites (14 - 40bp). The four main Homing Endonuclease families are: LAGLIDADG, GIY-YIG, His-Cys box and H-N-H [95]. Although most homing endonucleases share with restriction enzymes the ability to make a site-specific double-strand break in the DNA target, they differ in structure, recognition properties, and genomic location. Homing endonucleases are named using conventions similar to those of restriction endonucleases with intron-encoded endonucleases containing the prefix, “I-”. Homing endonuclease recognition sites are extremely rare. For example, an 18 base pair recognition sequence will occur only once in every 7×10^{10} base pairs of random sequence. This is equivalent to only one site in 20 mammalian-sized genomes

[80]. However, unlike standard restriction endonucleases, homing endonucleases tolerate some sequence degeneracy within their recognition sequence. As a result, their observed sequence specificity is typically in the range of 10-12 base pairs. Homing endonucleases do not have stringently-defined recognition sequences in the way that restriction enzymes do, i.e. single base changes do not abolish cleavage but reduce its efficiency to variable extents. The precise boundary of required bases is generally not known.

1.3.2 I-*Sce*I

I-*Sce*I is an intron-encoded site-specific homing endonuclease isolated from the mitochondria of Saccharomyces cerevisiae. I-*Sce*I belongs to the LAGLIDADG homing endonuclease family, whose members cleave long DNA substrates (>14 bp) to generate four base 3'-overhangs [95]. LAGLIDADG endonucleases (see Figure 7) are either monomers, such as I-*Sce*I, that are composed of two pseudosymmetric subdomains that recognize asymmetric substrates [96] or homodimers, such as I-CreI, that recognize palindromic or pseudopalindromic substrates [97]. The recognition sequence of I-*Sce*I is an 18 bp non-palindromic sequence. The insertion of I-*Sce*I recognition sites in the genomes of other organisms results in selective double-strand DNA cleavage at the inserted site, leaving the remainder of the genome intact. I-*Sce*I stimulates more than 1000 fold the frequency of recombination between a chromosomal locus containing the cleavage site and homologs located on exogenous DNA [98], making I-*Sce*I an ideal choice for gene targeting studies and studying DNA repair pathways like non-homologous end joining and HRR [99] [99-102] [103].

Fig. 7: Structure of PI-SceI, a LAGLIDADG family member. Endonuclease domains are shown in blue with orange β-sheets showing DNA-binding saddle [95].

1.4. Utilization of Transposons for study of DSB repair

Most studies till date have focused on creating a single DSB or 2 DSBs by Homing endonucleases like I-*Sce*I and studying aspects of DNA repair like recruitment of different proteins at these sites of breaks with kinetics of recruitment, uncovering repair pathways and their intermediates, monitoring the movement of open ends in the nuclear matrix, etc. We strived to differ from the above mentioned studies by introducing as many I-*Sce*I sites as possible into the mammalian cell genome. Random integration of sites in the genome with only transfection (nucleofection) yielded only one or two integrations, determined with Southern blotting. Thus to achieve our aim, we opted for a Transposon-based system which allows us to integrate our sequence of interest at many locations in the genome randomly.

1.4.1 Types of Transposable Elements

Transposable elements (TE) are characteristic segments of DNA which show the distinctive ability to move and replicate within genomes [104, 105]. Two major classes of transposable elements are known; the first class involves retrotransposons that transpose replicatively within their host genomes by using RNA intermediates [106]. As a result, the donor element does not move but instead a copy is produced, using reverse

transcription, which inserts elsewhere in the genome. In contrast to retroviruses, retrotransposons lack a glycoprotein envelope gene, which prevents the retrotransposon from forming an infectious virus particle and thus prevents it from leaving the host cell. Different types of retrotransposons exist, like long interspersed elements (LINEs), short interspersed elements (SINEs) and long terminal repeats (LTR).

Most of the repeat sequences, which comprise more than 50% of the human genome, are derived from retrotransposons. The L1 element consists of a 5` UTR, two ORFs encoding a RNA binding protein, an endonuclease, a reverse transcriptase and a 3`UTR. Alu, the only active SINE in the human genome, is derived from the 7SL RNA, a cytoplasmic RNA which functions in protein secretion as a component of the signal recognition particle [107]. In mammals, the L1 and Alu elements were inserted into new genomic locations during evolution. These elements are often truncated and rearranged to form inactive copies of their progenitors. Such mutations, if advantageous or neutral, may contribute on one hand to protein variability and versatility but on the other hand, if disadvantageous, they can generate genetic diseases.

The second class of transposable elements involves DNA transposons which move directly as DNA segments. DNA transposons are flanked by terminal inverted repeats (TIRs). The transposition is characterized by a “cut and paste mechanism” whereby the transposon is excised from the donor locus and reinserted randomly somewhere else in the genome. This process is catalyzed by the element-encoded transposase. The different classes of DNA transposons are divided into superfamilies. The following nine DNA transposon superfamilies are known in eukaryotes: CACTA, hobo/Activator/Tam3 (hAT), Merlin/IS1016, Mutator, P-element (Drosophila), PIF/Harbinger, PiggyBac, Tc1/mariner, and Transib [108]. The different superfamilies are characterized by a superfamily-specific transposase core domain, which is different from those of other superfamilies. Furthermore, superfamilies differ in the presence and size of the target site duplication (TSD), a short direct repeat that is generated on both flanks of a transposable element upon insertion [109].

Transposons occupy about 45% of the human genome, whereby the DNA transposons account for about 2-4% and the retrotransposons about 41%. Despite the fact that they make up such a significant fraction of the genome, no indication of DNA transposon

activity has been noticed in the human genome for the past 50 million years (International human genome sequencing consortium, Nature 2001).

1.4.2 The Sleeping Beauty Transposon system

Active DNA transposon systems are existent endogenously in invertebrates, but in vertebrates, they were inactivated millions of years ago. Since transposition offers unique advantages in experimental genome manipulation, efforts were made to generate active transposon systems in vertebrates.

As part of these efforts, a TC1/mariner-type transposon found in fish genomes was reconstructed by eliminating different inactivating mutations from the transposase gene, like insertions, deletions and point mutations. For this purpose, phylogenetic data of different teleost fish species and comparative analysis of functional transposase domains were used. The phylogenetic data comprised a multiple sequence alignment of salmonid TE sequences from twelve fish species. Five highly conserved regions, located in the transposase gene, were found: a nuclear localization signal (NLS), a glycine rich motif and three segments in the C-terminal region including an amino acid triad DDE domain. In the first step of reactivating the salmonid transposase gene, the TE open reading frame (ORF) was restored by combining parts of two inactive TEs of Atlantic salmon and a single part of rainbow troat and removing the premature translational stop codons and frameshifts. In the second step, non-synonymous nucleotide substitutions of the consensus sequence were eliminated in order to rebuild putative functional protein domains. Simultaneously, a full length gene was synthesized which is equal to the consensus sequence. This reconstructed synthetic transposase gene and a nonautonomous salmonid-type element from Tanichthys albonubes, that carries the inverted repeats of the transposon substrate DNA, constitute the active transposon system, named Sleeping Beauty (SB). Members of the TC1/mariner superfamily of transposable elements are extraordinarily widespread in nature, ranging from single cell organisms to humans. Therefore the salmonid SB transposon is able to mediate transposition in different species like fish, mouse and human cells [110].

1.4.3 Structure of the Sleeping Beauty Element

The SB transposon consists of a single gene encoding the transposase polypeptide, which is flanked by the inverted repeats (IRs) containing binding sites for the transposase. The SB transposon is nonautonomous and not able to transpose without an appropriate transposase encoding sequence. As long as transposons retain their IRs, the transposase can mobilize transposons in trans and can be physically separated from the transposon element. This gives the possibility to remove from the transposon the DNA segment coding for the transposase and insert other DNA sequences. The transposase binding sites of the SB element show a specific structure. Two binding sites are located at the ends of the 200-250 bp long inverted repeats and contain short 15-20 bp direct repeats (DRs). This special organization of the whole region is termed IR/DRs. The left IR contains the HDR sequence motif which is similar to the 3' half of the transposase binding sites.

The transposase has an N-Terminal, bipartite, paired like DNA-binding domain containing the two helix-turn-helix motifs PAI and RED separated by a GRRR-AT hook motif to mediate DNA binding to the DRs. Furthermore, it contains a nuclear localization signal (NLS) flanked by phosphorylation target sites of casein kinase II, which serve as a checkpoint in the regulation of transposition. At the C-terminal site, the catalytic domain is located, characterized by the conserved amino acid triad DDE [111]. Within the catalytic domain of the transposase, a glycine rich motif is present, but its function is unknown. The transposase used in this work is a hyperactive variant of the original SB transposase.

1.4.4 Mechanism of Transposition

The "cut and paste" transposition process involving the excision of the DNA element from its DNA context and the reintegration into a different locus in the genome, can be divided into four major steps (Figure 8):

In the first step, the transposase binds to the IRs of the transposon. The SB substrate recognition and transposition are highly specific. The SB transposase is able to distinguish its own substrate from a different substrate which differs in no more than two bps [112]. The specificity of DNA-binding is mediated by the PAI sub-domain of the

transposase through a base specific interaction. The 3' part of the transposon binding site is recognized by a PAI sub-domain whereas the 5' part is recognized by the RED sub-domain of the transposase. Furthermore, PAI binds to the HDR motif of the transposon and mediates interactions with other transposase units within the active tetramer.

In the second step, the synaptic formation takes place, where the two ends of the transposon element are paired and held together by the transposase. This step serves as a checkpoint for the transposition, controlling whether all molecular requirements are fulfilled. During synaptic complex formation, the complete IRs with four transposase binding sites forms transposase tetramers. The HDR motif of the transposon serves as a transpositional enhancer.

The third step, transposon excision, takes place when the synaptic complex formation is completed. The DDE catalytic sub-domain of the transposase catalyzes the cleavage at the ends of the SB element and generates overhangs of three nucleotides, GTC, at both ends of the transposon. The terminal nucleotides of the transposon which are left behind at the donor site, generate a three bp transposon "footprint" after NHEJ repair at the donor site.

In the fourth step, reintegration of the transposon takes place, catalyzed by the DDE subunit of the transposase. Sleeping Beauty shows a random pattern of integration in the human genome [113]. It prefers TA dinucleotides as integration sites which occur approximately every 20 base pairs in vertebrate genomes. Palindromic AT-repeats: ATATATAT were found to surround the integration site. The 3' ends of the excised transposon invade the target DNA molecule after the transposase has cleaved the TA dinucleotide target integration site. The TA target site is duplicated upon insertion.

1.4.5 Integration activity of SB in human cells

A two component assay was used to detect chromosomal integration events into the chromosomes of human HeLa cells [110]. Therefore two non autonomous transposon elements, the donor plasmid containing the neo selectable marker gene flanked by IRs and the helper plasmid expressing the transposase, were cotransfected in cultured vertebrate cells. The highest transposition rates were observed when the transposase

expressing plasmid was added in a ratio 1:10 dilution compared to the donor plasmid. If the ratio of the transposase is too high an effect called "overproduction inhibition" occurs which results in a decrease of transpositional activity. The number of cell clones resistant to the neomycin-analog drug G-418 served as the indicator for the integration and expression of the neo^R transgene [114]. Further details are explained in the experimental strategy section.

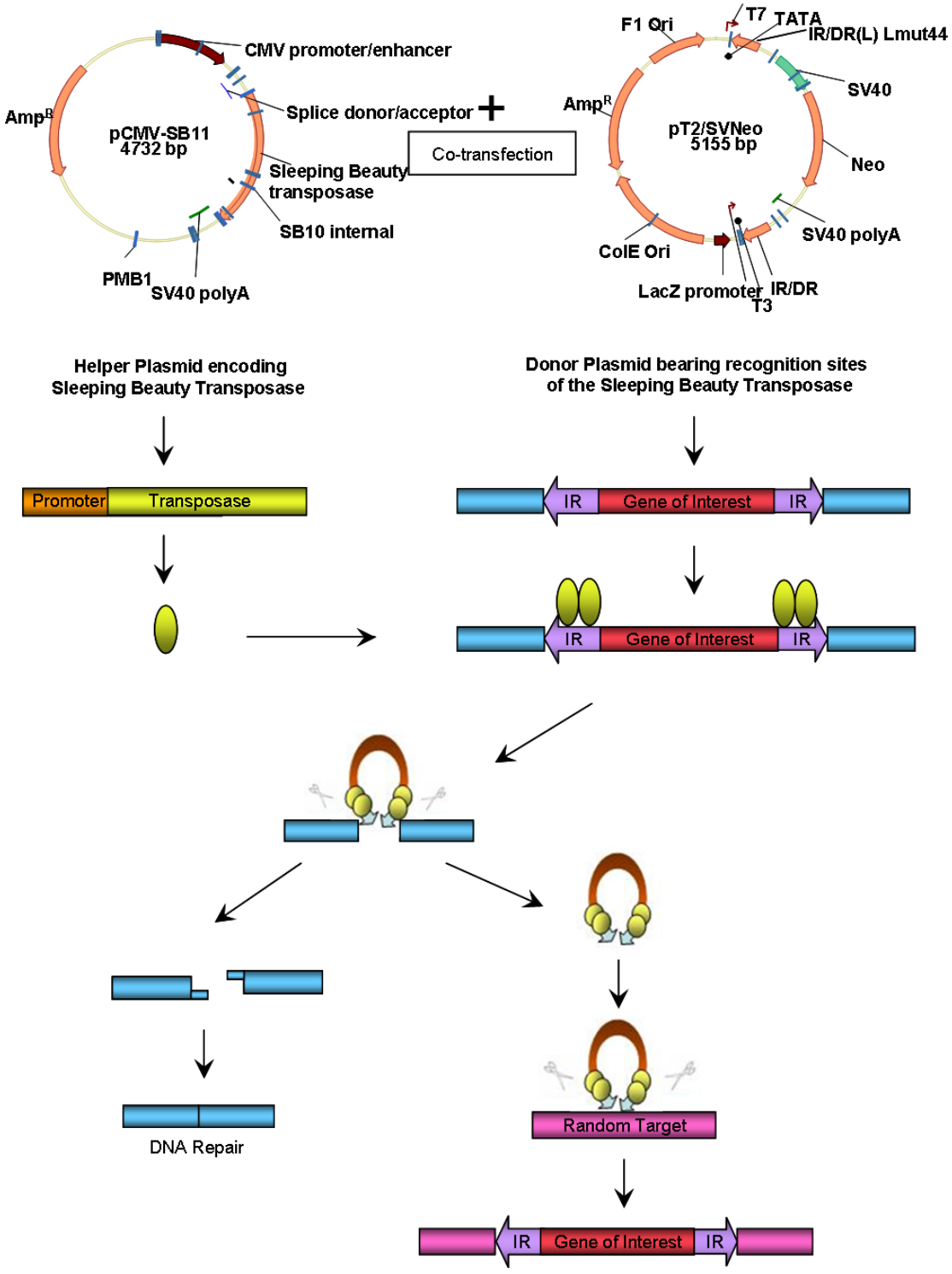

Fig. 8: Mechanism of Sleeping Beauty Transposition. Yellow circle denotes Transposase.

1.5. History of plasmid-based DNA repair assays

Analysis of the kinetics of repair of IR-induced genomic DSBs remains the golden standard in the field. However, the assays used, e.g. pulsed field gel electrophoresis, comet assay etc., and the random distribution of DSBs in the genome, as well as their generation at different genomic sites in each individual cell, preclude precise characterization and analysis of the joining event. Despite great progress in recent years, key aspects regarding the function of DSB repair pathways await elucidation. Progress in this direction will depend profoundly on robust assays allowing the elucidation and characterization of the underlying molecular steps and the definition of parameters determining functional requirements.

To overcome this limitation, assays were developed in which plasmid DNA appropriately digested in vitro using restriction endonucleases to generate DSBs with the desired ends is introduced using a spectrum of transfection methods into cells of different genetic background. Appropriately selected reporter genes allow quantification of repair efficiency, and plasmid rescue experiments offer means for analyzing the junctions generated.

These assays have been used extensively and have been instrumental in the characterization of the junctions generated by NHEJ. Numerous studies carried out with repair proficient cells demonstrated that D-NHEJ is an efficient but error prone repair process. That it only rarely utilizes homology in the form of local microhomologies, and that it is associated with nucleotide loss or gain, which can at times be extensive [115]. Importantly, these studies also showed that in D-NHEJ deficient mutants end joining (presumably by B-NHEJ) generates junctions using similar basic rules, albeit with increased use of microhomology, which rises from a few percent in wild type to over 30% in the mutant cells [116] [117] [118]. In addition, nucleotide deletions tend to be more frequent and larger extending to a few hundred base pairs.

While these plasmid assays have been very consistent when analyzing the architecture of the junctions generated by different forms of NHEJ, they generated quite divergent results when the efficiency of rejoining in D-NHEJ mutants was analyzed. Thus, while a defect in the repair of IR induced genomic DSBs is a uniform observation of all available

studies with D-NHEJ mutants, several studies using plasmid assays show no reduction in the rejoining efficiency [115] [119] [120] [121] [122] [123] [124] [125]. Since other studies show a measurable reduction in rejoining efficiency in D-NHEJ mutants and occasionally even strong effects are reported [116] [126] [127] [128], it is not possible to attribute this difference to a fundamental generally applicable property of the plasmid assay.

The spectrum of these divergent results masks the characterization and understanding of the components of DNA double strand break repair pathways in cells and has a direct bearing on human health, which makes it all the more imperative to solve this conundrum.

Since both projects discussed here involve transfection of constructs as DNA repair substrates and integration of DNA constructs in the genome of mammalian cells along with transfection of constructs expressing various chimeric proteins, in the following paragraphs, we discuss the principles of transfection methods used and the different methods available.

1.5.1 Transfection

Transfection is a term used for non-viral methods of introduction foreign substances into the cells. Transfection of animal cells typically involves opening of transient pores in the cell membrane to allow the uptake of material. Application of recombinant DNA technology to genetically manipulate the spectrum of cellular functions of a cell requires a suitable high efficiency transformation system. A number of conventional gene transfer techniques are available for transforming eukaryotic and prokaryotic cells.

These can be divided into three basic types:

A. Chemical-based transfection: Involves use of calcium phosphate, liposome-mediated transfection using cationic lipids, DEAE-Dextran, Polyethylenimine, etc.

B. Non-chemical methods: Electroporation, Nucleofection, Sono-poration, etc.

C. Particle based methods: Gene gun technique, Magnetofection, etc.

D. Viral methods utilizing viral transduction.

Since the transfection techniques utilized in this thesis are lipofection and nucleofection, a brief description of the methods is provided here.

1.5.1.1. Lipofection

Lipofectamine™ is a cationic lipid-mediated transfection reagent [129]. Cationic lipids are composed of a positively charged head group and one or two hydrocarbon chains. Negatively charged phosphate groups on DNA bind to the positively charged surface of the liposome forming the “transfection complex”, and the residual positive charge then presumably mediates binding to negatively charged sialic acid residues on the cell surfaces allowing the fusion of the liposome/nucleic acid complex into the cell membrane (see Figure 9). The transfection complex is thought to enter the cell through endocytosis, but the complex must escape the endosomal pathway and diffuse through the cytoplasm. It is generally believed that the transport of the nucleic acid into the nucleus happens when the nuclear membrane is broken down during cell division.

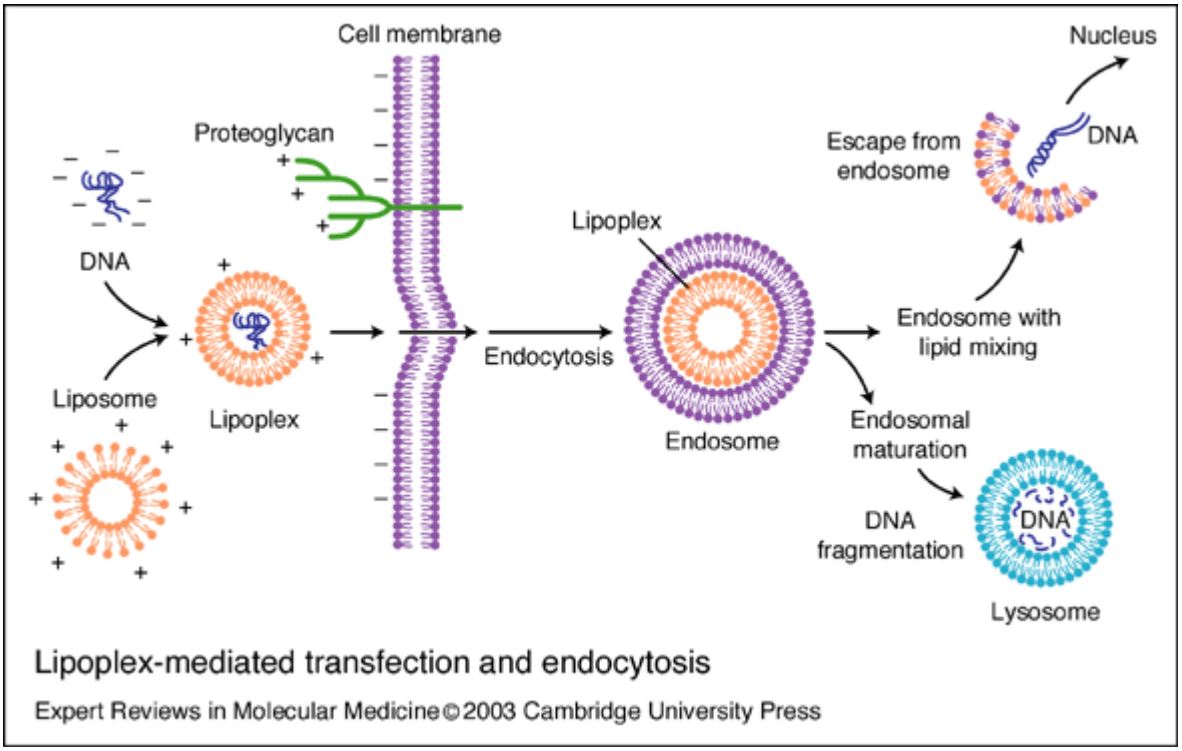

Fig. 9: Representation of liposome-mediated transfection method.

1.5.1.2. Nucleofection

Nucleofection is a technique based on electroporation. ‘‘Electropermeabilization’’ or ‘‘electrotransfection’’ or ‘‘electroinjection’’, as it is also called, is a technique where reversible electrical breakdown of cell membranes is associated with the change in permeability and sequestering of nucleic acids, proteins or antibodies through the cell membrane, utilizing brief, high intensity pulse(s) to create transient pores in the cell membrane. The survival of the electrically transfected cells is ensured by removal of the external electrical field, which leads to the resealing of the membrane electropores. Nucleofection/Nucleofector® technology is a specialized electroporation technique where a combination of electrical parameters with cell-type specific reagents allows the delivery of substances directly into the cell nucleus and the cytoplasm, thus allowing transfection in hard-to-transfect non-dividing and primary cells.

1.6. Objectives

The molecular analysis of DSB repair has benefited from assays allowing more precise substrate fate analysis. We focus our attention here to the various conflicting and intriguing results published to date about the effects of mutations of the principal components of D-NHEJ pathway on double strand break repair ability of the cells, studied principally utilizing DNA reporter substrates digested in vitro using restriction endonucleases to generate DSBs with the desired ends. These substrates were then introduced into the cells utilizing a myriad of transfection methods and the reporter system allowed quantification of efficiency of repair. Plasmid rescue experiments also allowed determining the spectrum of junctions generated after repair. Several studies over the years have reported little or no effect on DSB repair capacity of cells devoid of the core components of D-NHEJ pathway measured by various plasmid end joining assays in vivo. The spectrum of these divergent results masks the characterization and understanding of the components of DNA double strand break repair pathways in cells and has a direct bearing on human health, which made it all the more imperative to solve this conundrum.

The objective of this project was to determine the reasons for these observed discrepancies in results obtained with plasmid end joining assays, which sometimes were in complete disagreement to the results obtained with standard DNA repair assays like pulsed field gel electrophoresis, comet assay, etc. We also hypothesized that these divergent results reflect methodological differences that affect important parameters of the plasmid rejoining reaction. Results obtained with a plasmid-based DNA repair assay [130] in various D-NHEJ mutants utilizing Lipofection and Nucleofection techniques are presented here.

The second part of the thesis involves study of complex lesions utilizing homing endonuclease-based model systems. Energy deposition by ionizing radiation (IR) in cells takes place along the particle tracks in close vicinity and are not uniformly distributed in space. The distance between ionizations vary on a particle track but the distance between ionizations are known to be reduced along a track as the particle loses energy. Electrons are known to show this phenomenon and to form clustered lesions at the end of their tracks, which is referred to as the high LET component of a low LET radiation. These complex/clustered DSBs arising from these events are thought

to be the prime factor behind cell lethality with increasing LET. Repair of these lesions would require extensive processing leading to deletions and probably oncogenic transformation.

The purpose of our study was to devise model systems which would allow us to study simple and complex types of DSBs that are potentially lethal for a living mammalian cell. It was also an aim to investigate whether the processing of single DSBs differs from complex/clustered types and to determine the outcome of repair of the same. Discussing DNA repair in the context of chromatin, a recent review from our group [34] explains that out of the three major repair pathways available to a cell, NHEJ requires the least chromatin modification for operating successfully, with single strand annealing (due to its search for homology) and homologous recombination (due to its template-based approach) requiring the most. With the switch in preferences for repair pathway choice moving from lower to higher eukaryotes, it was hypothesized that maintaining chromatin integrity has taken precedence in evolution over the restoration of local sequence integrity in higher eukaryotes.

The present project tests the hypothesis that clustering of DSBs at distances affecting nucleosomal stability is highly lethal and mutagenic for the cell. In our experimental strategy, DSB clusters are induced in the genome of human tumor A549 cells through enzymatic restriction of I-*Sce*I sites integrated at different combinations and at multiple sites using transposon technology. To address complexity, we generate constructs harboring one and two I-*Sce*I sites separated by 200bp. To add another degree of complexity, we also generated a construct harboring the two I-*Sce*I sites in incompatible orientations. The transposon-based vector used contains the neo^R gene as a selectable marker and its integration at multiple sites is facilitated by co-expression of a hyperactive transposase artificially reactivated from the “Sleeping Beauty” transposon. The number of integration sites is measured in randomly selected G418 resistant clones using Southern blotting and sets are generated with clones harboring 1-20 integration sites for each DSB arrangement. These clones were then utilized to perform assays like clonogenic survival assays, determination of chromosomal aberrations, γ-H2AX foci determination, etc. for determining the cellular effects arising from these enzyme-induced lesions.

1.7. Experimental Design

To evaluate DNA end joining in vivo, we employed a fast-readout plasmid-rejoining assay using the plasmid pEGFP-Pem1-Ad2, as described earlier [130]. The plasmid is a derivative of pEGFP-Pem1 (7,139 bp) that was generated by L. Li from pEGFP-N1 (Clontech, Palo Alto, CA) by interrupting the enhanced green fluorescent protein (EGFP) sequence with the Pem1 intron. It was constructed by inserting the wild-type adenoviral major late mRNA leader sequence adenoviral exon 2 (Ad2) into the polylinker site within the Pem1 intron of pEGFP-Pem1 after appropriate modifications to generate HindIII and I-SceI cutting sites, as well as splice sites on both sides of Ad2. In this configuration, the EGFP gene is normally disrupted by the Ad2 exon and therefore transfection of supercoiled plasmid generates no EGFP signal. When Ad2 is removed before transfection, by digestion at both sides, either with HindIII or I-*Sce*I, EGFP activity can be recovered if the transfected cell possesses end joining activity to re-circularize the linear plasmid. Partly digested plasmid that retains the Ad2 sequence generates no signal.

In the experiments reported here, the pEGFP-Pem1-Ad2 plasmid was digested with HindIII to remove Ad2 and generate cohesive ends with 4-bp 5' protruding single strands. Supercoiled pEGFP-Pem1 was used as a positive control to standardize the transfection and analysis conditions. The pDsRed2-N1 plasmid (Clontech) was cotransfected with either linearized pEGFP-Pem1-Ad2 or supercoiled pEGFP-Pem1 to evaluate the transfection efficiency utilizing Lipofection and Nucleofection. The ratio of GFP+ to Red+ cells was plotted as a function of the amount of GFP-Pem1 vector. The percentage of rejoining was then calculated as equivalent circular DNA over concentration of linear DNA transfected x 100%.

All plasmids were prepared in XL-1 Blue bacteria and purified using CsCl/EtBr gradients. The HindIII linearized pEGFP-Pem1-Ad2 was purified by gel electrophoresis to remove the Ad2 fragment. Plasmid rejoining efficiency was tested in MEFs and CHO cells both proficient and deficient in D-NHEJ pathway components.

Our experimental design for the second project involves creation or induction of simple and complex homing endonuclease-induced DNA double strand breaks. This was accomplished by stably integrating I-*Sce*I homing endonuclease sites into the genome at

various sites in “simple” and “complex” orientations. The terms “simple” and “complex” denote the I-*Sce*I sites in compatible and incompatible orientations to each other respectively. The constructs are designed bearing I-*Sce*I sites in compatible and non-compatible orientation separated by 200bp. Compatible ends are defined as overhanging sequences which are complementary at both I-*Sce*I sites after restriction and the loss of the 200bp spacer. The term incompatible is defined here as overhanging DNA sequences exclusively formed when the 200 bp spacer is lost in the construct bearing reversely oriented I-*Sce*I sites, where complementary sequences at the DNA ends are not available for direct rejoining.

For punctuating the genome with I-*Sce*I sites at various locations randomly, we utilized the Sleeping Beauty Transposon system developed by Ivics et al. [104, 105, 110-112, 114, 131, 132], which functions by inducing global mutagenesis via non-homologous end joining (NHEJ) in the genome. The system utilizes two constructs, one called as the “Donor” plasmid and the other “helper” plasmid expressing the modified “hyperactive” variant of the Sleeping Beauty transposase. The donor plasmid is a construct in which our sequence of interest is cloned upstream of the Neo^R gene and flanked on both sides by Inverted Repeats/Direct Repeats (IR/DRs), which are the recognition sequences of the Sleeping Beauty Transposase (Figure 8). The hyperactive version of the Sleeping Beauty Transposase cleaves the plasmid at the IR/DR sites, carries the sequence of interest along with the Neo^R gene marker and integrates it randomly in the genome by a transposon-mediated cut-and-paste mechanism. We utilized two variants of I-*Sce*I constructs for expression in vivo, one in which I-*Sce*I is constitutively expressed, called as pCMV-I-*Sce*I-3xNLS [92, 94, 102] and the other construct expressing a chimera of EGFP-I-*Sce*I-GRLBD, which is inducible by addition of triamcinolone acetonide (TA) [82, 89].

2 Materials and Methods

2.1 Materials

2.1.1 Laboratory apparatus

Al Filter	GE Healthcare, USA
ÄKTA FPLCpurifier 10/100 UPC-900	GE Healthcare, Germany
Avanti J-20XP	Beckman Coulter, USA
Beckman Tabletop GS-6R centrifuge	Beckman Coulter, USA
BioFuge (Fresco)	Thermo Scientific, Germany
Cell culture “Herasafe” hood	Thermo Scientific, Germany
Coulter Counter	Beckman Coulter, USA
Electro-Transfer Unit	Bio-Rad, USA
Express Pipet-Aid	BD Falcon, USA
Flow Cytometer	Beckman Coulter, USA
Heating unit	Peter Oehman, Germany
Hybridizer HB-1000	UVP LLC, USA
CO_2 Incubator	Sanyo, Japan
Magnetic Stirrer	Heidolph, Germany
Inverted Microscope	Olympus, Japan
Molecular Imager VersaDoc	Bio-Rad, USA
Nanodrop	Thermo Scientific, Germany
Overnight Culture Shaker	Infors, Germany
Pasteur pipette	BD Falcon, USA
Peristaltic pump	Ismatec, Switzerland
pH Meter	InoLab, Germany
Pipettes	Eppendorf, Germany
Rocky Shaker	Peter Oehmen, Germany
Roller drum	Bellco Biotechnology, USA
SDS PAGE mini gels	Mini PROTEAN, Bio-Rad, USA
Scintillation Counter	Beckman Coulter, USA

Thermo-mixer	Eppendorf
Typhoon Scanner	GE Healthcare, USA
Ultracentrifuge	Beckman Coulter, USA
UV Spectrophotometer	Shimadzu Corp., Japan
Vortexer (Vortex-Genie 2)	Scientific Industries, USA
Water Bath	GFL Instruments, Germany
Weighing Balance	Sartorius (BP110 S)
X-ray machine (320KV)	GE Pantak, Germany

2.1.2 Disposable elements

0.2µm filter	Millipore, USA
1.5 and 2 ml tubes	Eppendorf, Germany
15 & 50 ml Centrifuge Tubes	BD Falcon, USA
Cell Culture Dishes	Cell Star, USA
Dounce homogenizer	KonTes, Kimble Chase, USA
Flasks and beakers	Schott Duran, Germany
Nitrocellulose membrane	Schleicher Schuell, Germany
Nylon membrane	Roche, Germany
Rainin Pipettes	Mettler Toledo, Germany
PVDF membrane	GE Health care, USA
Spinner Flask	Bellco, USA
UV Cuvettes	Hellma, Germny
Parafilm	Lab Depot Inc. USA

2.1.3 Chemical reagents

The chemicals used were of analytical grade

Acrylamide-Bis-acrylamide (37:5.1)	Roth, Germany
Albumin Bovine	Sigma-Aldrich, USA
Bromophenol Blue	Sigma-Aldrich, USA
DMEM	Sigma-Aldrich, USA
dNTPs	Promega, USA

DTT	Roth, Germany
EDTA	Roth, Germany
Ethanol	Roth, Germany
FCS/FBS	Gibco Life Sciences, USA
Glycerol	Roth, Germany
Glycine	Roth, Germany
Grace's Insect Medium	Gibco Life Sciences, USA
Isopropanol	Roth, Germany
KCl	Roth, Germany
Lactalbumin hydrolysate	Sigma-Aldrich, USA
Luria Broth	USB Corp, USA
Luria Agar	USB Corp, USA
McCoy's5A	Sigma-Aldrich, USA
MEM	Gibco Life Sciences, USA
Methanol	Sigma-Aldrich, USA
NaCl	Roth, Germany
Non-Fat dry milk	Roth, Germany
Nonidet P40	Roche, Germany
Phusion Hot-Start High Fidely Polymerase	Finnzymes-NEB, USA
Poly L-Lysine	Biochrom AG, Germany
ProLong Gold Antifade solution	Invitrogen, USA.
Propidium Iodide	Sigma-Aldrich, USA
RNase	Sigma-Aldrich, USA
TEMED	Roth, Germany
TRIS Base	Roth, Germany
Tris-HCL	Sigma-Aldrich, USA
Triton X-100	Roth, Germany
Trypsin	Biochrom, Germany
Coommassie brilliant blue G-250	Serva, USA
Tween 20	Roth, Germany

2.1.4 Commercial kits and columns

α-^{32}P CTP	Perkin Elmer, USA
Label IT CX Rhodamine Labeling kit	Mirus Bio, USA
DNA cellulose resins	Sigma-Aldrich, Germany
ECL Western Blotting Reagent	GE Healthcare, USA
DNA Maxi-prep Kit	Qiagen, USA
FlexiGene DNA Kit	Qiagen, USA
Hi Load (26/60) SuperDex 200	GE Healthcare, USA
HiTrap™ Heparin prepacked column	GE Healthcare, USA
ProbeQuant G-50 Columns	GE Healthcare, USA
Prime-It II Random Primer Labeling kit	Stratagene, USA.
QuikHyb Hybridization Solution	Stratagene, USA
QIAquick Nucleotide removal Kit	Qiagen, Germany
Salmon Sperm DNA	Roche, Germany

2.2 Methods

2.2.1 Cell Culture and chemicals

For experiments, we used mouse embryo fibroblasts (MEFs) from *p53*$^{-/-}$ as well as *LIG4*$^{-/-}$*/p53*$^{-/-}$ animals [133]. Chinese hamster cells *(CHO9)* were used as a repair proficient control to the *xrs-6* mutant [134], which is defective in Ku80, and the *XR-C1-3* mutant, which is defective in *DNA-PKcs* (a kind gift from Dr. M. Zdzienicka). *xrs-6/KU80*, is a corrected cell line generated by transfecting *xrs-6* with the human *KU80* under the control of the Rous sarcoma virus long terminal repeat promoter [135]. MEFs were maintained in D-MEM supplemented with 10% fetal calf serum (FCS). CHO cells were cultured in McCoy's 5A medium supplemented with 10% FCS. Propidium iodide (40 µg/ml) was used for staining cells for Flow Cytometry (Beckman Coulter Epics XL-MCL).

2.2.2 In vivo plasmid DNA end joining

For Nucleofection, the appropriate plasmids were transfected using the MEF1 Nucleofector^{R} kit in the Nucleofector^{R} device (Lonza) according to the instructions of the manufacturer. Typically, a suspension of 2 x 10^6 cells was transfected by Nucleofection with 0.2 µg pEGFP-Pem1, or HindIII linearized pEGFP-Pem1-Ad2 substrate, together with 0.2 µg of the transfection-efficiency marker pDsRed2-N1.

In case of Lipofection, increasing concentrations from 0.05 µg of pEGFP-Pem1 or HindIII linearized pEGFP-Pem1-Ad2 plasmids with 2 µg of pDsRed2-N1 were transfected in near confluent exponentially growing cells in 60 mm dishes according to the manufacturer's protocol. Green (EGFP) and Red (RFP) fluorescence were measured by flow cytometry 24 hours later. For this purpose, cells were trypsinized and resuspended in fresh growth medium at 10^6 per ml.

Analysis was carried out in a Beckman Coulter Epics XL-MCL flow cytometer equipped with an argon ion laser emitting at 488 nm. Red fluorescence was collected at 540 nm with 740 V PMT gain, whereas green fluorescence at 490 nm with 490V PMT gain. Electronic compensation was 12.8% of green signal for red and 6.7% of red signal for

green. Transfection with supercoiled pEGFP-Pem1 was used to calibrate the system. To include the transfection efficiency in the calculation of percent rejoining, the EGFP+/Red+ ratio was calculated and compared between treated and non-treated cells. To calculate the percent rejoining of the linearized GFP plasmid, the GFP+/Red+ ratio obtained from various concentrations of NHEJ substrate was converted to an equivalent amount of circular GFP plasmid by extrapolating the points back on the curve obtained from the ratio of circular GFP+/Red+ cells. The percentage of rejoining was then calculated as equivalent circular DNA over concentration of linear DNA transfected x 100%. This method was used to calculate the rejoining efficiency of all cells used in all experiments carried out. The results were confirmed in X-Y independent experiments.

2.2.3 Plasmid preparation and CX-Rhodamine labeling of plasmid DNA

Plasmid DNA was prepared by culturing green fluorescent protein (EGFP)-expressing plasmid (pEGFP-Pem1-AD2) containing bacteria overnight and using CsCl Density Gradient protocol for the large-scale purification of the plasmid DNA. Plasmid purity was confirmed by Agarose gel electrophoresis, spectrofluorometrically and spectrophotometrically. The day prior to transfection experiments, 10μg of circular plasmid DNA encoding GFP was labeled with CX-Rhodamine using a Mirus Label IT Tracker CX-Rhodamine kit as per the manufacturers' instructions (Mirus, Madison, WI). Briefly, Rhodamine reagent was incubated with plasmid DNA (at a ratio of 0.75:1) at 37ºC for 90 minutes and precipitated using 100% ethanol and 5M NaCl. To confirm plasmid labeling, absorbance was read at 576 nm (the appropriate wavelength for CX-Rhodamine) and found to be 0.09 for labeled plasmid compared to 0.0 for unlabeled plasmid when using equivalent quantities of DNA (as determined by absorbance at 260 nm). Successful plasmid labeling was also confirmed by spectrofluorimetric analysis and dilutions of labeled DNA were spotted onto glass slide and visualized under fluorescence microscope Leica DMI 6000 (Leica Microsystems).

2.2.4 Immunofluorescence, confocal microscopy and image analysis

For immunofluorescence experiments, sterile coverslips in 35 mm dishes were coated with Poly L-Lysine (Biochrom AG, final concentration 0.01 mg/mL) the night before and cells were seeded as described above. In preparation for fixation media was aspirated and cells washed once with PBS (pH 7.4). Then, 2 ml of 2% Paraformaldehyde (PFA) was added for 15 min at room temperature (RT). PFA was aspirated and cells were washed with PBS. Cells were permeabilized with 2 ml solution P (100mM Tris, pH 7.4, 50mM EDTA, 0.5% Triton X-100) for 10 min at RT. After a PBS wash, 1 to 2 ml of DAPI solution (Sigma Aldrich, 25 ng/ml working concentration) was added for 5 min at RT. After three PBS washes coverslips were mounted on slides using 15 µL anti-fade solution. Slides were stored in the dark before analysis using a Leica TCS SP5 Confocal microscope.

Sequential scans at 0.5 µm steps were carried out with a 63X (N.A. 1.4) oil immersion Leica Objective for DAPI – GFP – CX-Rhodamine and DIC. For all images, a resolution of 512 x 512 and a pixel size of 240.74 nm X 240.74 nm were selected. For detection and measurement of DAPI, a laser diode of 405 nm was used at 40% power output was used for excitation. Fluorescence was collected at 410 – 550 nm using a smart gain of 800 V and a smart offset of -2.0%. For detection and measurement of expressed GFP, an Argon laser at 488 nm and 25% power output was used for excitation. Fluorescence was detected between 495 – 550 nm using a smart gain of 750 V and a smart offset of -5.0%. For the detection and measurement of CX-Rhodamine-labeled plasmid DNA, a laser diode at 461 nm and 25% power output was used for excitation. Fluorescence was detected between 570 – 650 nm using a smart gain of 950 V and a smart offset of -5.0%. The last channel in the sequential scan was the transmission channel generating the DIC (Differential Interference Contrast) images of the cells. For the transmission channel, a 488 Laser was utilized with the laser intensity set at 25% using a smart gain of 350V and a smart offset of 0%.

The statistical analysis of data obtained for the signal intensities of CX-Rhodamine-labeled plasmid DNA was carried out using the Leica Application Suite^{TM} and Imaris® Image Processing Software.

2.2.5 Nuclease inhibitor experiments

Triammonium salt of Aurintricarboxylic acid or ATA was dissolved in Milli-Q water (Millipore Corporation) and filtered with a 0.2 µM syringe filter (Minisart^R Sartorius). It was used at a final concentration of 100nM to treat *LIG4* and *DNAPKcs* mutant as well as wild type cells.

2.2.6 Plasmid preparation

Supercoiled plasmids were prepared using CsCl/EtBr gradients or a Qiagen Midi Plasmid purification kit. For CsCl/EtBr gradients, a 1 liter culture of plasmid-transformed E.coli was grown overnight and collected by centrifugation for 30 minutes at 1300g, 4°C. The pellet was resuspended in 10 ml Sucrose/Tris/EDTA solution and 2 ml of freshly prepared lysozyme was added and gently mixed. Cells were incubated for 30 minutes at room temperature and then 4 ml Triton lysis mix was added and culture was incubated at 37°C. Subsequently, lysates were centrifuged for 1 hour at 25,000 rpm (48,400g) in a Beckman JA25.50 rotor. Supernatant was removed and volume determined to add 0.95 g cesium chloride per ml while making sure that it was completely dissolved. Then 0.1 ml of 10 mg/ml EtBr solution was added per ml supernatant. Mixture was centrifuged for 20 min in a Beckman JA 25.50 rotor at 7.000 rpm to remove protein and debris. Then it was transferred to an ultracentrifuge tube (Beckman: 4.2 ml, 6.3 ml or 8 ml) and centrifuged for 16 hours at 20°C in an ultracentrifuge (Beckman Optima Max) in a near vertical rotor MLN80 at 70,000 rpm (240,000g). Subsequently, the lower band was removed that contained the supercoiled plasmid and was transferred to another 4.2 ml ultracentrifuge tube. CsCl/TE solution containing 0.2 mg/ml EtBr was added to fill the tube, which was centrifuged again as described above. The lower band was removed and extracted with 1:1 phenol/chloroform twice and precipitated with ethanol overnight at –20°C. Pellet was extracted once more with phenol/chloroform and precipitated with ethanol. The resulting pellet was dissolved in TE buffer and followed by dialysis and concentration determination.

2.2.7 Methodology to determine percent rejoining in the plasmid rejoining assay

GFP-Pem1-Ad2 was prepared with the above mentioned protocol and linearized by digestion with Hind III and purified by gel electrophoresis. Plasmid rejoining was tested in *LIG4*$^{-/-}$/*p53*$^{-/-}$mouse embryo fibroblasts. The appropriate plasmids were transfected in these cells using the Lonza Nucleofector and kit-MEF1 according to the instructions of the manufacturer. Transfection and analysis conditions were optimized using GFP-Pem1 or pDsRed2-N1, alone or in combination. Typically 2x10^6 cells, in suspension, were transfected by electroporation with 0.2 µg GFP-Pem1, or Hind III linearized GFP-Pem1-Ad2 substrate, together with 0.2 µg of the transfection-efficiency marker pDsRed2-N1. Green (EGFP) and Red (DsRed) fluorescence were measured by flow cytometry 24 or 48h later. For this purpose, cells were trypsinized and resuspended in fresh growth medium at 10^6 per ml. Analysis was carried out in a Beckman Coulter Epics XL-MCL flow cytometer equipped with an argon ion laser emitting at 488 nm. Red fluorescence was collected at 540 nm and 740 V PMT gains, while green fluorescence at 490 nm and 490V PMT gain. Electronic compensation was 12.8% of green signal for red and 6.7% of red signal for green. For calibration purposes and as standard to calculate rejoining efficiency, we used supercoiled GFP-Pem1 plasmid. Percent rejoining was calculated by dividing the signal generated from a given amount of linearized GFP-Pem1-AD2 by the signal generated from the same amount of supercoiled GFP-Pem1. Equal signal is defined as 100% rejoining as it will require circularization of all transfected linear GFP-Pem1-AD2; half signal is then equivalent to 50% rejoining etc. In order to include the transfection efficiency in the calculation of percent rejoining the EGFP+/dsRed+ ratio was calculated first and then compared between the linear and the circular plasmid, as indicated above. There was an approximately linear increase in the EGFP signal with increasing amount of DNA in the range of concentrations employed. Results shown here have been confirmed in three or more independent experiments.

2.2.8 Tissue culture

Tissue culture was performed in Sanyo MCO-18 O_2/CO_2 incubator at 37°C with 5% CO_2 (Sanyo). A549 cells were maintained in McCoy's 5A medium (M4892, Sigma-Aldrich) supplemented with 10% fetal bovine serum (FBS) (S0615, Biochrom AG).

Cells were grown in 100 ml tissue culture dishes (664160, CELLSTAR) with 15ml growth media. Exponentially growing cells were passaged every 3 days while avoiding confluency levels above 80%. For passage, medium was removed and cells were rinsed with ice-cold PBS. Cells were rinsed with 5 ml Trypsin-EDTA solution and incubated for 5 min at 37°C. Detached cells were resuspended in 10 ml cold media supplemented with 10% FBS. Single cell suspensions were obtained by passing cells through the Pasteur pipette. Cells were counted and appropriate numbers of cells were further incubated for experiments or for subculture. When frozen cells were taken to subculture, they were passed at least 2 times before being used in experiments. Cells were discarded after about 50 passages, since their genomic stability could not be guaranteed.

2.2.8.1 Drug treatments

Caffeine (C8960 Sigma-Aldrich) was dissolved in Milli-Q water (Z00QSV001, Millipore, 18.2 MΩ·cm at 25°C) to prepare a 200mM stock solution. The solution was sterilized by passing through a 0.22μm filter and stored in RT. 4mM caffeine was used as the working concentration.

2.2.8.2 Cell synchronization

Cell populations enriched in G1 or G2 cells were obtained by centrifugal elutriation. Briefly, 1 million cells were seeded in 15 ml growth media supplemented with 10% FBS in 100 mm dishes. At least, 40 dishes were prepared for each elutriation. After 48 h, cells were washed, trypsinized, suspended in the fresh growth medium supplemented with 10% FBS and counted. About 140 million exponentially growing cells could be collected for elutriation. Cells were loaded into an elutriation rotor (Avanti J-20 XP, BECKMAN COULTER). Fractions were collected by gradually reducing the rotor speed. Cell cycle analysis was carried out by flow cytometry.

2.2.8.3 Ionizing radiation (IR)

Cells were exposed to 320 kV X-rays with a 1.65 Al filter (GE-Healthcare). The dose rate was about 2 Gy/min. An even radiation was ensured by rotating the radiation table. Cells were returned to the incubator immediately after IR.

2.2.8.4 Clonogenic survival assay after IR-induced DSBs

For the clonogenic survival assay, wild type A549 cells along with clones bearing pairs of I-*Sce*I sites were irradiated with 4, 8 and 12 Gy of X-rays, trypsinized immediately and plated in multiples with variable cell numbers according to the dose of radiation delivered. The cells were allowed to grow for 14 days and then stained for counting colonies.

2.2.8.5 Clonogenic survival assay after I-*Sce*I-induced DSBs

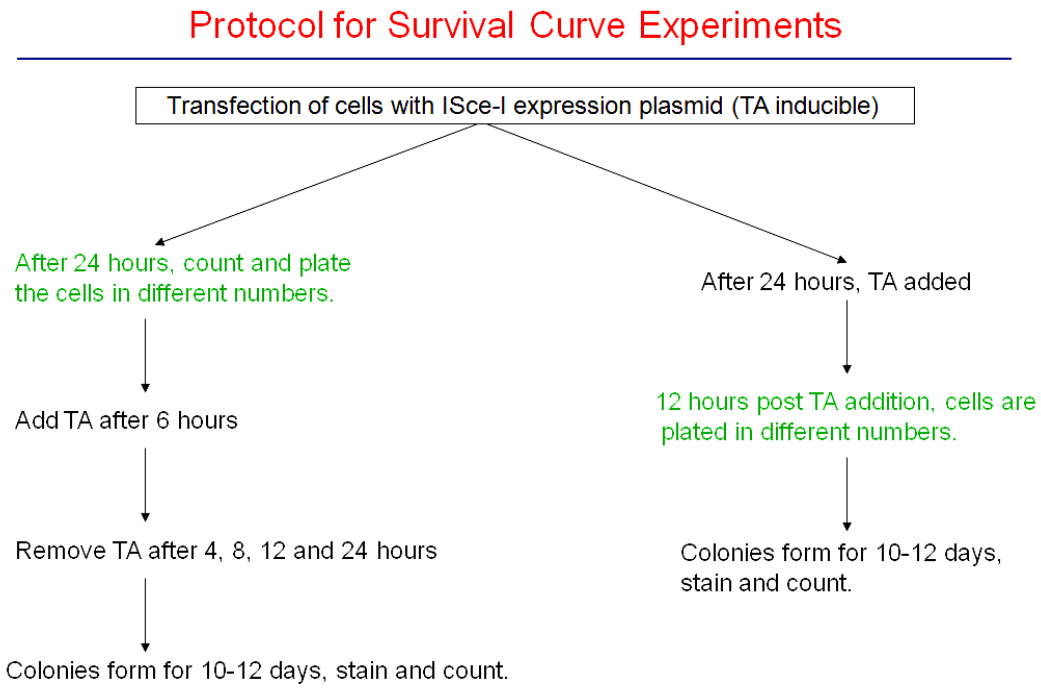

Fig. 10: Flowchart of the two protocols used for survival assay.

A similar protocol was employed for colony formation assay with pCMV-I-*Sce*I-3xNLS construct, where 2 Mio. cells were transfected with 2µg of the construct utilizing nucleofection. 24 hours post transfection, the cells were trypsinized and plated in duplicates of 100 and 200 cells. The cells were then allowed to form colonies for the

next 10-12 days, after which they were stained with crystal violet stain and counted (see Figure 10).

2.2.9 Flow cytometry

2.2.9.1 Cell cycle analysis by flow cytometry

Propidium iodide binds to DNA proportional to its mass. Cell cycle distribution was assessed by measuring Propidium iodide (PI) fluorescence on a flow cytometer. Cells were washed with cold PBS and trypsinized at 37°C for 5 min. Single cell suspensions were prepared in 5ml cold fresh media. About 1 million cells were collected and centrifuged at 1500 RPM, 4°C for 5 min. The cell pellets were washed with cold PBS and fixed in 70% ethanol at -20°C overnight. Supernatant was removed by centrifugation at 1500 RPM for 5 min. Pellets were washed with cold PBS and incubated in PBS containing PI (40 µg/ml) (81845, Sigma-Aldrich) and RNase (62 µg/ml) (R4875, Sigma-Aldrich) at 37°C for 30 min in dark. Samples were measured on Epics XL MCL flow cytometer (Beckman Coulter) according to pre-established protocols. 20,000 cells per sample were counted and the single cell population was gated to obtain standard histograms. Histogram files (*.HST) were generated by counting the frequency of the cell with same PI signal intensity.

The fractions of cells in the different phases of the cell cycle were calculated using the Wincycle® software. HST files were loaded into the Wincycle®. The parameter “S-phase growing order” was carefully chosen between 0, 1 or 2, until the prediction model fitted the histogram shape. Cell cycle distributions were automatically calculated. G2 arrest kinetics was obtained by plotting the G2 fraction as a function of time after IR.

2.2.9.2 Bivariate flow cytometry

Bivariate flow cytometry was used to simultaneously measure DNA content and the levels of proteins of interest, e.g. phosphorylation of Histone 3 at serine 10 (H3-pS10). Briefly, 0.6-0.8 million cells were prepared as single cell suspension in cold fresh media. After centrifugation at 1500 RPM, the cell pellets were washed with cold PBS and fixed in 70% ethanol at -20°C overnight. Supernatants were removed by centrifugation at 1500 RPM for 5 min. Cells were further permeabilized in 2ml permeabilization solution (PBS + 0.25% Triton X-100) on ice for 15 min. Supernatants were removed by

centrifugation at 1500 RPM and the pellets were washed with cold PBS. Cells were blocked in blocking buffer (PBS + 0.05% Tween-20 + 1% BSA (8076.2, Roth)) at RT for 45 min in the dark with gentle agitation. Primary antibody H3-pS10 (06-570, upstate) was diluted 1:150 in blocking buffer. After centrifugation at 1500 RPM for 5 min, the pellets were suspended in 100 µl diluted primary antibody and incubated for 2 h at RT in the dark with gentle agitation. The primary antibody was diluted in 5ml PBS and the cells were washed 3 times with PBS. Secondary antibodies, such as Mouse IgG-FITC (F0257, Sigma), Rabbit IgG-FITC (AP307F, Chemicon), were diluted in blocking buffer (1:200). Cell pellets were incubated with 100 µl conjugated secondary antibody for 90 min at RT in the dark. Secondary antibodies were removed by diluting in 5ml PBS and washing with PBS for three times. Cells were then incubated with PI plus RNase at 37°C for 30 min in the dark before measuring on a flow cytometer. Totally 20,000 cells were measured. Proper gating was applied to detect H3-pS10 positive cells and to calculate their fraction in the total population. Compensation was applied when necessary (for details, see Appendix 1 and 2).

2.2.10 Electrophoresis and Immunoblotting

2.2.10.1 Cell extracts preparation and protein concentration determination

Cells were collected by trypsinization and washed once with cold PBS and then washed once with hypotonic buffer. Pellet was resuspended in three packed cell volume of hypotonic buffer (see Appendix 4). The cells are lysed by three times freezing at -80ºC or liquid Nitrogen and thawing at 37ºC. Subsequently, the concentration of KCl was adjusted to 500mM. Incubate the mixture at 4ºC for 30 min on a rotating platform. Centrifuge mixture at 14,000 rpm at 4ºC for 40 min, remove supernatant and dialyze. After dialysis, centrifuge at 13.000 rpm for 20 min. The supernatant is WCE.

2.2.10.2 Electrophoresis

20 µg whole cell extract was mixed with 2x SDS-PAGE loading buffer. Samples were denatured at 95°C for 5 min and cooled down on ice for 5 min. They were centrifuged at 3000 RPM for 15 sec before loading. SDS-PAGE mini gels were cast (165-8000, Bio-Rad) according to the instructions of the manufacturer. Proteins were resolved in gels with different concentrations according to their sizes; for example 15% gel for proteins

smaller than 50 kDa, 12% for proteins between 50-100 kDa, 10% for proteins between 100-200 kDa, and 8% for proteins larger than 200 kDa. Samples were loaded and run at constant voltage (150 V) for 1.5 h at RT.

2.2.10.3 Immunoblotting/Western Blotting

After the electrophoresis, the gels were removed from the cassette and briefly rinsed with MQ water. PVDF membranes (RPN303F, GE Healthcare) and the blotting paper (GB004 Whatman) were cut to the desired size. PVDF membranes were pre-soaked in 100% methanol for 1 min and rinsed in MQ water for 15 min. PVDF membranes, blotting paper and the transfer unit sponge were equilibrated in 1x transfer buffer (Glycine 200mM (3908.2, Roth), Tris-HCl 25mM (4855.2 Roth), 10% Methanol (32205, Sigma-Aldrich)) at 4°C for at least 30 min. The Gel, blotting papers, sponge and PVDF membrane were assembled and loaded into an electro-transfer unit (170-3930, Bio-Rad) according to the instructions of the manufacturer. Wet electro-transfers were run at 100 V, 0°C for 1 h.

After completion of the transfer, the unit was disassembled and the side of the membrane on which proteins were transferred was marked. PVDF membranes were briefly rinsed with PBST (PBS + 0.05% Tween-20) and blocked in blocking buffer (PBS + 0.05% Tween-20 + 5% milk (T145.2, Roth) at RT for 1h with gentle agitation. Primary antibodies, for instance GFP for I-*Sce*I (Abcam) 1:100, GAPDH (Mab374, CHEMICON), 1:20,000. Membranes were incubated with primary antibodies at 4°C overnight with gentle agitation. The secondary antibodies, such as mouse IgG-HRP (7076, Cell Signaling), rabbit IgG-HRP (7074, Cell Signaling) were diluted 1:2000 in blocking buffer. After removing primary antibodies and washing with PBST (3 x 10 min), membranes were incubated with secondary antibodies at RT for 1 h. After washing with PBST (3 x 10 min), the membranes were ready for development. The ECL developing solution (RPN2132, GE Healthcare) was prepared according to the instructions of the manufacturer and evenly distributed on the side of the membrane on which the proteins were transferred. After 1 min incubation at RT in the dark, images were obtained using the molecular imager VersaDoc MP 4000 System (170-8640, Bio-Rad).

2.2.11 Immunofluorescence and data analysis

2.2.11.1 Confocal microscopy

Sterilized cover slips (2 mm x 2 mm, 8404, Invitrogen) were incubated in 1 mg/ml poly-L-lysine (L7240, Biochrom) solution for 1 h. Solution was removed and cover slips were stored at 4°C in the dark. Cells were plated with 2 ml growth medium in a 35 mm dish with poly-L-lysine coated cover slips. At each time point, growth media were removed, cells were washed in cold PBS 3 times and fixed in 2% Paraformaldehyde (PFA, 76240, Fluka) for 15 min at RT. PFA was removed and cells were washed 3 times with PBS. Cells were permeabilized in P-solution (100mM Tris pH7.4, 50mM EDTA, 0.5% Triton X-100) for 10 min at RT. After washing 3 times with PBS, cells were blocked in the PBG solution (0.2% Gelatin, 0.5% BSA in PBS) at 4°C overnight.

Primary antibodies, such as γ–H2AX were diluted 1:300 in PBG. 100 µl diluted primary antibodies were dispensed on parafilm (52858-032-CS, The Lab Depot, Inc.). The cover slips were mounted on top of the solution containing the primary antibodies. After incubating at RT for 2 h in the dark, slides were returned to the dishes and washed with PBST (PBS + 0.05% Tween 20) at RT 3 x 10 min. Conjugated secondary antibodies, such as Alexa488 mouse IgG (A11001, Invitrogen), Alexa568 mouse IgG (A11004, Invitrogen) were diluted in PBG 1:400. Slides were incubated with 100µl secondary antibody solution at RT for 1h in the dark. After 3 washes with PBST, cells were counterstained with 100ng/ml DAPI (Invitrogen) at RT for 5 min. The cover slips were washed 3 times with PBS and mounted on slides with 15µl ProLong Antifade Mounting Media (P-7481, Invitrogen). The slides were kept in the dark at RT and allowed to solidify for 48 h before analysis.

Scanning of the slides was carried out on a Leica TCS SP5 confocal microscope. For each slide, at least 5 fields were scanned (about 150 nuclei). Resolution was set at 1024 x 1024 and the zoom factor at 1.2. Bidirectional scans were applied to avoid bleaching of the fluorophore. Due to the differences in foci formation patterns, different proteins required different scanning parameters, such as laser intensity, PMT voltage, Smart Gain offset, filter spectrum range, etc. LIF files were generated after each scan, which were used for foci quantification using the Imaris® software (see below). TIFF Images shown in the text were obtained from the maximum intensity projection of the field scanned.

2.2.11.2 Foci scoring

Foci numbers were enumerated using Imaris® (Imaris 6.0; Bitplane). At least 150 target nuclei were scored. The LIF files were loaded onto Imaris using default settings. “Bright dots” with a size larger than 0.5 µm and intensity above the threshold value (between 17–21) were confirmed as foci. Foci were grouped in each nucleus, and the number of foci per nucleus was obtained. In some cases, the mean number of foci per nucleus was calculated from data obtained by analyzing many nuclei (for details, see Appendix 3). For data analysis, Microsoft Excel 2003® was used.

2.2.12 Live cell imaging

Live-cell imaging technique provides critical insights into the fundamental nature of cellular and tissue functions. Studies of cellular dynamics and cell physiology require live observation over time. For successful live cell imaging, the environment provided to the cells under the microscope is of utmost importance. The cells are also required to be plated in dishes or cell chambers with coverslip bottoms. The requirement for maintaining the cells at 5% CO_2 during the span of investigation could be avoided by using HEPES buffered medium (L-15 Leibovitz medium) which does not require a controlled atmosphere, but suitability of the medium for the cells should be determined before. Cellular function is also exquisitely sensitive to temperature, hence objective and stage warmers are used. Heating of both the dish and the objective prevents temperature gradients across the dish. In live cell imaging experiments, instability of Z-positioning happens over time. This focus drift is nearly always due to thermal expansion that occurs due to a temperature gradient. That is why both a stage warmer and an objective heater are used when z-stability is required for an experiment. Figure 11 represents a schematic illustration of basic live cell imaging equipment.

Fig. 11: Representation of a typical setup of a live cell imaging experiment. Image courtesy: Nikon microscopy.

For the experiment, the construct expressing EGFP-53BP1 was transfected using Nucleofector technology and the cells were directly plated in 3-well culture chambers. The cells were maintained in L-15 Leibovitz medium and 24 hours post transfection, pCMV-I-*Sce*I-3xNLS was transfected using Lipofectamine 2000 reagent to the cells (to prevent cell lethality owing to trypsinization and electroporation for two consecutive days). For measurement of foci kinetics, a 63x Leica oil immersion objective was used with a numerical aperture of 1.3 and a zoom factor of 1.2. For measuring EGFP, 488 nm Argon laser was utilized with photomultiplier tube (PMT) setting in the range of 495-600 nm. For DAPI channel, a 405 nm Laser diode was utilized with a PMT setting of 410-550 nm range. Up to 5 field per well were tracked for the next 24 hours at an interval of 20 min and the fields were selected to accommodate a number of green cells per view. Controls included 1 Gy X-ray irradiated samples, cells transfected with only EGFP-53BP1 construct and untreated cells.

2.2.13 Cytogenetic assays

The experiments are designed in such a way that DSB induction and repair are studied through their transformation to chromosome breaks that can be visualized by cytogenetic approaches in the G2 and M-phases of the cell cycle. The assay allows measurement in specific phases of the cell cycle and at very low radiation doses, which is not easily possible with other techniques of DSB repair such as PFGE, the comet assay etc.

2.2.13.1 Assay to study the kinetics of G2-chromosome breaks at metaphase

Exponentially growing cell cultures were either irradiated with 1Gy X-rays or transfected with I-*Sce*I expression construct. Following irradiation and 24 hours post transfection, Colcemid was added for the duration of 4 hours. Cells were trypsinized, treated with hypotonic solution (75mM KCl) for 10 minutes at room temperature (RT) and fixed in Carnoy's fixative (3X). The fixed cells were dropped on clean glass slide and stained with 3% Giemsa stain prepared in Sorenson's buffer. For each experimental point about 50 metaphases were scored for chromatid damage from three independent experiments. Standard criteria were used for scoring. During scoring, chromatid breaks and gaps were considered, the latter only when longer than the chromatid width. The chromosome exchanges were counted as two chromatid breaks. Bright field microscopy (Olympus, Japan) was employed to facilitate scoring.

2.2.14 Premature chromosome condensation (PCCs)

To study the influence of G2 checkpoint on chromosome break repair kinetics, exponentially growing cell cultures were irradiated with 1 or 2Gy X-rays (positive control) or transfected with I-SceI expression construct. 24 hours post transfection and 1 to 4 hours post irradiation, 50nM Calyculin A was added for 45 minutes before harvesting the respective time point to induce PCCs. This time for Calyculin A treatment was considered in the repair time. Cells were harvested and prepared for cytogenetic analysis in a similar way as for the metaphases. About 50 G2-PCCs were scored for each experimental point from three independent experiments. During scoring excess PCC fragments were considered. The chromosome exchanges were counted as two

chromatid breaks. Bright field microscopy (Olympus, Japan) was employed to facilitate scoring.

2.2.14.1 G2-PCC of cells after treatment with β-AraA

To visualize the homing endonuclease-induced DSBs and to prevent their repair, cells were treated with the nucleotide analog β-AraA, which is known to inhibit DNA synthesis[136, 137]. 500µm β-AraA was administered to the transfected cells (24h post transfection) one hour prior to the addition of TA. Colcemid was added one hour after TA for two and a half hours. 30 min prior to collection, Calyculin A was added to the cells. The induction of chromosomal breaks by β-AraA is known, when it is added during DNA synthesis (S Phase) for a long period. We added β-AraA for a maximum of four hours so that the cells undergoing DNA synthesis while being treated with β-AraA are not scored in the G2-PCC. The following steps were as mentioned above. Untransfected cells treated with β-AraA served as a control.

The dishes prepared for irradiation were treated with β-AraA 1h prior to irradiation. Two hours post irradiation, Colcemid was added and finally Calyculin A was added for 30min before fixation (Fig. 12). The cells were then fixed in Fixative (3:1 Methanol: Acetic Acid). Metaphase spreads were prepared and stained in 10% Giemsa in 1x Sörensens buffer for 15min.

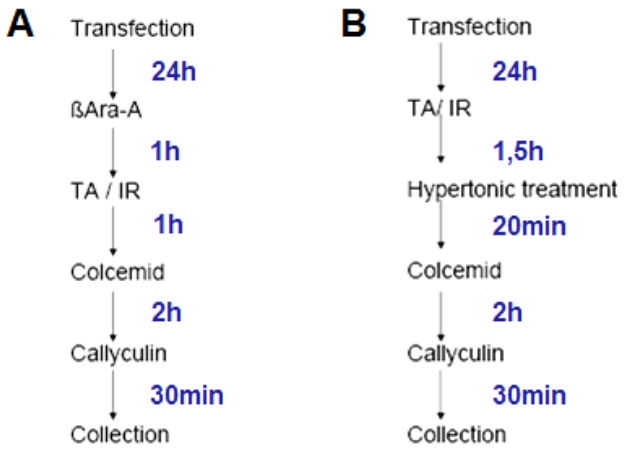

Fig. 12: Flowcharts of the protocols used to induce G2-PCC with ß-AraA and Hypertonic treatment. Protocol 1 shows cells treated with β -AraA before irradiation and transfection. Protocol 2 shows the steps used for hypertonic treatment of transfected and irradiated cells.

2.2.14.2 G2-PCC of cells after hypertonic solution treatment

pEGFP-I-*Sce*I-GR transfected cells (24h post transfection) along with X-ray irradiated controls were treated with hypertonic solution for 20min (500mM NaCl in PBS) 1.5 hours after addition of the drug TA or after irradiation. After 20 min, hypertonic solution was removed and colcemid was added for 2 hours. Calyculin A was added 30 min prior to collection of cells. The cells were then trypsinized, centrifuged, medium was removed and the pellet was dissolved in the remaining 1ml of Media. 10ml of hypotonic solution (75mM of KCl) was added for 10 min at room temperature and the cells were centrifuged. Finally the cells were fixed in Fixative (3:1 Methanol: Acetic Acid). Metaphase spreads were prepared and stained in 10% Giemsa in 1x Sörensens buffer for 15min.

2.2.15 Restriction of genomic DNA

For the digestion of genomic DNA, 15 µg of genomic DNA was used for each reaction. Per µg DNA, 0.3 Fast Digest Unit (FDU) of the enzyme were used. The following components were added to the reaction:

DNA	X µL (15 µg)
FD Restriction Enzyme	4.5 µL (4.5 x 1FDU)
FD Restriction Enzyme Buffer (10x)	20 µL
Water	200 µL

For complete digestion, the reaction mixture was incubated without the enzyme for 30 min at 4°C shaking in a Thermo mixer. After adding the enzyme the reaction was incubated for 5 hours at 37°C and shaken every 15 min for 15 min.

2.2.15.1 Ethanol precipitation of digested genomic DNA

Ethanol precipitation was carried out by adding 0.1 Vol. of 5M NaCl and 2.5 Vol. of 100% Ethanol to 200 µL of digested DNA. The mixture was incubated at - 80°C for one hour before centrifuging for 30 min at 1300rpm at 4°C. The supernatant was decanted

and 200 µL of 70% ethanol was added to the DNA pellet. After repeating the centrifugation step the supernatant was removed and the pellet was dried for 10 min at 37°C. The pellet was dissolved in 25 µL TE. To remove residual Ethanol, the cap of the micro centrifuge tubes were opened and incubated at 65°C for 10 min.

2.2.16 Agarose DNA Gel-electrophoresis

Agarose DNA Gel-electrophoresis was used to separate DNA Sequences according to their size. For running Gels with genomic DNA an 0.8% Agarose gel was prepared by adding 0.8 g Agarose to 100mL 1 x TAE Buffer and heating in the microwave. After complete melting of the Agarose, it was poured into a gel chamber of 10 x 7 cm and was left for polymerization. After completely covering the gel with TAE buffer the samples were loaded on the gel with 1/10 Vol. of Fermentas Loading Buffer (6 x). The gel was run at 0.5Volts/cm for 6 hours. The DNA was stained in 50ml 1 x TAE with 1% Ethidium bromide (EtBr) for 30 min while shaking.

2.2.17 Southern Blot

With the southern Blot Technique, described by Southern in 1975, it is possible to detect specific DNA sequences in the genome of cells. In the first step, 15 µg genomic DNA is digested with a specific restriction endonuclease and resolved by Agarose gel electrophoresis. Subsequently, the DNA is transferred onto a Nylon membrane through capillary transfer. After cross-linking the DNA with the membrane, specific sequences of the fixed DNA will be hybridized with a radioactive labeled probe.

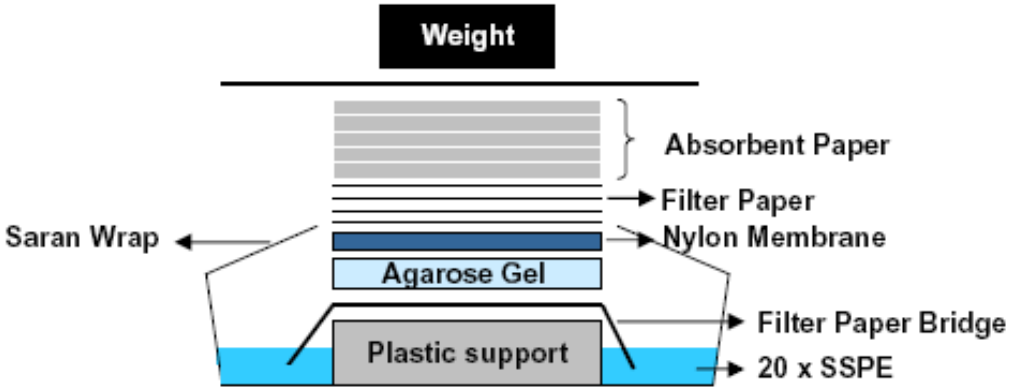

Fig. 13: Schematic illustration of the capillary transfer of Southern blot apparatus. The DNA from the Agarose gel is transferred to the Nylon membrane through capillary forces. A stream of 20xSSPE solution moves through the gel into the paper towels eluting the DNA from the gel and depositing it on the nylon membrane.

2.2.17.1 Blotting via capillary transfer

Depurination

After Gel electrophoresis, the gel was rinsed in distilled water and slowly shaken on a platform shaker in Depurination solution for seven minutes. The Depurination treatment with 0.2N HCl leads to strand cleavage which allows better transfer of large DNA fragments.

Denaturation

The gel was rinsed twice in distilled water and treated with denaturation solution twice for 15 min. Denaturation solution is required to unzip the DNA and produce single stranded DNA for further hybridization.

Neutralization

After rinsing twice in distilled water, the gel was shaken two times for 15 min in neutralization solution, which elevates the pH above nine to allow binding to the membrane.

Depurination Solution: 0.2NHCl

Denaturation Solution: 1.5M NaCl
0.5M NaOH

Neutralization Solution: 1M Tris (pH7.4)
1.5 M NaCl

2.2.17.2 Construction of the transfer apparatus

The construction of the capillary blot was carried out according to Fig. 13. A container was filled with 20xSSPE solution containing a plastic support. A long piece of Whatman paper wetted with 20xSSPE was placed on a piece of glass plate which was put over the plastic support. The gel was placed upside down on the Whatman paper. A wet Nylon membrane was placed on the gel. Between every step, bubbles were rolled out

using a glass pipette. Four pieces of plastic wrap were placed on the sides of the nylon membrane and stretched over the sides of the plastic container to avoid contact between the paper towels and the Whatman paper. Four pieces of Whatman paper wetted in 20xSSPE were one by one put over the nylon membrane taken care that bubbles between the papers are removed carefully by rolling. A stack of paper towels were placed on the top of the Whatman paper to provide capillary action. Finally, a glass plate was placed on the top of the paper towels with a 500g weight at the top.

The transfer was set for 18-20 hours. After the transfer, the membrane was marked with a pencil on the opposite side. The membrane was washed briefly in distilled water and equilibrated in 6xSSPE. To crosslink the DNA to the membrane, it was baked for 45min at 110°C.

20 x SSPE (pH7.4): 3M NaCl

0.2M $NaH_2PO_4H_2O$

0.02M EDTA

2.2.17.3 Preparation of the probe

For the preparation of the probe for hybridization, the pT2SVNeo plasmid was digested with HindIII RE following the protocol described above. Various fragments of the digested DNA were separated on a 1% Agarose-gel running at 2Volts/cm. The fragment of interest (1.7kb) was purified with the Qiagen gel purification kit according to the manufacturer's protocol.

2.2.17.4 Radioactively-labeled DNA probes

For preparing the radioactive labeled probe, the "Prime-It II Random Prime Labeling Kit" from Stratagene was used.

25ng template DNA with distilled water and 10µL of random oligonucleotide primers were prepared in a total volume of 34 µL in a 1.5 mL micro centrifuge tube. After 5 min incubation in a boiling water bath, the reaction tube was briefly centrifuged at RT. In the

next step, 10µL of dCTP Primer buffer, 5µL of [α-^{32}P] dCTP and 1 µL of Klenow enzyme (Exo-) was added to the reaction mixture and incubated at 37°C for 20min. Finally, the reaction was stopped by adding 2µL of stop mix.

Table 1: Reaction Mixture for radioactive probe labeling

Components	Volume
25 ng DNA template	x µL
Sterile double-distilled H_20	x µL
5X Random primers solution	10 µL
Total Volume	**34 µL**
5X dCTP buffer	10 µL
α- ^{32}P dCTP	5 µL
Exo (-) Klenow Enzyme	1 µL
Stop Mix	2 µL

2.2.17.5 Purification of radioactively-labeled probe

For the removal of unincorporated nucleotides from the DNA labeling reaction, the illustra^{TM} ProbeQuant G-50 Micro Columns (GE Healthcare) was used according to the manufacturer's protocol. The activity of the generated probe was then determined by Scintillation counting.

2.2.17.6 Prehybridization and hybridization of the nylon membrane

Prehybridization of the nylon membrane

The nylon membrane was prehybridized for 1h at 65°C in a roller bottle with prewarmed Prehybridization solution. Single stranded salmon sperm DNA 10mg/ml was added to the solution. To prepare single stranded DNA, 100µL of salmon sperm DNA was heated in a 1.5 mL micro centrifuge tube for 5 min in a boiling water bath and was cooled down on ice.

Hybridization of the membrane

The radioactive labeled probe, 22µL or 2 x 10^7 cpm was denatured for 5 min at 100°C together with 100µL of salmon sperm DNA and chilled on ice for two min before adding to the hybridization solution. The membrane was hybridized in a roller bottle overnight.

Washing the hybridized membrane

Four washing solutions were prepared ranging from high stringency (1) to low stringency (4). After Hybridization, the membrane was washed in solution 1 at RT for 5 min. The membrane was kept shaking in solution 2 at RT for 15 min. The Solution 3 was prewarmed at 65°C before adding to the beaker containing the membrane and incubated for at least 1 hour. The membrane was wrapped in a Saran wrap and measured in the interim till the Geiger-Müller counter showed counts of approx. 200Bq. In the last step the membrane was washed in Solution 4 for 5 min at RT.

Washing Solution I:	2 x SSPE
	0.5% SDS
Washing Solution II:	2 x SSPE
	0.1% SDS
Washing Solution III:	0.1 x SSPE
	0.1% SDS

Washing Solution IV: 0.1 x SSPE

2.2.18 PCR

The Polymerase chain reaction was used for the amplification of single DNA sequences to obtain DNA fragments for further cloning. The PCR reaction was set up in a total Volume of 20µL with concentrations of template DNA ranging from 1ng-10pg. Furthermore the reaction contained 100mM dNTP Mix, 1 x PCR-Buffer, 2.5U Taq- or Phusion^{R} Polymerase and dist. H_20. For primer sequences, refer Appendix, Table 2.

The amplification reactions were performed in a Thermo-Cycler with the following programs:

Program	Cycles	Temperature	Time
Denaturation	1	94°C	80 sec
		94°C	30 sec.
Annealing	32	51-62°C	30-50 sec.
Elongation		72°C	15sec-60sec.
	1	72°C	10 min.

2.2.19 Cloning

2.2.19.1 Ligation of PCR Products with the pGEM-T Easy vector

The PCR products eluted from the Agarose gel with the Qiagen gel extraction kit were ligated into the pGEM-T Easy Vector (Promega) in the ratio of 3:1. The Vector contains a 3` Deoxythymidine residue at the site of insertion. During PCR amplification, the Taq polymerase adds a Deoxyadenosine at the 3` end of the DNA.

Ligation reaction mixture: 2.5 µL 2 x rapid ligation Buffer

0.5 µL pGEM-T easy Vector

0.5 µL T4-DNA-Ligase

The reaction was made up to 10 µL after addition of the PCR product. The ligation was incubated at 22°C overnight.

2.2.19.2 Ligation of PCR products

The Ligation of PCR- products were carried out in a total volume of 20 µL. A 1:5 relation of Vector insert was used. The reaction mixture contained additionally 0.1 Vol. 10 x ligation buffer and 1U T4 Ligase. The reaction mixture was incubated at 22°C overnight.

2.2.19.3 Heat shock transformation

For the heat shock transformation, 100 µL competent E.coli cells were transformed with 10ng of plasmid DNA. The reaction was incubated for 40 min on ice. In the next step, heat shock was carried out at 42°C for 45 sec. in the Thermo Mixer and immediately incubated on ice for 2 min. 800 µL LB Media was added to the bacterial culture and incubated for 1.5 h at 37°C with the speed of rotation set at 220rpm. In the final step, 200 µL of the culture were plated on LB-Agar plates and incubated at 37°C overnight.

2.2.19.4 Preparation of competent E.coli cells

A 100 µL aliquot of frozen cells were inoculated in 200ml LB-Media on a shaker at 37°C until they reached an OD_{600} of 0.4. The culture was chilled on ice for 15min. Also the 0.1M $CaCl_2$ solution and 0.1M $CaCl_2$ plus 15% glycerol were chilled on ice. The cells were centrifuged at 3300g at 4°C for 10 min. The pellet was resuspended in 30 mL cold 0.1M $CaCl_2$ and incubated on ice for 30 min. After centrifuging the cells again, the pellet was dissolved in 6 ml 0.1 M $CaCl_2$ solution plus 15% glycerol. 500 µL aliquots were prepared and frozen at -80°C.

3 Results

3.1 Transfection approach versus repair pathway choice

3.1.1 Repair of DSBs in plasmids transfected by lipofection show only marginal defects in D-NHEJ mutants

IR induced DSBs are randomly generated in the genome, and neither their number nor their location are precisely known. Furthermore, in an irradiated cell population, each cell sustains DSBs at different locations of the genome, at different numbers, spread around a known mean.

Some of these limitations can be mitigated by analyzing repair of DSBs in plasmid DNA *in vitro*, after transfection into cells of different genetic background. The *in vitro* manipulation of the plasmid DNA allows the generation of DSBs with different but well-defined ends, usually generated by treatment with appropriate combinations of restriction endonucleases. The efficiency of repair is quantitated by end rejoining dependent restoration of a reporter gene, e.g. EGFP, and end processing after ligation analyzed in bacteria after plasmid rescue. These valuable properties give plasmid assays considerable popularity. Yet, the results generated appear highly variable suggesting that undefined parameters determine the outcome.

As a first step toward the characterization of these parameters, we analyzed rejoining of DNA ends using the plasmid shown in Figure 14A and described in detail under Material and Methods. Digestion of this plasmid with *Hind*III removes the Ad2 exon and generates the compatible DNA ends shown in the inset. Upon successful rejoining in the cell, EGFP expression was used to detect and quantitate the event.

Figure 14B shows the principle of the approach and the signal generated after transfection of CHO cells using lipofectamine with a circular version of the plasmid that lacks the Ad2 exon (see Materials and Methods). A robust signal is evident that indicates a transfection efficiency of nearly 50%.

An analysis of DSB repair efficiency is summarized in Figure 14D and E. Transfection using lipofectamine of the *DNA-PKcs* deficient mutant *XR-C1-3* and their wild type

counterpart *CHO9* shows efficient plasmid rejoining in both types of cells. The results summarized in Figure 14D and the relative inhibition plotted as a function of the amount of DNA transfected in Figure 14E show marginal effects at best with a trend for stronger effect with increasing amount of transfected DNA.

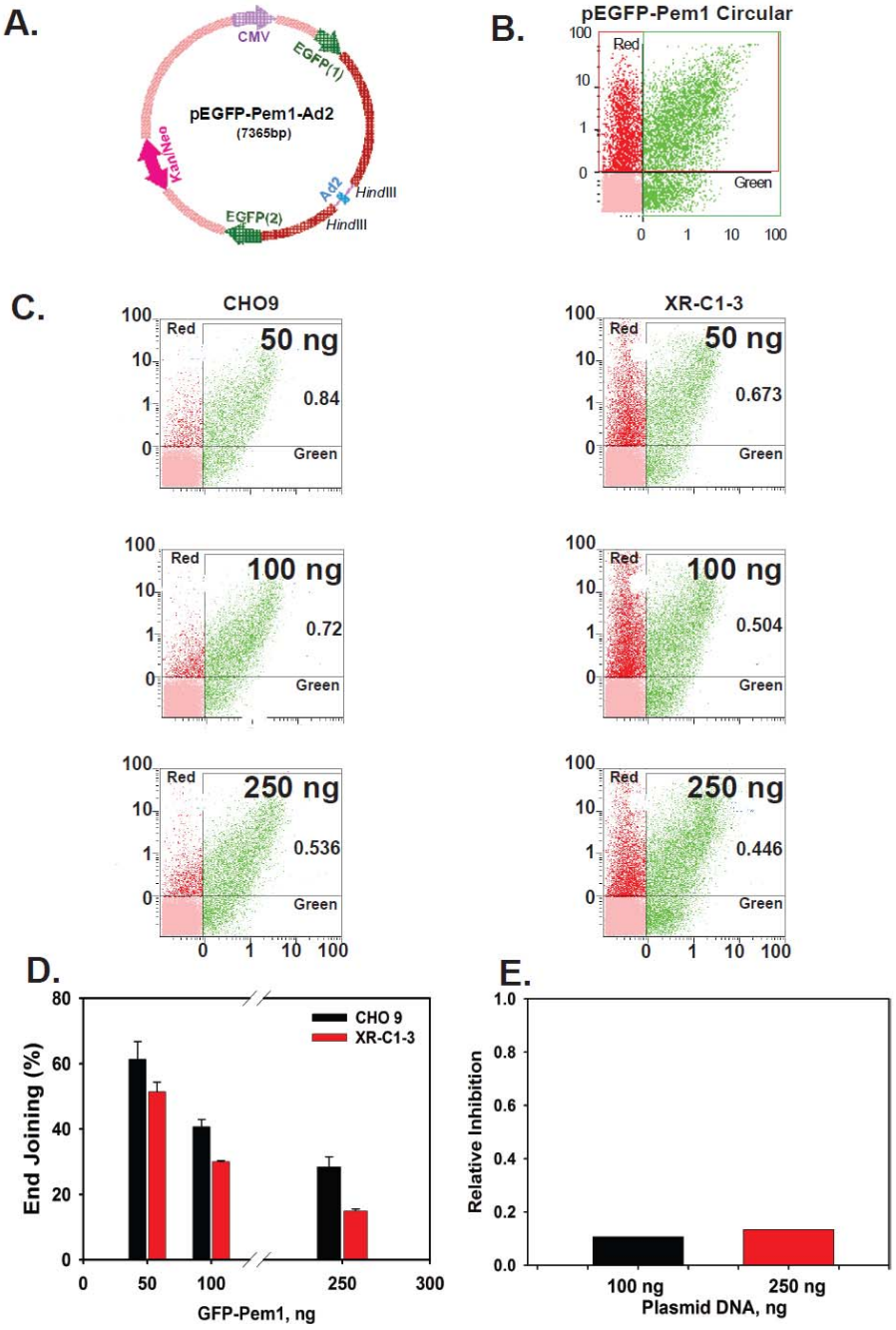

Fig. 14: A. Map of pEGFP-Pem1-Ad2 plasmid used. Digestion with either HindIII or I-*Sce*I removes the Ad2 exon and allows, upon successful intracellular plasmid circularization, EGFP expression, which is quantified by flow cytometry.

B. Flow cytometry histogram depicting EGFP expression from circular (pEGFP-Pem1) plasmid together with supercoiled DsRed (to monitor transfection efficiency) after nucleofection in wild type cells.

C. Flow cytometry histograms of EGFP and RFP expression 24 hours post transfection of HindIII-linearized pEGFP-Pem1-Ad2 plasmid at different DNA concentrations together with supercoiled DsRed (to monitor transfection efficiency) in *XR-C1-3* mutant and wild type *CHO9* cells by lipofection.

D. Determination of Percent Rejoin in *DNA-PKcs*-deficient *XR-C1-3* and wild-type *CHO9* cells in lipofection by *in vivo* plasmid assay. Two million cells (for nucleofection) and 70-80% confluent cells (60mm dishes for lipofection) were transfected with HindIII-linearized pEGFP-Pem1-Ad2 together with supercoiled DsRed (to monitor transfection efficiency). The ratio of GFP+ to Red+ cells was calculated (values inserted in the individual dot plots) and used to determine the percent rejoining efficiency of cells. Cells were transfected with various amounts of circular and linear pEGFP-Pem1 vector and transfection control pDsRed plasmid and the percentages of red and green cells were determined by FACS analysis 24 hours post transfection. The ratio of GFP+ to Red+ cells was plotted as a function of the amount of pEGFP-Pem1 vector and used as a measure of NHEJ efficiency. The above experiments were repeated at least 3 times.

NB: Higher signals are observed in FACS data from lipofection as compared to nucleofection although transfection efficiency is less. This is due to the fact that nearly double the number of cells were counted in lipofection (all the cells).

E. A bar plot depicting the relative inhibition of rejoining efficiency at different concentrations of HindIII-linearized pEGFP-Pem1-Ad2 plasmid after lipofection.

Figure 15 I A summarizes results similar to those described above but for MEFs with defect in *LIG4*. Here again a relatively small inhibition in end joining efficiency is observed in *LIG4*$^{-/-}$*p53*$^{-/-}$ cells that reaches significance only at high concentrations of transfected DNA. A slightly stronger effect has been observed when examining *Ku80* deficient cells in Figure 15 I C.

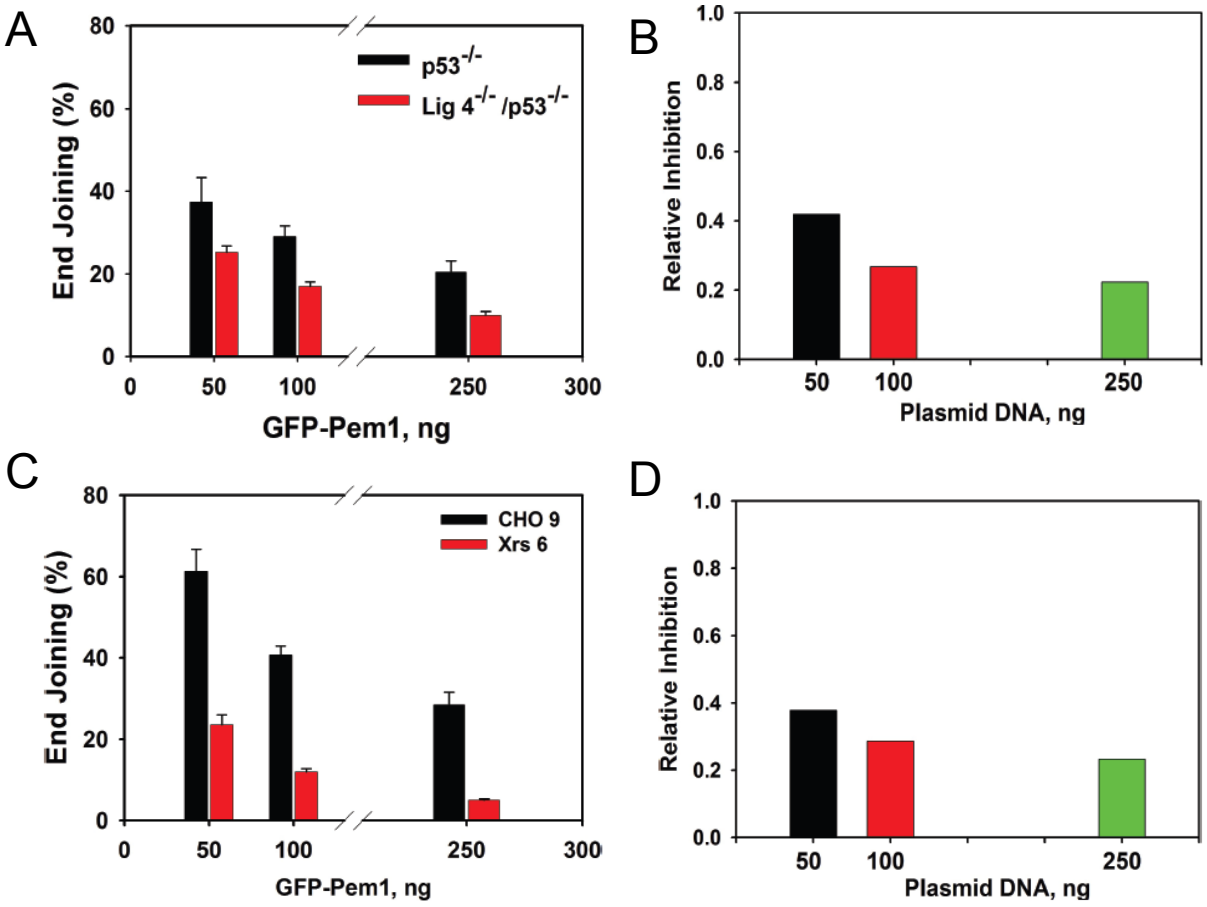

Fig. 15 I: A. Determination of percent rejoining in *Lig4*$^{-/-}$*p53*$^{-/-}$ mutant and *p53*$^{-/-}$ wild-type MEF cells after lipofection using an *in vivo* plasmid assay. Details of the experiment as explained above in Fig. 14D. The experiments were repeated at least 3 times.

B. A bar plot depicting the relative inhibition of rejoining efficiency at different concentrations of HindIII-linearized pEGFP-Pem1-Ad2 plasmid after lipofection.

C. Determination of percent rejoining in *Ku80*-deficient *xrs-6* and wild-type *CHO9* cells by in vivo plasmid assay. Details of the experiment as explained above in Fig. 14D. The experiments were repeated at least 3 times.

D. A bar plot depicting the relative inhibition of rejoining efficiency at different concentrations of HindIII-linearized pEGFP-Pem1-Ad2 plasmid after lipofection.

3.1.2 Repair of DSBs in plasmids transfected by nucleofection show dramatic defects in D-NHEJ mutants

The generally reduced end joining defects measured in D-NHEJ mutants when plasmid DNA is used might indicate different processing by the repair apparatus of extrachromosomal *versus* genomic DNA. It is for example possible that B-NHEJ operates on extrachromosomal substrates more efficiently than in genomic DNA, concealing thus D-NHEJ defects. To examine this possibility we carried out plasmid assay experiments using alternative transfection methods. We reasoned that if an alternative transfection method generates results similar to lipofection, it will support the hypothesis of enhanced function of B-NHEJ on extrachromosomal substrates. If, on the other hand, different results were obtained, it would suggest the contribution of as of yet uncharacterized parameters. There are reports in the literature pointing to the transfection method as a contributing parameter to end joining efficiency when using plasmid assays.

As an alternative transfection method, we chose nucleofection, a special application of electroporation that is characterized by very high transfection efficiency. Figure 15 II A summarizes the results obtained with *DNA-PKcs* deficient cells. Notably, when linear DNA is introduced into cell using this transfection method, a marked decrease in end joining efficiency is observed. When the normalized relative inhibition is plotted for the different amounts of DNA transfected a nearly 80% inhibition is observed. For a direct comparison with the results obtained after lipofection, the curve measured has been transferred from Figure 14E and is included in Figure 15 II B.

A similar trend is also observed in the results obtained with *LIG4*$^{-/-}$*p53*$^{-/-}$ cells that are summarized in Figure 15 II D. The trend is also confirmed in the results with *Ku80* deficient cells summarized in Figure 15 II F, although as expected with these cells the difference between lipofection and nucleofection is reduced.

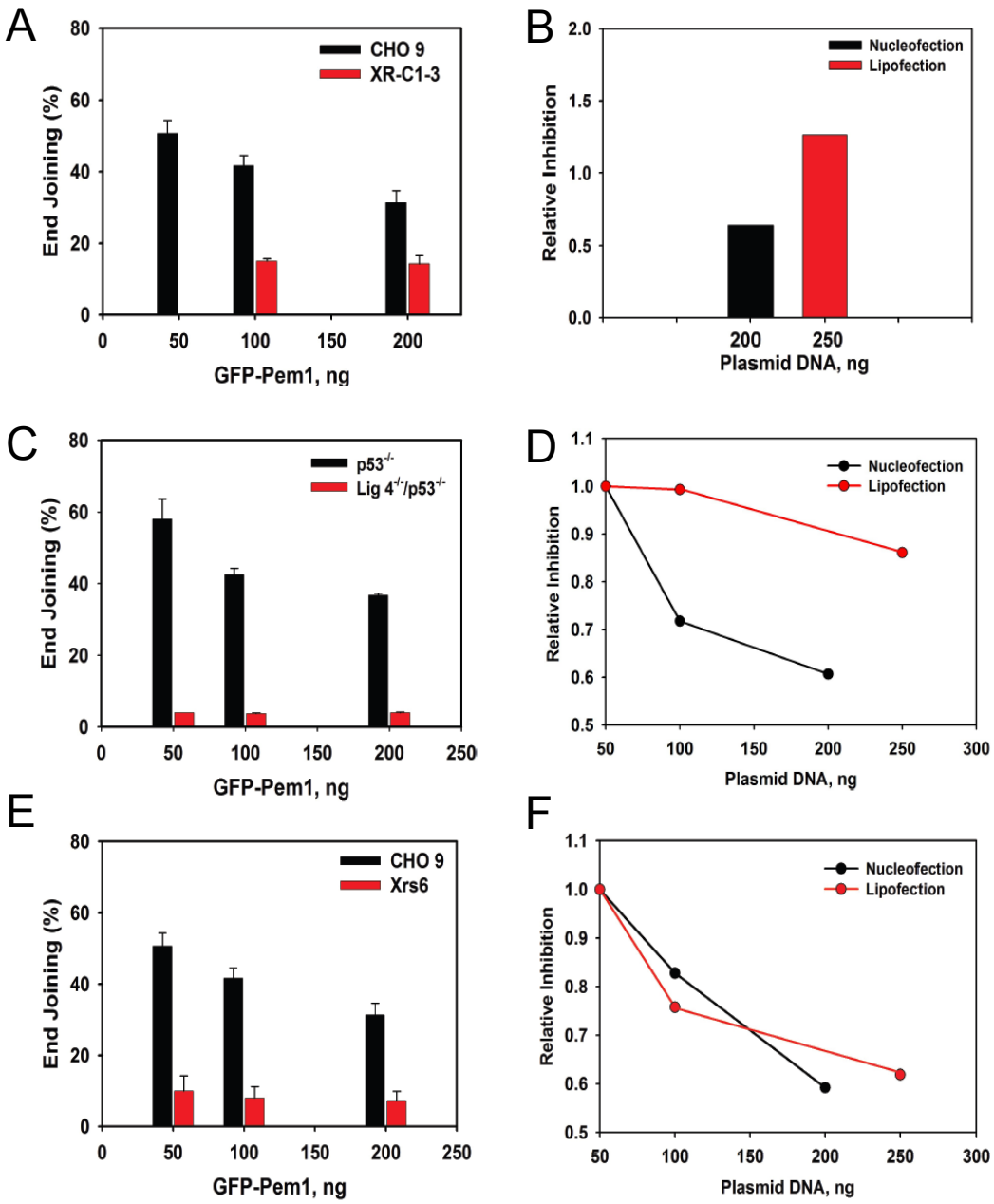

Fig. 15 II: A. Determination of percent rejoining in *DNA-PKcs*-deficient *XR-C1-3* and wild-type *CHO9* cells after nucleofection using an in vivo plasmid assay. Cells were transfected with various amounts of circular and linear pEGFP-Pem1 vector and transfection control pDsRed plasmid and the percentages of red and green cells were determined by FACS analysis 24 hours post transfection. The ratio of GFP+ to Red+ cells was plotted as a function of the amount of pEGFP-Pem1 vector. The ratio of GFP+ to Red+ was used as a measure of NHEJ efficiency. The percent rejoining graphs were generated as mentioned in Fig. 14D. The above experiments were repeated at least 3 times.

B. A bar plot depicting the relative inhibition of rejoining efficiency at different concentrations of HindIII-linearized pEGFP-Pem1-Ad2 plasmid in both nucleofection and lipofection.

C. Determination of percent rejoining in *Lig4*$^{-/-}$*/p53*$^{-/-}$ mutant and *p53*$^{-/-}$ wild-type MEFs after nucleofection using an in vivo plasmid assay. Details of the experiment as explained above in Fig. 14D. The experiments were repeated at least 3 times.

D. Plot depicting the relative inhibition of rejoining efficiency at different concentrations of HindIII-linearized pEGFP-Pem1-Ad2 plasmid in both nucleofection and lipofection.

E. Determination of Percent Rejoining in *Ku80*-deficient *xrs-6* and wild-type *CHO9* cells after nucleofection using an in vivo plasmid assay. Details of the experiment as explained above in Fig. 14D. The experiments were repeated at least 3 times.

F. Plot depicting the relative inhibition of rejoining efficiency at different concentrations of HindIII-linearized pEGFP-Pem1-Ad2 plasmid in both nucleofection and lipofection.

Percent rejoining was also calculated from the standard error line and scatter plots with 2-parameter curve fitting (as earlier) and was found to be 26%, 24% and 18.4% for *p53*$^{-/-}$ cells, 20%, 14% and 9.4% for *Lig4*$^{-/-}$*p53*$^{-/-}$ cells, 46%, 29%, and 15.2% for *DNA-PKcs* mutant *XR-C1-3* cells, 22%, 12%, and 4.8% for *Ku80* mutant *xrs-6* cells and 60%, 41% and 25.6% for wild type *CHO9* cells. For all above experiments, percent rejoining efficiency was also calculated from plots without any curve fitting where all points were joined to calculate the percent rejoining at each point denoting the concentration of DNA transfected. The rejoining percentages were very similar to the ones obtained above and did not significantly differ at any concentration of DNA transfected (data not shown). The requirement for *CHO9* cells as control for both *DNA-PKcs* mutant and *Ku80* mutant cells was further accentuated by the fact that *Ku80* complementation in *xrs-6/Ku80*$^{+}$ cells was not complete and the rejoining efficiency was not very comparable to wild type *CHO9* cells.

3.1.3 Non-specific inhibition of nucleases leaves end-joining characteristics unaffected

When plasmid DNA is transfected in cells and gene expression is allowed the levels of signal and their duration will also dependent upon the degradation characteristics of the

plasmid by the cellular apparatus. This degradation is thought to involve DNA nucleases. It is possible that the different results obtained above after nucleofection and Lipofection is due to different kinetics of degradation by the two methods.

To address this possibility, we inhibited nuclease activity during the initial stages of the transfection and measured the outcome of the repair reaction. A widely reported nuclease inhibitor ATA (100nM) was used to treat *Lig4* and *DNA-PKcs* mutants and wild type cells. The results summarized in Figure 16A and B show that no effect is observed in the outcome with nucleofection suggesting that nucleases do not modify the outcome. On the other hand, transfection was completely inhibited when the cells treated with ATA were used for lipofection and signals were barely detected by flow cytometry.

3.1.4 Difference in the intracellular distribution of transfected DNA between lipofection and nucleofection

An alternative possibility is that the intracellular distribution of plasmid DNA is different between the two methods of transfection and causes the observed differences in the results. To test this possibility, we carried out plasmid DNA labeling and tracking experiments to visualize intracellular plasmid localization after transfection. Two types of experiments were designed and carried out with 5µg of CX-Rhodamine-labeled circular pEGFP-Pem1 using either lipofection or nucleofection in repair proficient MEFs. Plasmid was localized by confocal microscopy 16, 20, and 24 hours after transfection. The total DNA-bound CX-Rhodamine signal in the nucleus and the entire cell was determined to calculate total cytoplasmic signal by subtracting the former from the latter. A more than 3 fold higher CX-Rhodamine signal intensities were observed in the nucleus of nucleofected cells as compared to lipofected ones. Controls included unlabeled DNA transfected with both lipofection and nucleofection, mock transfected cells without DNA and untransfected cells. Whole cell, nuclear and cytoplasmic signal intensities from individual cells were plotted as an average of the intensity values (Figure 17A).

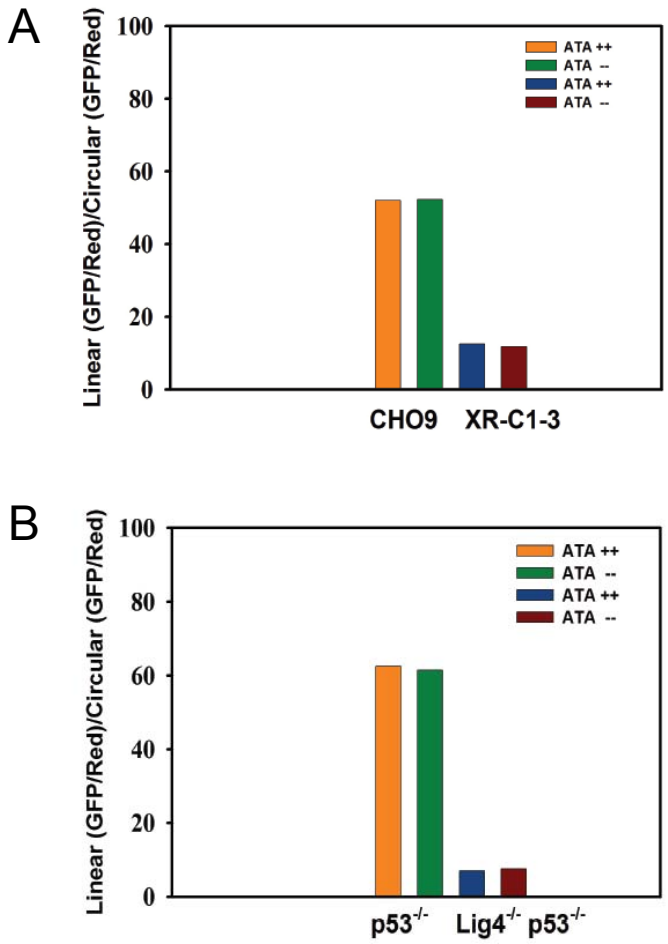

Fig. 16 A. Effect of the nuclease inhibitor Aurintricarboxylic acid (ATA) on DNA double strand break rejoining efficiency of *XR-C1-3* mutant and *CHO9* wild-type cells: 100nM ATA was used to treat cells before transfection. 200ng of circular and linear pEGFP-Pem1 plasmid was used for nucleofection for all the cells with pDsRed2-N1 plasmid used as transfection control. The ratio of EGFP+/Red+ was used as a measure of NHEJ efficiency. Percent rejoining was calculated as described in Fig. 14D. ATA completely inhibited transfection by lipofection.

B. Effect of nuclease inhibitor ATA on double strand break rejoining efficiency of *Lig4*$^{-/-}$*p53*$^{-/-}$ mutant and *p53*$^{-/-}$ wild-type cells. 100nM of ATA was used to treat the cells before transfection. 200ng of circular and linear pEGFP-Pem1 plasmid was used for nucleofection for all the cells with pDsRed plasmid as transfection control. The ratio of GFP+ to Red+ was used as a measure of NHEJ efficiency. The percent rejoin graph was generated as mentioned in Fig. 14D.

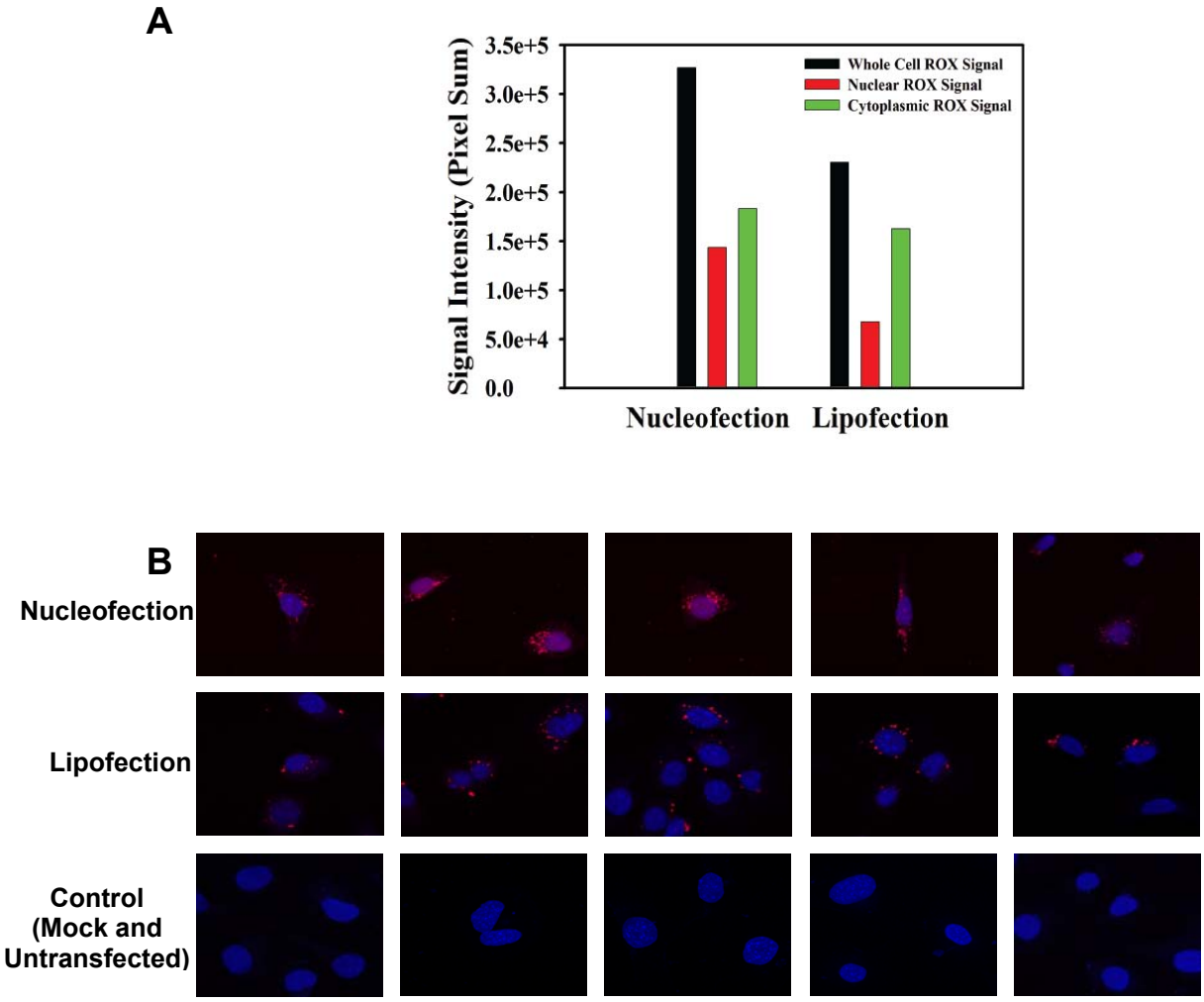

Fig. 17: A. Total CX-Rhodamine signal intensities from whole cell, nuclear and cytoplasmic fields: Average intensity from > 50 cells was measured for each transfection and nuclear, cytoplasmic, or total signal intensities calculated. CLSM color allocation: DAPI-stained nucleus (blue) and CX-Rhodamine-stained plasmid DNA (red).

B. Intracellular DNA Localization experiment: *p53*$^{-/-}$ MEF cells were nucleofected or lipofected with 5µg of CX-Rhodamine-labeled pEGFP-Pem1 plasmid and fixed 16, 20 and 24 hours later. Cells were stained with DAPI and visualized under a Leica TCS SP5 confocal microscope

3.2. Models of complex lesions using special arrangements of I-*Sce*I recognition sites

Part II of my thesis deals with the design and development of model systems to study the effects of complex DNA lesions based on Sleeping Beauty Transposon technology. In this part, we utilize the knowledge gained from experiments of Part I that nucleofection is a more effective technique for transfection as compared to Lipofection and thus we use nucleofection extensively to establish and authenticate our model systems.

The following results describe how we established the model system which models complex types of DSBs as described in the objectives of the project (1.7), and outline some of their biological consequences. Finally, the results obtained with the I-*Sce*I based system are compared to results obtained by low doses of ionizing radiation.

3.2.1 Synthesis of oligonucleotides bearing I-*Sce*I sites

Three different oligonucleotides containing I-*Sce*I sites were commercially procured from Cloning Biotech (for oligonucleotide sequences, please refer Appendix Table 2). The first oligonucleotide (NS) was designed bearing a single I-*Sce*I site, which will serve as a control to elucidate the effect of single DSBs on cells. The second (200C) and third (200I) oligonucleotides were synthesized consisting of two I-*Sce*I sites separated by 200 bp. This distance was chosen, since it is known that the length of DNA wrapped around a nucleosome is approximately 146 bp, and thus according to our hypothesis, the two DSBs induced would be in adjacent nucleosomes, with the possibility that simultaneous breaks at both sites may lead to loss of a nucleosome, leading to genomic instability and eventually cell death. 200C (C stands for compatible) contains both sites in direct, compatible orientation. To increase the degree of DSB complexity, the 200I (incompatible) oligonucleotide has the two I-*Sce*I sites in reverse orientation. This prevents the direct head-to-head rejoining of the DNA ends, as some sort of processing and polymerization will be required before rejoining. These oligonucleotides were shipped cloned in the pPCRScript vector at KpnI and SalI sites.

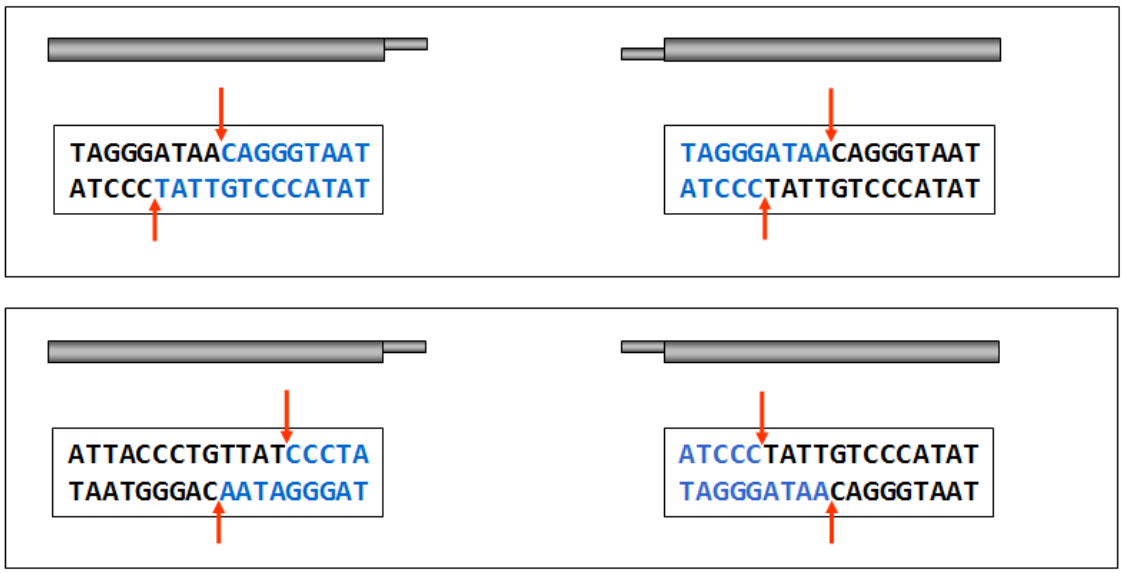

Fig. 18: Schematic illustration of I-*Sce*I in compatible and incompatible orientation
A: I-*Sce*I sites are located in compatible orientation. **B:** I-*Sce*I sites are located in incompatible orientation. The red arrows indicate the site of restriction. The blue bases will be cut out after restriction. The black bases will remain as "sticky" ends after restriction.

3.2.2 Cloning of the Transposon Donor plasmid

All three oligonucleotides were cloned into Transposon donor plasmids for multiple, random integration into human A549 cells using the SB system.

The multiple cloning site (MCS) of the Transposon donor plasmid pT2SVNeo along with the SV40 Promoter and the Neomycin resistance conferring gene (Fig. 19A) are located between the IR/DRs, the Transposase binding sites. The EcoRI site at the MCS was selected for non-directional cloning of the oligonucleotides. The oligonucleotides were excised from the pPCRScript vector by EcoRI restriction and cloned into pT2SVNeo plasmid. The cloning was confirmed by restriction with EcoRI and SacII (Fig. 19B). The plasmid containing the oligonucleotide NS was named as pT2SVNeoNS. Post cloning, the other two plasmids containing the two sites' oligonucleotides 200C and 200I were named pT2SVNeo200C and pT2SVNeo200I to indicate the compatible and incompatible nature of the ends.

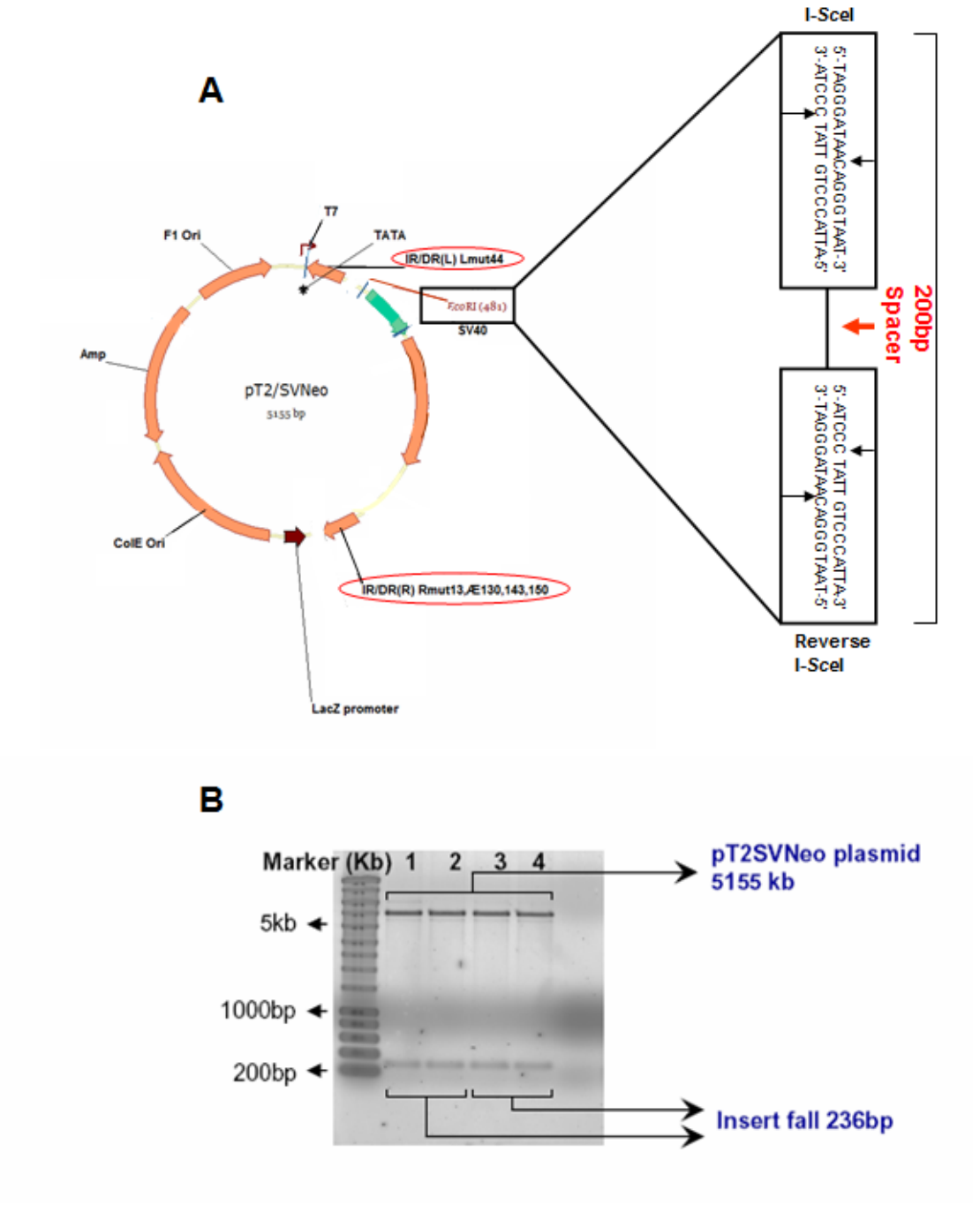

Fig. 19: pT2SVNeo plasmid with integration of oligonucleotide bearing I-*Sce*I sites in incompatible orientation. A. The red arrow indicates the 200bp spacer. The IR/DRs are marked with a red circle. The EcoRI site marked in black was used as the cloning site. On the right the I-*Sce*I Sequences are represented. The cutting sites are indicated by a black arrow. **B.** 0.8% Agarose-Gel illustrating the test restriction of the clones pT2SVNeo200C and pT2SVNeo200I. The lanes 1 and 2 show the 236bp insert fall of pT2SVNeo200I. The insert fall of pT2SVNeo200C is illustrated in the lanes 3 and 4.

3.2.3 Generation of A549 clones harboring different numbers of I-*Sce*I integration sites

3.2.3.1 Cell line used to establish clones bearing I-*Sce*I sites

A549 cells were selected (ATCC Number: CCL-185^{TM} human lung carcinoma cells of epithelial origin) for our experiments. This cell line has a positive p53 status; it is easy to grow and has a relatively stable karyotype. A549 cells are hypotriploid (chromosome numbers range from 64-67) and they are devoid of the limited life-span problems associated with primary fibroblasts.

3.2.3.2 Testing efficiency of the Sleeping Beauty Transposon system

Before applying the Transposon technology to integrate the oligonucleotides bearing I-*Sce*I sites into the genome of A549 cells, we checked the integration efficiency of the original Sleeping Beauty Transposon system in A549 cells using transposases of different activity kindly provided by Dr. Z. Ivics. The two SB expressing constructs, pCMV(CAT)SB100X and pCMV(CAT)SB80X, express transposases with 100 times and 80 times higher activity than the original transposase. The SB100X yielded the highest number of integrations and was therefore chosen for further experiments. On the average, 7-8 integrations were achieved with unmodified constructs, as estimated by Southern blotting.

3.2.3.3 SB-mediated integration of I-*Sce*I oligonucleotides in A549 cells

The above described plasmids were co-transfected into A549 cells with the transposase-expressing helper construct pCMV(CAT)SB100X at a ratio of 10:1 using nucleofection.

For transfection experiments cells in the exponential phase of growth, as well as elutriated G1 cells were used. Transfections with G1 cells were explored arguing that better conditions for plasmid integration may be reached in the subsequent S-phase, where chromatin is opened for replication.

After transfection, cells were plated at different dilutions, ranging from 100 to 5000 cells/dish for 14 days while selecting for integration using G418. 20 colonies from each of the three transfections (60 colonies in total) were picked and tightly selected with G418. These 20 clones were passaged, collected and frozen. In total a pool of 5 X 60 clones (300) of three different kinds of I-*Sce*I clones (clones with one I-*Sce*I site and 2 I-*Sce*I sites in compatible and incompatible orientation) were generated. In the next step, genomic DNA was extracted from a wide number of randomly selected clones from this pool and the number of integrations was determined by Southern Blotting.

3.2.3.4 Selection of stable transfectants with G418

To determine the concentration of G418 required for the selection of Neo^R positive clones, a kill curve of wild-type A549 cells was prepared using increasing drug concentration (G418 solution in 100mM Hepes, pH 7.3). 500µg/mL was determined as the required concentration for tight selection.

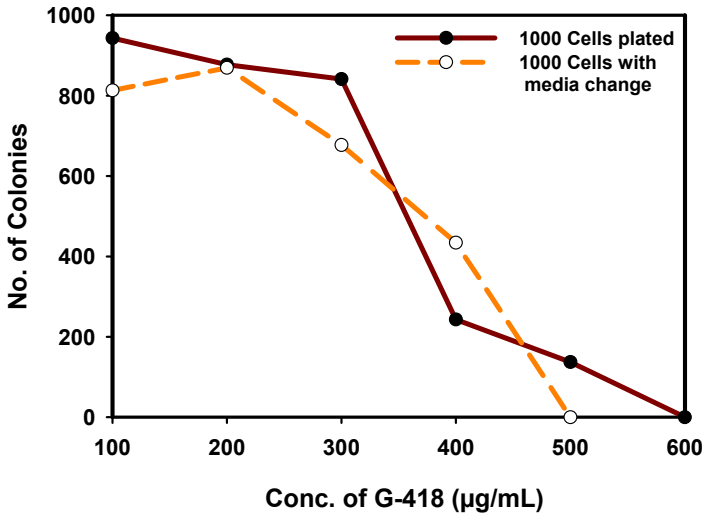

Fig. 20: Effect of G418 on A549 cells. A549 cells were treated with different concentrations of G418, with (orange line) and without (red line) medium change.

The experiment was performed both without and with medium change (fresh G-418 added every 2 days) so as to determine whether G-418 needs to be replenished to maintain its effectiveness. As no significant difference was observed, it was decided to proceed without medium change.

3.2.4 Southern blotting to estimate the number of integration sites

Southern blotting was performed to estimate the number of integration sites in the different clones.

A probe was generated which can be used for single I-*Sce*I site clones as well as for clones bearing two sites. For this purpose, the pT2SVNeo plasmid was digested with HindIII to digest the sites located between the two IR/DRs downstream of the EcoRI site, which was used to clone the I-*Sce*I constructs. The sequence has a size of 1.72kb, contains the Neo^R gene and a CMV promoter (Figure 21), which is complementary to a part of the integrated cassettes in the different clones. The eluted sequence was labeled with α-^{32}P radioisotope (α-^{32}P dCTP) utilizing standard protocols (2.11.4).

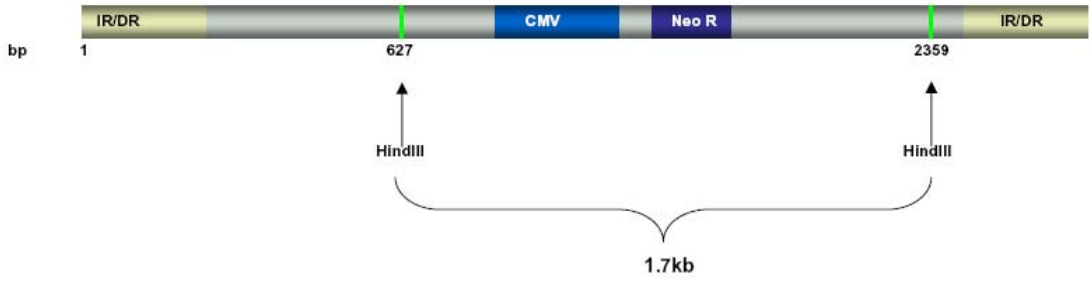

Fig. 21: Illustration of the DNA fragment between the IR/DRs of the pT2SVNeo plasmid utilized to generate the probe. Two HindIII restriction sites are located in the sequence. The first is located at position 627 (starting from Position 1 as the first bp in the IR/DR) and the second at position 2359.

In total, 24 clones bearing two I-*Sce*I sites and seven clones bearing a single I-*Sce*I site were checked for the number of integrations. The results obtained are shown below. In Fig. 22A and B, Southern blotting results are shown for clones with two I-*Sce*I sites in compatible (Fig. 22A lanes 1-4, Fig. 22B, lanes 4-7) and incompatible orientations (Fig. 22A lanes 5-9, Fig 22B lanes 1-3). The number of integrations ranges from 3 to 12. Fig. 22C shows the results of clones generated from transfected G1 cells (lanes 1-4 incompatible, lanes 5-8 compatible). Compared to the results obtained from exponentially growing cells, the number of integrations in G1 cells is not significantly increased. The clone in lane 3 shows the highest number of integrations. Southern Blot with clones bearing a single I-*Sce*I site (Fig. 22D) shows integrations ranging from 3 to 7.

All clones were named according to the number of integration sites. The following clones from sets of C (compatible) and I (incompatible) were selected for further experiments: 200SA549C4(8), 200SA549C9(18), 200SA549C11(22), 200SA549I8(16), 200SA549I3(6). 200SA549I6(12) 200SA549I12(24). In brackets, the number of I-*Sce*I sites are indicated, which is double in clones bearing integrations with two I-*Sce*I sites and the same in clones bearing a single I-*Sce*I site. 200S stands for the 200bp spacer and A549 for the parent wild type cell line without integrations.

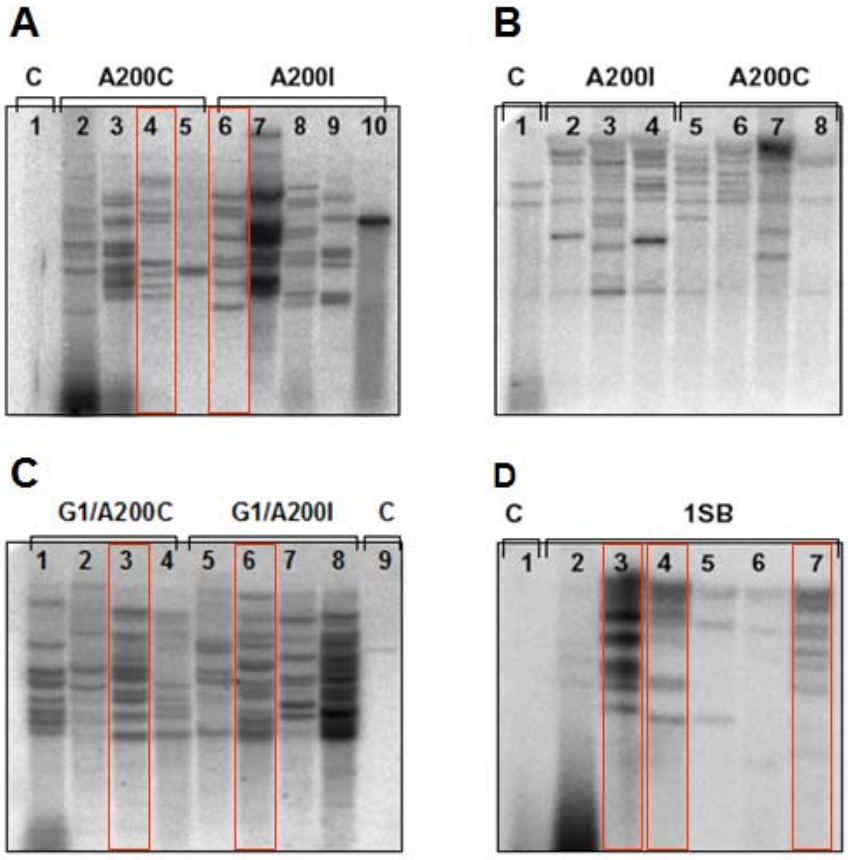

Fig. 22: A. Southern blot of neo^R resistant clones from different transfection. Southern blots show the number of integration sites estimated from the generated signal. **A.** Clones with integrations of two I-*Sce*I sites and control cells. **B.** As in A for different clones. **C**. Clones from transfected G1 cells with two I-*Sce*I sites. **D.** Clones with integrations bearing a single I-*Sce*I site. **NB**: C: A549 control, A200C: clones with compatible I-*Sce*I sites and 200bp spacer, A200I clones with incompatible I-*Sce*I sites. 1SB: clones with a single I-*Sce*I site. Clones used in Experiments are marked in red.

3.2.5 Clonogenic cell survival assay

The clonogenic assay or colony formation assay[138], measures the ability of a single cell to grow into a colony and is extensively used to measure the effect of cytotoxic agents. By convention, a colony must consist of at least 50 cells. A cell survival curve is therefore the relationship between the dose of the agent used to introduce damage and the fraction of cells retaining their ability to form colonies. Clonogenic cell survival assays were initially described for studying the effects of IR, but are now widely used to examine the effects of other agents like chemotherapeutic drugs and cytokines. In our case, we introduced this assay to estimate the effect of DSBs generated by the I-*Sce*I homing endonuclease at the sites of integration in the above described clones.

3.2.5.1 Radiosensitivity of clones with transposon integrations

As mentioned in the last section, a range of clones were selected for further experiments depending upon the number of integrations of single or double I-*Sce*I sites. Since the SB Transposase-mediated integrations are random, mutagenic events that affect cell radiosensitivity to killing cannot be ruled out. Therefore, we tested the radiosensitivity to killing of the following clones, two with compatible I-*Sce*I ends (9 and 11 integrations), and one with incompatible I-*Sce*I ends (12 integrations) along with untransfected A549 cells.

Cells were irradiated with 4, 8 and 12Gy of X-rays, trypsinized immediately and plated in a way aiming to the same number of colonies per dish, irrespective of the dose of radiation delivered. Colonies were allowed to form for 14 days, then stained and counted.

Figure 23 shows the survival curves obtained. As it can be deduced from the graph, equivalent cell killing was observed at all delivered doses for all cell lines tested irrespectively of whether they had been transfected with I-*Sce*I containing constructs.

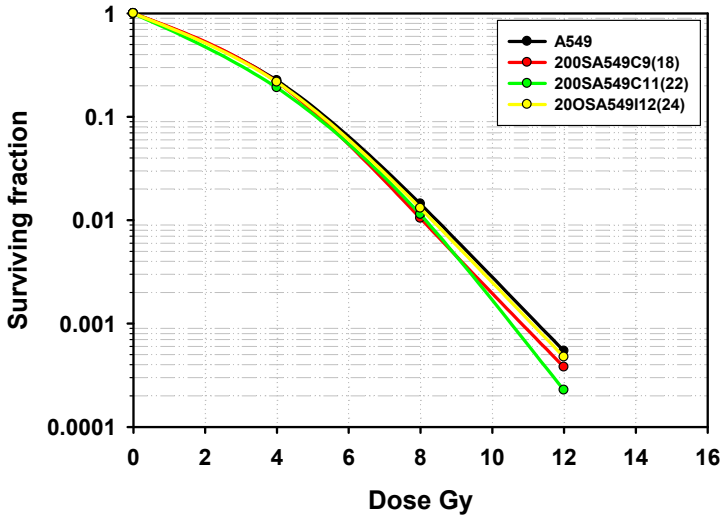

Fig. 23 Survival curves of wild type A549 cells and clones bearing I-*Sce*I sites in compatible and incompatible orientations. Cells were plated in duplicates and allowed to form colonies for 14 days.

3.2.5.2 I-*Sce*I expression constructs

The aim was now to perform colony formation assays with clones bearing defined number of integrated I-*Sce*I sites along with the parent A549 control, based exactly on the principle of colony formation assays performed with IR. For the following experiments, we utilized two different types of expression constructs of I-*Sce*I. The first one, named pCMV-I-*Sce*I-3xNLS, expresses I-*Sce*I constitutively with three nuclear localization signals to facilitate transfer of expressed I-*Sce*I to the nucleus.

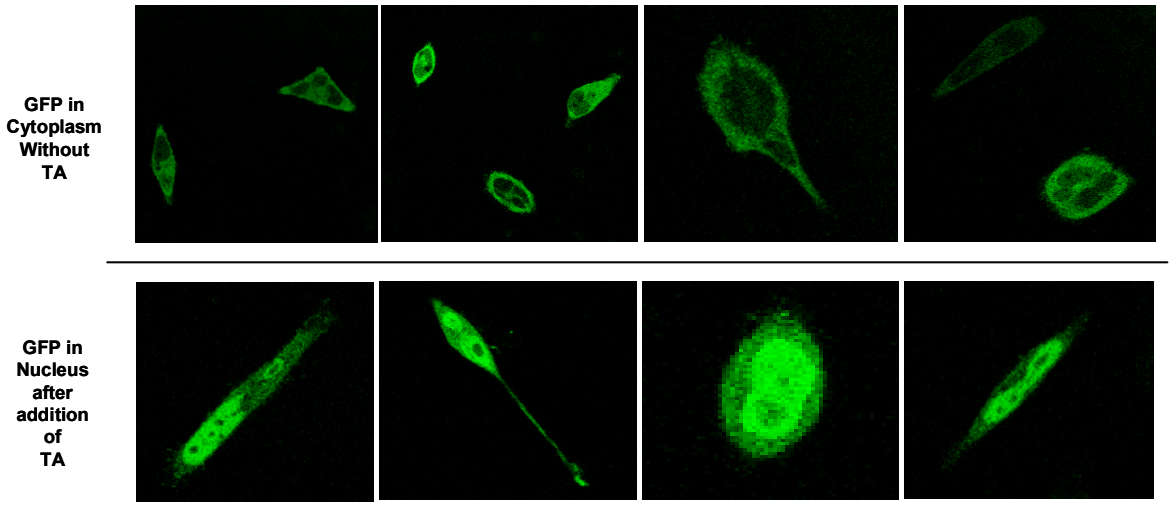

Fig. 24: Live cell imaging pictures depicting transport of EGFP-tagged I-*Sce*I from cytoplasm into the nucleus. The above Figure utilizes live cell imaging to show the transport of EFGP-I-*Sce*I-GR chimera from the cytoplasm to the nucleus upon addition of the ligand TA. The upper panel shows cells with the chimera in the cytoplasm 24 hours post transfection with pEGFP-I-*Sce*I-GR plasmid. Note the GFP signal primarily seen only in the cytoplasm in the absence of TA, with the nucleus mostly clear. The lower panel shows cells treated with the ligand TA. The images were acquired 5 min after addition of TA. Note the transport of the GFP signal to the nucleus which is now seen in bright green color.

The second is an inducible construct named pEGFP-I-*Sce*I-GR, which expresses a chimeric protein of EGFP, I-*Sce*I and a Glucocorticoid Receptor Ligand binding domain, which remains cytoplasmic until supplied with triamcinolone acetonide (TA). On addition of TA, the expressed chimera is immediately transported into the nucleus leading to excision at the recognition sites of I-*Sce*I, which in our case are integrated into the genome of A549 cells.

This system theoretically mimics the effects of IR, as all the DSBs should be triggered simultaneously.

Figure 24 shows live cell imaging pictures depicting the expression of GFP tagged chimeric I-*Sce*I in the upper panel, which gets transported into the nucleus within 5 min of addition of TA, as seen in the lower panel. Despite the impressive compartmentalization indicated here using imaging technologies, functional assays described below indicate that the system may be leaky (see 2.3.3).

3.2.5.3 Cells survival after transfection with I-*Sce*I

We measured cell survival in clones bearing single I-*Sce*I and double I-*Sce*I sites at different numbers. This assay has never been utilized before for determining the effect of homing endonuclease-induced DSBs on cell survival.

We devised two different protocols (see Figure 10) for these experiments in which the I-*Sce*I expressing construct was transfected using Nucleofection. In the first step, 2 million cells of each clone were transfected with 2µg of I-*Sce*I expression plasmid. According to the first protocol, the cells were plated in duplicates of 100 and 200 cells immediately after transfection. After 24h hours, TA was added to the cells and was removed after 8-10 hours of addition.

The second protocol was designed to exclude cells killed by the transfection. Therefore, cells were returned to culture for 24h at high numbers after transfection and were subsequently treated with TA 10-12 hours under the same conditions. Only at this point, cells were trypsinized and plated in duplicates of 100 and 200 cells. We observed similar results with both protocols.

3.2.5.4 Determination of transfection efficiency

All experiments included controls for determining the transfection efficiency. Transfection experiments have the inherent weakness that transfection efficiency is rarely 100%. Ideally, in our experiments, all transfected cells should receive the I-*Sce*I expression construct to ensure that DSBs are induced in all cells. Since this is not possible in practice it generates a complication that must be considered in the interpretation of the results obtained. For determining the transfection efficiency in our experiments, a construct supplied with the Lonza Nucleofector® kit (pMaxGFP) expressing EGFP was transfected in parallel and the percentage of green cells was determined by FACS, 24 hours post transfection. Transfection efficiency typically varied between 75 – 90%.

3.2.5.5 Survival of clones bearing single I-*Sce*I site integrations

Survival assays were performed with clones bearing 3, 6 and 7 integrations of single I-*Sce*I sites NSA5493(3), NSA5496(6) and NSA5497(7). NS stands for no spacer.

The survival is plotted as of function of the number of integrated I-*Sce*I sites. As it is shown no substantial killing was observed with any of the clones (Figure 25). The survival curve is a straight line starting from origin and running parallel to the dose axis. Comparable results were obtained with constitutive and inducible I-*Sce*I expression constructs, and the effect of the latter was independent of the presence of the inducing agent. No clear increase in cell killing was witnessed with increasing number of I-*Sce*I integration sites.

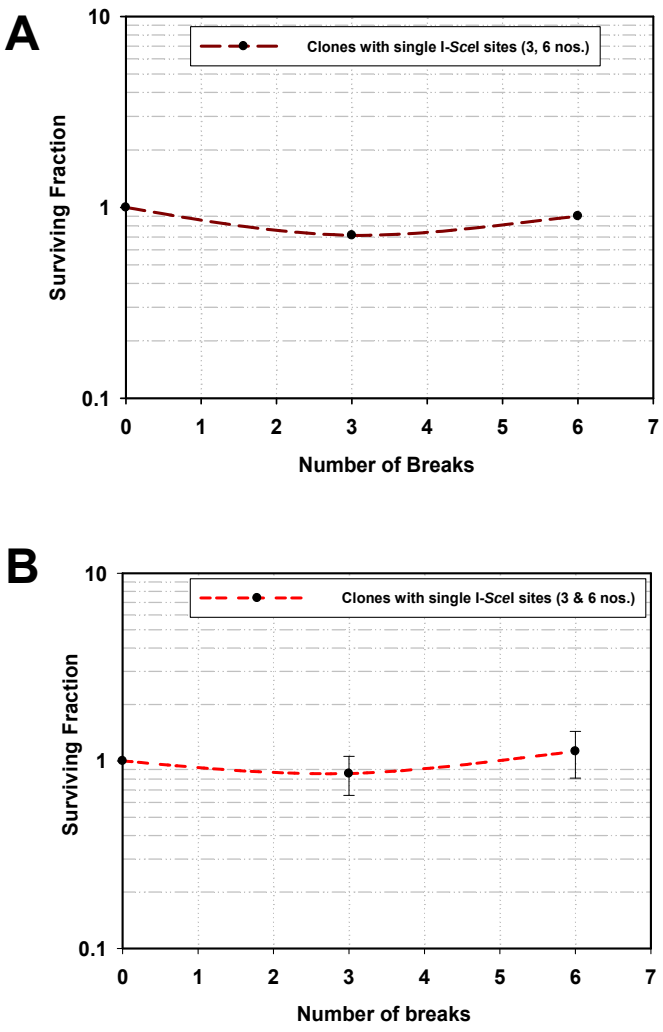

Fig. 25: .Survival Curves of clones bearing single I-*Sce*I sites with 3, 6 and 7 integrations (NSA5493(3), NSA5496(6) and NSA5497(7)). A: Clones were transfected with pCMV-I-*Sce*I-3xNLS .**B**: Clones were transfected with pEGFP-I-*Sce*I-GR

3.2.5.6 Clonogenic Survival assay with clones bearing pairs of I-*Sce*I sites

As colony formation with clones bearing single I-*Sce*I sites in multiple numbers showed no killing, we proceeded to test clones bearing pairs of I-*Sce*I sites separated by a distance of 200 bp. Similarly to clones with single I-*Sce*I sites, initially 4 clones were selected on the basis of number of integrations determined by Southern Blotting. Two of these clones were with the two I-*Sce*I sites in compatible orientations (200SA549C9(18) and 200SA549C11(22)) and two with sites in incompatible orientations (200A549I8(16) and 200A549I12(24)). In Fig. 26A the results are shown obtained from transfection experiments of the different clones with the pCMV-I-*Sce*I-3xNLS construct.

In the graph representing cells harboring the pairs of I-*Sce*I sites in incompatible orientation 200SA549I8(16) and 200SA549I12(24), the results point to an initial strong killing effect. The dose-response curve is a straight line starting from origin and showing approx. 80% killing for the clone bearing 16 I-*Sce*I sites (200SA549I8(16)). It reaches a plateau at this point and it is not further increased in the clone bearing 24 I-SceI sites (200SA549I12(24)). Clones with pairs of I-*Sce*I sites in compatible orientations show a consistent increase in cell killing with increasing number of integration sites. The clone bearing 18 I-*Sce*I sites (200SA549C9(18)) shows no initial killing, but the 200SA549C11(22) clone with 22 sites shows killing greater than 50%.

To investigate the initial points of the survival curves, we performed experiments with clones bearing lower numbers of integrations. Figure 26B shows the results obtained. As can be deduced from the plot, the clones bearing the I-*Sce*I sites in incompatible orientations still show substantial killing with the clone bearing 6 I-*Sce*I sites (200SA549I3(6)) showing approx. 70% lethality, and the clone bearing 12 sites (200SA549I6(12)) leading to a cell lethality of nearly 90%. The clone with 24 sites ((200SA549I12(24) again shows a killing of 90%, which is in agreement with the results obtained earlier.

On the other hand, clones bearing two I-*Sce*I sites in compatible orientation show less killing. Here, the clone with 4 sites (200SA549C2(4)) showed approx. 30% killing and the clone with 18 I-*Sce*I sites (200SA549C9(18)) 70%.

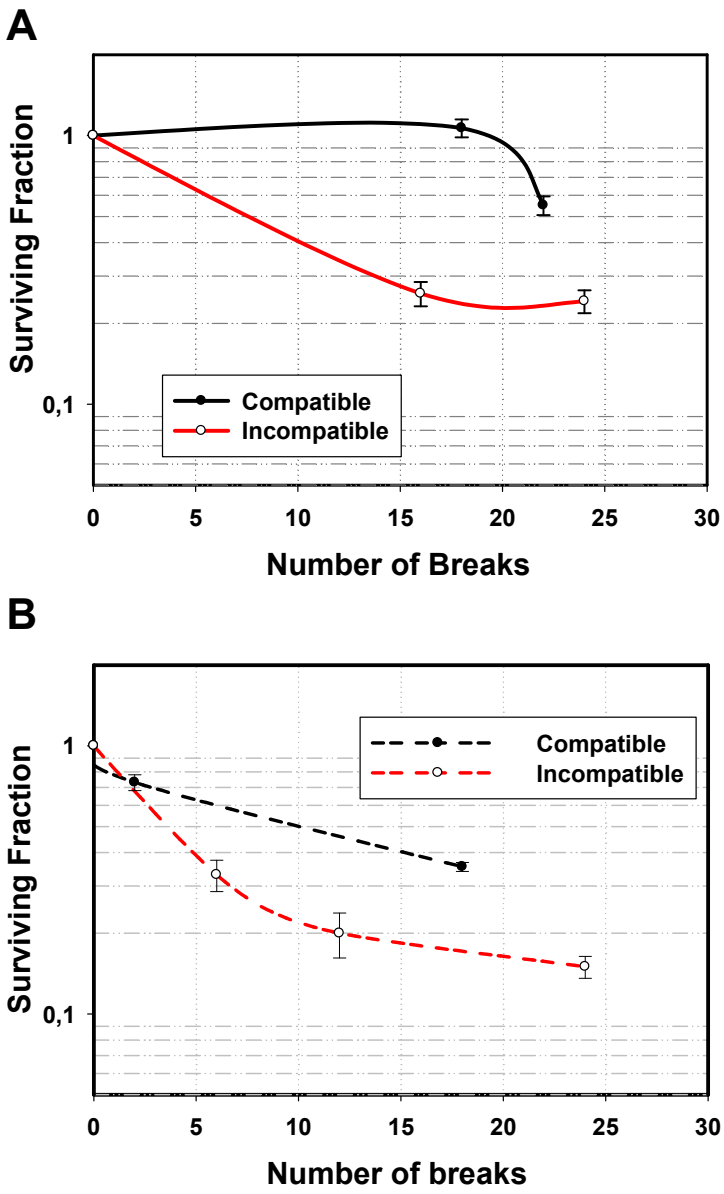

Fig. 26 Survival curves of clones bearing pairs of I-*Sce*I sites. **A.** The different clones were transfected with pCMV-I-*Sce*I-3xNLS. The survival experiment was carried out with two clones with sites in compatible orientations and 9 or 11 integrations (200SA549C9(18), 200SA549C11(22), black curve) and two clones with sites in incompatible orientations, with 8 and 12 integrations (200SA549I8(16) and 200SA549I12(24) red curve). **B** The clones were transfected with the pEGFP-I-*Sce*I-GR Plasmid. Two clones with compatible sites bearing 4 (200SA549C4(8)) and 9 (200SA549C9(18)) integrations and three clones with incompatible sites bearing 3,6 and 12 integrations (200SA549I3(6), 200SA549I6(12) and 200SA549I12(24)) were used in this experiment.

3.2.6 Results of G2-PCC - Determination of chromosomal aberrations

The cell survival data clearly implies that DSB pairs show an increased killing potential compared to single DSBs. In the following steps, we inquire how this strong killing is mediated.

For this purpose and in order to validate the results obtained with survival assays, we attempted to visualize the transformation of the enzyme-induced DSBs to chromatin breaks. We analyzed metaphases in I-*Sce*I plasmid transfected cells treated with Colcemid, but chromosome breaks or other forms of chromosome aberrations were only rarely observed. To increase the sensitivity of the assay we performed G2 Premature Chromosome Condensation (G2-PCC) to visualize I-*Sce*I-induced chromosome breaks before repair.

Two sets of experiments were designed to examine chromatid breaks induced by I-*Sce*I. In the first set of experiments, cells were additionally treated with β-AraA and in the second cells were treated with hypertonic solution (500mM NaCl). The repair inhibitor β-9-D-arabinofuranosyladenine (β-AraA) is a nucleoside analog known to inhibit DNA polymerases alpha and beta, thus inhibiting DNA synthesis [136, 139]. Hypertonic solution is thought to act by condensing chromatin, thus potentiating the effect of radiation or of DSBs [140, 141]

3.2.6.1 Calyculin-induced G2-PCC

Chromosome damage was analyzed in G2 after induction of premature chromosome condensation using Calyculin A. G2-PCC can be induced by the Serine/Threonine Phosphatase inhibitor Calyculin A [142]. It dephosphorylates the Serine/Threonine Phosphatases PP1 and PP2A which regulate the activity of the cell cycle checkpoint protein Cdc25. Cdc25 is a Tyrosine Phosphatase that activates the maturation mitosis promoting factor (MPF), a complex of p34cdc2/cyclinB. MPF promotes chromosome condensation and is active in its dephosphorylated form. MPF is normally active only in the M phase of the cell cycle corresponding to the high Cyclin B1 concentration at this cell cycle phase. Calyculin A indirectly activates the MPF factor by dephosphorylating PP1 and PP2A and forcing interphase cells into premature mitosis that is associated

with premature chromosome condensation (PCC). Due to the oscillation of Cyclin B1 through the cell cycle, PCC is predominantly induced in G2 phase followed by S Phase.

3.2.6.2 G2-PCC in cells transfected with pEGFP-I-*Sce*I-GR

The induction of DNA damage at the chromosome level was measured by G2-PCC [143]. All experiments were performed with exponentially growing cells. In the first step, four million of A549 human cells and four million of each of four different clones with different number of I-*Sce*I integration sites (200SA549C9(18), 200SA549C11(22), 200SA549I8(16) and 200SA549I12(24)) were transfected with the I-*Sce*I expressing plasmid pEGFP-I-*Sce*I-GR (1µg/Mio cells). The transfected wt A549 cells, as well as the four different clones were plated in 90-mm dishes, one million cells/dish in 15 ml McCoy's medium supplemented with 10% FCS. As a control, one million cells/dish of untransfected cells from each cell line were plated at the same time. In the following steps, the controls were treated the same way as the transfected cells. 24h post transfection, TA was added to the cells to initiate the transport of I-*Sce*I into the cell nucleus. Cells were harvested at 4h post addition of TA. Calyculin A was added 30 min before fixation at a final concentration of 100nM. Colcemid was also added four hours prior to fixation to enable a metaphase block and prevent the loss into G1 (where chromosome analysis is not possible) of cells that could otherwise be analyzed.

3.2.6.3 G2-PCC of 0.5 Gy X-ray treated cells

Simultaneously, a set of irradiated cells were prepared to compare the number of DSBs induced by 0.5Gy X-rays to the number of breaks induced by restriction of I-*Sce*I sites. 0.5 Mio. cells/dish of A549, 200SA549C9(18), 200SA549C11(22), 200SA549I8(16) and 200SA549I12(24) were radiated with 0.5Gy X-rays which corresponds to the induction of 15-20 DSBs, similar to the putative number of DSBs induced by restriction of I-*Sce*I sites in the selected clones. The cells were harvested 4h after irradiation and after treatment with Calyculin A for 30 min and with Colcemid block for four hours. In the last step, the cells were fixed for analysis.

3.2.6.4 Effect of β-AraA treatment on pEGFP-I-*Sce*I-GR transfected and irradiated cells

Treatment with β-AraA significantly enhanced the incidence of G2-PCC breaks in clones after induction of DSBs as compared to wild type A549 cells, suggesting the activation of DNA repair systems upon induction of DSBs by I-*Sce*I. A two to three fold higher incidence was observed in cells harboring two closely spaced DSBs than in wild type A549 cells (Fig. 27). Compared to the wild type A549 cells, which have in general one chromatid break per cell, all clones show a significant increase in G2 PCC breaks/cell, which is two to four fold higher. The 200SA549C9(18) clone with 9 integrations of I-*Sce*I sites in compatible orientation show two chromatid breaks/cell, whereas the clone 200SA549I8(16) with 8 integrations of I-*Sce*I sites in incompatible orientations showed approx. 4 chromatid breaks per cell. The other two clones 200SA549C11(22) and 200SA549I12(24) with higher number of integrations and with sites in compatible and incompatible orientations respectively did not show much variation and also had approx. 4 chromatid breaks per cell. The black bars represent transfected cells, which were not treated with β-AraA. A549 and all untreated clones bear approx. 0.1 chromatid breaks. The low number of breaks in cells not treated with β-araA further points out the lack of correlation between cell killing and chromosome aberration formation in all these clones. The results with β-araA will require additional analysis and controls to exclude artifacts.

In the cells irradiated with 0.5Gy X-rays, the number of G2 PCC breaks ranged for all clones from 3.8 to 5.2 breaks per cell. The black bars representing the irradiated controls without treatment show a similar number of breaks among all clones, which are approx. 0.4 G2PCC breaks per cell.

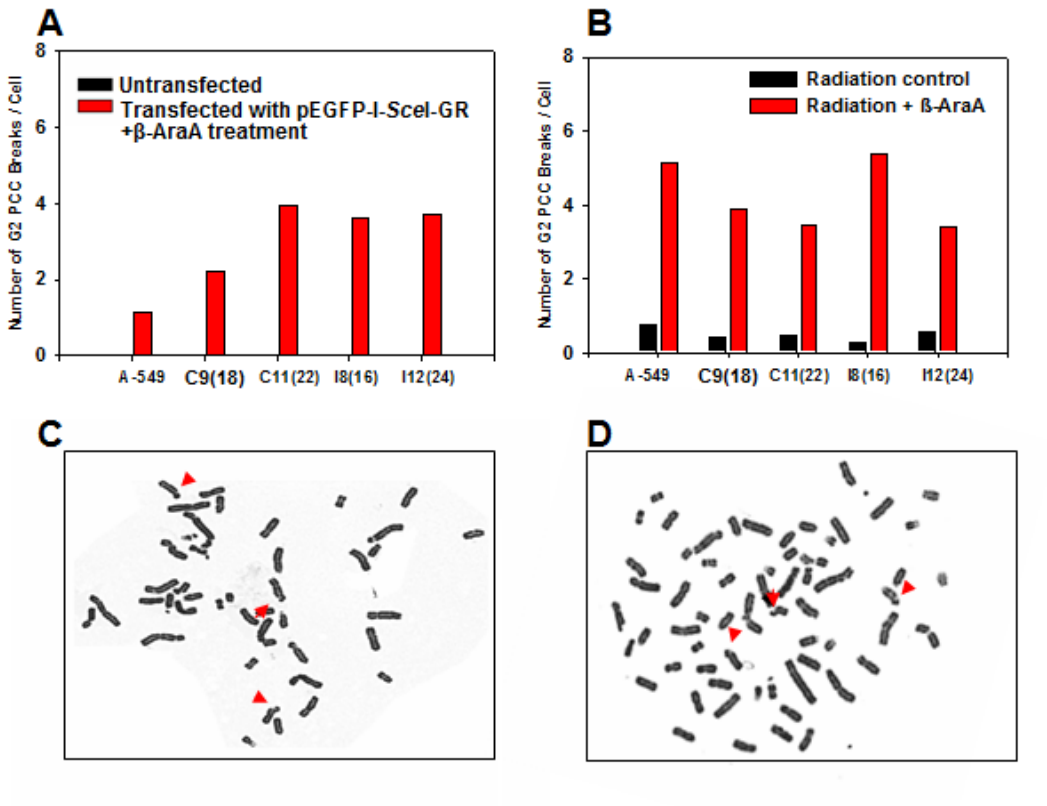

Fig. 27: G2-PCC fragments in clones harboring the indicated number of integrations of pairs of I-*Sce*I sites separated by 200bp after treatment with β-AraA. **A**. Bar graph with respective representative micrographs of clones transfected with TA-inducible pEGFP-I-*Sce*I-GR construct to generate DSBs, as well as untransfected controls. The red bars represent the number of G2-PCC breaks/cell in β-AraA treated cells. **B.** Radiation Control (0.5 Gy X-rays). Red bars represent irradiated cells treated with β-Ara A. **C** Picture of Chromosomes transfected and treated with β-AraA. **D.** Picture of Chromosomes irradiated and treated with β-AraA. **N.B**.: C9(18) and C11(22) represent 200SA549C9(18) and 200SA549C11(22)clones respectively with pairs of I-*Sce*I sites in compatible orientations with 9 or 11 integrations, resulting in 18 and 22 DSBs respectively. I8(16) and I12(24) represent 200SA549I8(16) and 200SA549I12(24) clones respectively, with the pairs of I-*Sce*I sites in incompatible orientations. Red arrows indicate the G2-PCC breaks.

3.2.6.5 G2-PCC of cells after hypertonic solution treatment

In the second set of experiments with the identical objective of preventing the repair of I-*Sce*I-induced DSBs, the cells were treated with hypertonic solution (500mM NaCl in PBS) 3h prior to fixation for a duration of 20min. Hypertonic treatment of cells is performed to induce condensation of chromatin [140]. It is hypothesized that repair proteins have difficulty to access DSBs in condensed chromatin; therefore repair of DSBs is thought to be inhibited in hypertonic solution treated cells. Furthermore, chromatin destabilization may allow the transformation of DSBs into chromosome breaks, which would have missed detection otherwise.

3.2.6.6 Effect of hypertonic treatment on pEGFP-I-*Sce*I-GR transfected and irradiated cells

Compared to A549 which has 0.1 G2-PCC breaks/cell, all clones show significant increase in breaks, up to seven fold. The number of G2-PCC breaks ranges from 0.4 in 200SA549C11(22)and 200SA549I8(16), to 0.5 in 200SA549I12(24) and 0.7 breaks/cell in 200SA549C9(18). The black bars represent untransfected cells treated with hypertonic solution. The untransfected clones show breaks ranging from 0.1 to 0.4 G2-PCC breaks per cell (Figure 28A). Irradiated cells of all clones have approx. 0.3 - 0.6 G2-PCC breaks per cell (black bars, Figure 28B). The G2-PCC breaks of irradiated cells (0.5 Gy) with hypertonic treatment vary between the different clones from approx. 1.8 in A549 to 0.4 in 200SA549C11(22).

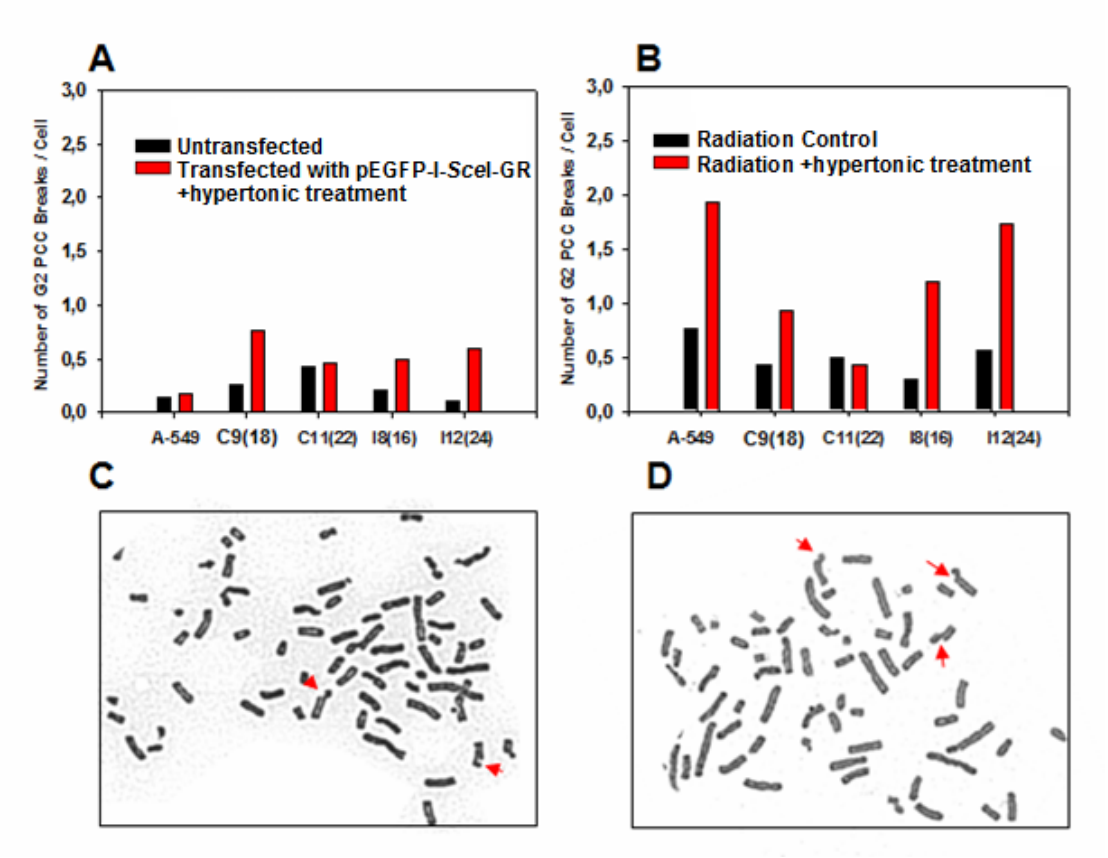

Fig. 28 G2-PCC fragments in clones harboring the indicated number of integrations of pairs of I-*Sce*I sites separated by 200bp after Hypertonic treatment (500mM NaCl) A. Bar graph with representative micrographs of clones transfected with TA-inducible pEGFP-I-*Sce*I-GR construct, together with untransfected controls. **B**. Radiation control (0.5 Gy X-rays). Red bars represent irradiated cells treated with hypertonic solution. **C** Picture of chromosomes transfected and treated with hypertonic solution. **D.** Picture of chromosomes irradiated and treated with hypertonic solution.

N.B.: C9(18) and C11(22) represent 200SA549C9(18) and 200SA549C11(22) clones respectively, with two I-*Sce*I sites in compatible orientations with 9 and 11 integrations, resulting in 18 and 22 DSBs, respectively. I8(16) and I12(24) represent 200SA549I8(16) and 200SA549I12(24) clones, respectively, with the pairs of I-*Sce*I sites in incompatible orientation. Red arrows indicate the G2-PCC breaks.

3.2.7 Determination of the fate of I-*Sce*I sites after restriction analyzed by PCR

3.2.7.1 Genetic consequences of simultaneous restriction of two closely spaced I-*Sce*I sites

Previous results demonstrated that the induction of DSBs by I-*Sce*I has deleterious consequences for the cell in terms of survival. Now, the question arises as to how the repair mechanisms deal with such DSBs. For this purpose, we used PCR to analyze the DNA sequence at the repair junction between two I-*Sce*I sites. Primers were designed which flanked the two I-*Sce*I sites 57bp upstream and 138bp downstream. As template DNA from the clone 200SA549I8(16) was used, bearing 8 integration sites in incompatible orientations. Theoretically, in untreated cells all eight sites should give rise to the same product. After digestion and successful rejoining, the PCR products could be of different sizes depending on how repair modified the junction. To enable the sequencing of this mixture of PCR products, the DNA fragments were cloned into the pGEM-T Easy vector system (Figure 29). After transformation in E.coli cells, every plasmid should bear a single PCR product of one integration site. In the next step, PCR was performed in 10 randomly picked clones and two clones were sequenced.

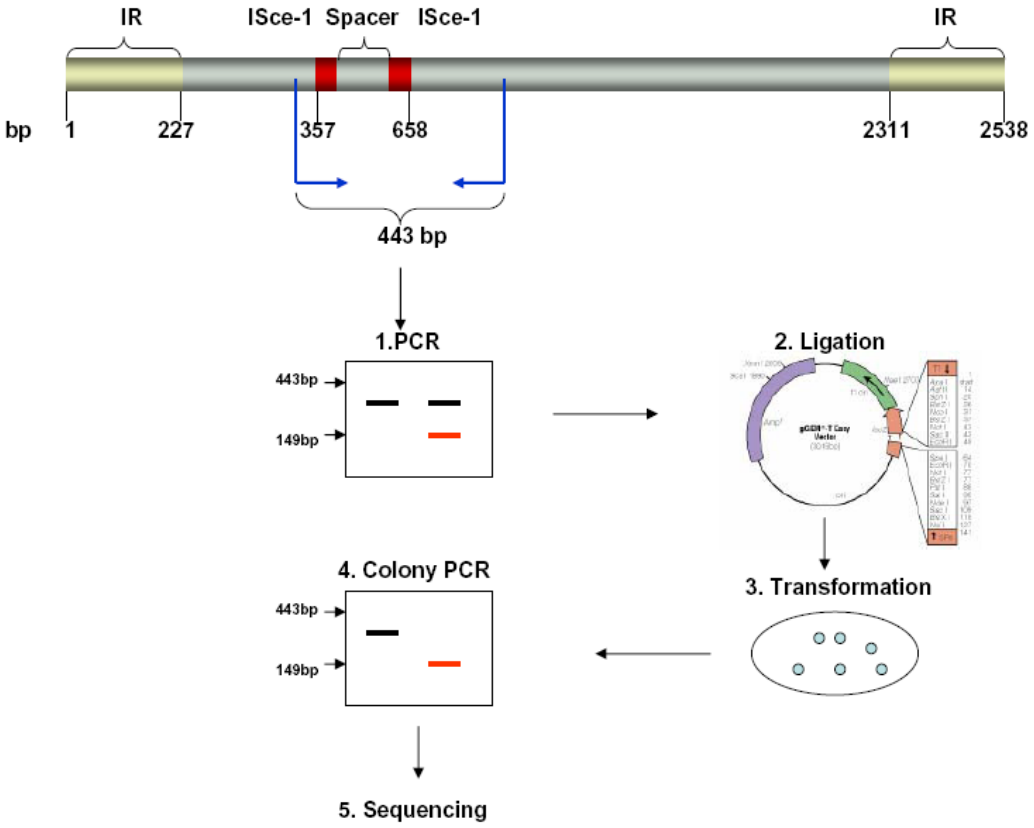

Fig. 29: Schematic illustration of the PCR analysis of the sequence containing the two I-*Sce*I sites. After the sequences were amplified by PCR, products were run in agarose gels and the different bands were eluted and cloned into the pGEM-T Easy vector. 10 colonies were picked for colony PCR and run on 1% Agarose gel. Colonies containing 149 bp sequence and 450 bp sequence were subsequently sequenced. The blue arrows indicate the forward and reverse primers. 1. PCR, left band - A549, right bands – 200SA549I8(16), 4. Colony PCR, left band - A549, right band - 200SA549I8(16).

3.2.7.2 Deletion of intervening sequence between the two I-*Sce*I sites

Two different DNA sequences were obtained after sequencing the different E.coli clones obtained from the pEGFP-I-*Sce*I-GR transfected 200SA549I8(16) cells. One clone showed the original sequence where no genetic changes could be detected. The other sequence showed a 294bp deletion, see Fig. 30. In this sequence, both the I-*Sce*I sites had been deleted by the repair machinery and additionally 45 bp had been deleted upstream of the first I-*Sce*I restriction site and 23bp downstream of the second site. This suggests that two simultaneously induced DSBs are repaired as a single DSB by error prone NHEJ repair machinery using extensive trimming of ends. Also, it must be noted that there was a loss of the intervening fragment between the two I-*Sce*I sites suggesting destabilization of chromatin.

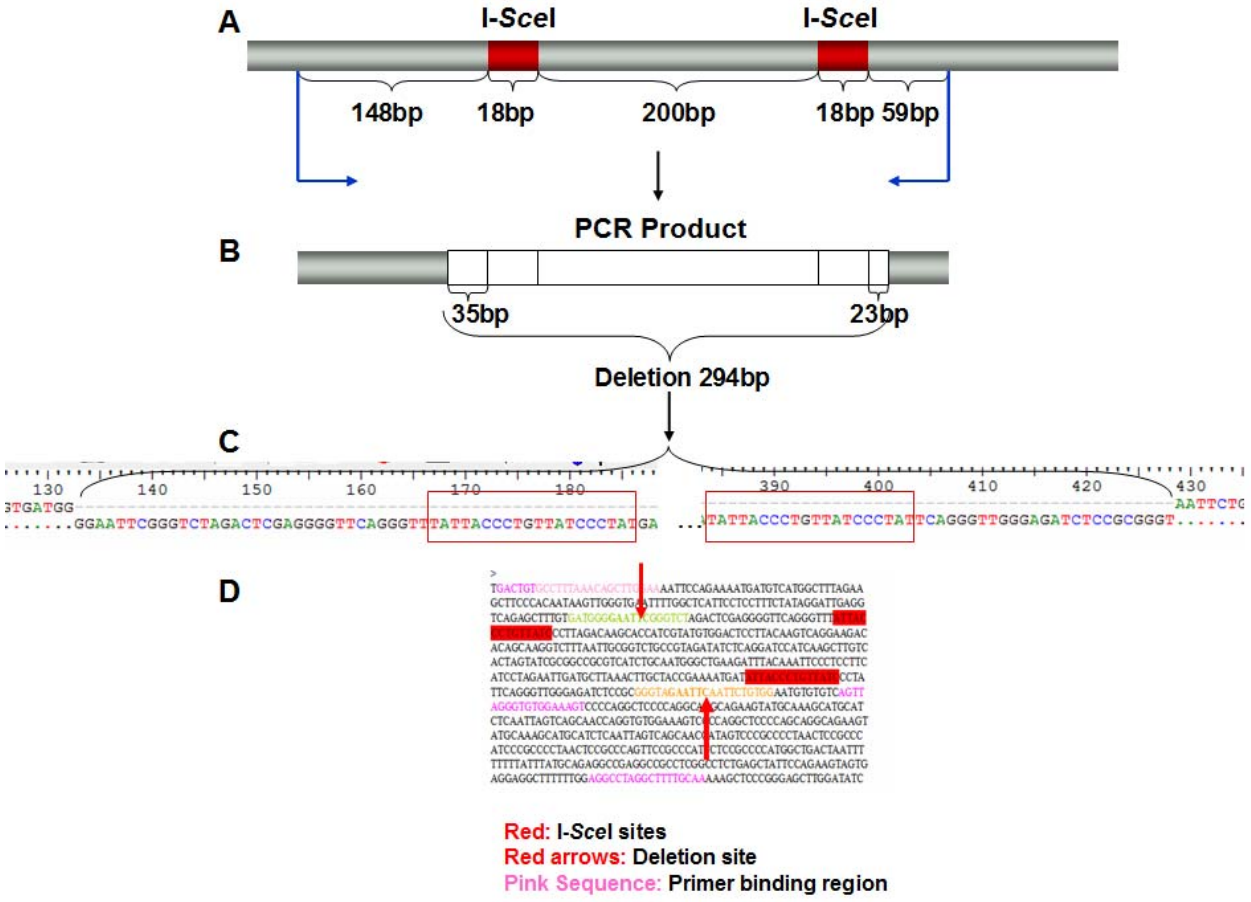

Fig. 30: Schematic illustration of the sequence deletion due to error prone repair of I-*Sce*I-induced DSBs. A: Schematic illustration of the sequence harboring two I-*Sce*I sites. The blue arrows indicate the primer binding sites. **B:** The white area in the PCR product sequence indicates the site of deletion which spans 294bp. **C:** The sequences are illustrated in Bioedit program format. In the top panel, the deletion is shown, ranging from position 130bp to 430bp (starting at base pair 1 from the forward primer binding site). The lower panel of the Bioedit figure shows the original sequence integrated in the genome before incision with I-*Sce*I. The red boxes indicate the two I-*Sce*I sites in the uncut sequence. **D:** Original Sequence in FASTA format.

3.2.8 Immunofluorescence: Determination of γ-H2AX foci induction in response to I-*Sce*I-induced DSBs

In higher eukaryotes, DSBs promptly induce the phosphorylation of the histone H2A variant, H2AX, at Serine 139 to generate γ-H2AX[34]. Regions with γ-H2AX are conveniently detected in chromatin by Immunofluorescence Microscopy. It has been shown that there is an approx. one-to-one relationship of γ-H2AX foci with number of DSBs induced and this has quickly become a standard for microscopic determination of DSB induction and repair kinetics.

We determined γ-H2AX foci induction upon I-*Sce*I-induced DSBs by utilizing confocal microscopy. In these experiments, exponential phase cells at a concentration of 2 x 10^6 were nucleofected with 4µg of pEGFP-I-*Sce*I-GR plasmid and plated in 35 mm dishes containing poly L-Lysine-coated coverslips. 24 hours post transfection, the cells were treated with the drug TA and cells were fixed with 2% Paraformaldehyde after 90 min for γ-H2AX foci analysis. DAPI was used as a nuclear stain. Controls were included in the experiments where TA was not added along with blank and only transfection reagent treated cells. Due to the high cell toxicity of nucleofection, the experiment was then performed with Lipofectamine^{TM} 2000 reagent and a transfection efficiency of 35-40% (determined by EGFP-FACS) with lesser cell toxicity was observed. In experiments with Lipofectamine^{TM}, cells were first plated in 35 mm dishes containing poly L-lysine-coated coverslips at a concentration of 0.2 x 10^6. The cells were transfected the following day with 4µg of pEGFP-I-*Sce*I-GR plasmid including all appropriate controls.

Since, we could not distinguish between background and induced γ-H2AX foci, we determined total number of γ-H2AX foci per cell for several fields and plotted the focus distribution pattern for transfected and untransfected clones. As seen in Figure 32, in A549 cells, the distribution of foci remains more or less constant in untransfected and transfected cells. In cells bearing 9 pairs of I-*Sce*I sites in compatible orientations, a general increase in number of cells with γ-H2AX foci ranging from 1 to 17 was observed after transfection as compared to the untransfected cells.

Similarly, in a clone bearing 8 pairs of I-*Sce*I sites in incompatible orientations, a general increase in number of cells with γ-H2AX foci ranging from 1 to 16 was observed after transfection as compared to untransfected cells. Thus despite the pronounced killing observed in this clone, γ-H2AX foci formation could not be conclusively established.

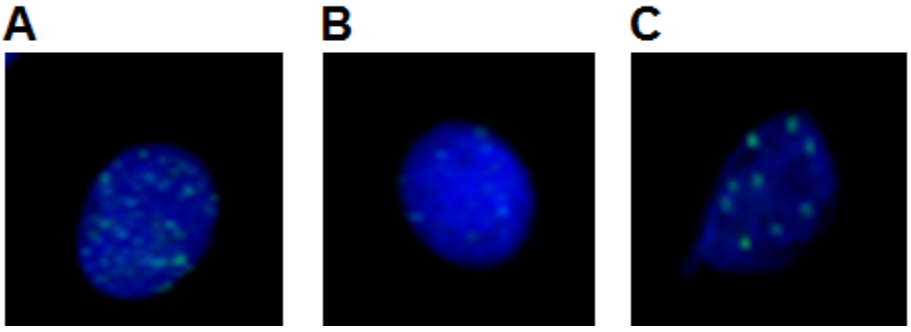

Fig. 31: Representative images of cells with γ-H2AX foci. A. 1Gy X-rays irradiated sample. **B**. Wild type A549 control after transfection with I-*Sce*I expression construct. **C**. 200SA549I8(16) clone after transfection with I-*Sce*I expression construct.

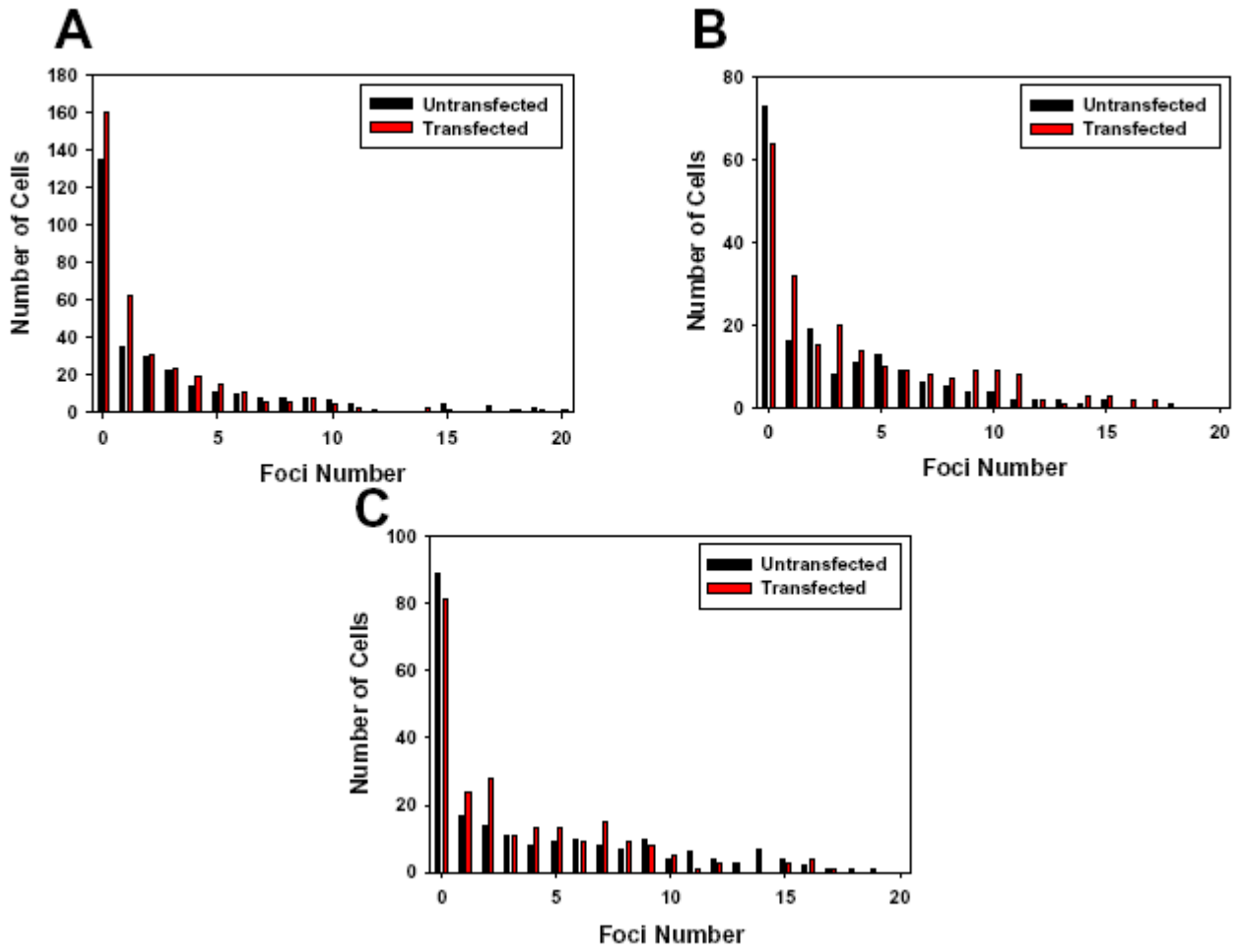

Fig. 32: Determination of γ-H2AX foci upon induction of DSBs by I-*Sce*I. A. Plot representing distribution of γ-H2AX foci across wild type A549 cells. **B.** Plot representing the distribution of γ-H2AX foci across cells of a clone bearing 9 pairs of I-*Sce*I sites in compatible orientation. **C**. Plot representing the distribution of γ-H2AX foci in cells of a clone bearing 8 pairs of I-*Sce*I sites in incompatible orientation. Black bars represent untransfected cells bearing γ-H2AX foci. Red bars represent cells with γ-H2AX foci, which were transfected with I-*Sce*I expression construct. Note the different scales.

3.2.9 DNA damage leads to activation of the G2 checkpoint

As the name suggests, checkpoints in the cell cycle facilitate repair of damaged chromatin before a cell transits into the next phase of the cell cycle. Of the three known and well characterized G1[144], S[145] and G2 checkpoints[146], the G2 checkpoint is the most potent. It is located at a sensitive juncture of the cell cycle phase before the cell enters mitosis. IR is known to induce a strong G2 checkpoint, lasting several hours depending upon the dose delivered. Thus, activation of G2 checkpoint after DNA damage leads to altered distribution of cells throughout the cell cycle, which can be determined either by measuring the DNA content of the cells by PI staining at various time points after induction of the damage, or by determining the Mitotic index at these time points after damage induction, since arrest in G2 will quickly reduce the number of cells reaching mitosis.

3.2.9.1 Determination of G2-Checkpoint on induction of DSBs by I-*Sce*I

IR is known to induce a strong G2 arrest, which can be easily visualized by the accumulation of cells in G2. We tried to determine if the DSBs induced by I-*Sce*I have the same effect. In the following experiment, we utilized a clone with compatible I-SceI sites 200SA549C9(18) and one with incompatible ends 200SA549I8(16) along with A549 controls. All three cell lines were transfected with pEGFP-I-*Sce*I-GR and the expressed I-*Sce*I was induced with TA 24 hours post transfection. Cells were collected at various time points post transfection and fixed with 70% ethanol for PI staining (described in materials and methods). Figure 33 shows plots with the percentage of G2 cells as a function of time post TA. As can be deduced from the plots, a clear increase in G2 population is witnessed after approximately 24 hours post transfection with both the clones, whereas no increase in G2 population is witnessed in wild type A549 cells. This 24 hour time point exactly corresponds to the time of addition of TA to the cells, and presumably is a result of the induction of DSBs by I-*Sce*I. However, the similar size fluctuations observed in the controls preclude a conclusive interpretation.

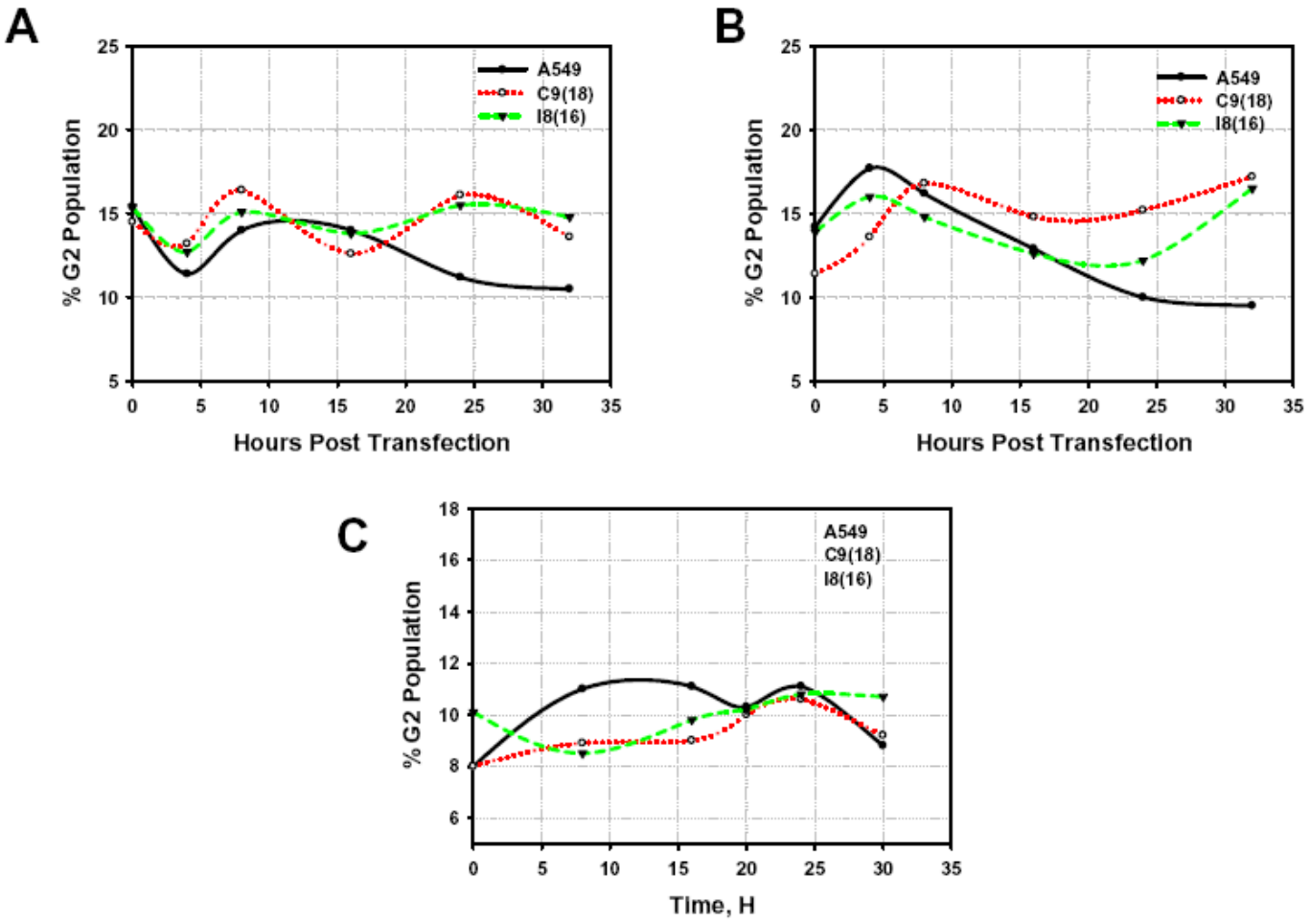

Fig 33. Determination of G2 checkpoint activation upon induction of DSBs by I-*Sce*I. A, B. Plots representing two independent experiments depicting the G2 population of clones bearing 9 and 8 pairs of I-SceI sites in compatible and incompatible orientations along with wild type A549 controls after transfection with pEGFP-I-*Sce*I-GR construct with samples collected at various time points up to 33 hours post transfection. **C.** Plot representing the G2 population of untransfected clones bearing 9 and 8 pairs of I-*Sce*I sites in compatible and incompatible orientations respectively along with wild type A549 control with samples collected at various time points until 30 hours post transfection. Black splines represent wild type A549 cells. Red splines represent a clone with 9 pairs of I-*Sce*I sites in compatible orientations. Green splines represent a clone with 8 pairs of I-*Sce*I sites in incompatible orientations.

It must be mentioned though that there was no significant difference observed in the G2 population of clones with compatible or incompatible I-*Sce*I ends at the 25 hour time point. It is also important to note that since the G2 population in both clones started to increase 20 hour post transfection, this could potentially be due to the leakiness of expressed I-*Sce*I into the nucleus (as discussed earlier).

3.2.9.2 Determination of G2-Checkpoint activation upon induction of DSBs by I-*Sce*I homing endonuclease by measurement of Mitotic Index

In the next step, we studied the activation of G2-checkpoint by determining mitotic index through flow cytometry. Mitotic index (MI) variations also reflect the G2 checkpoint activation and provide a higher sensitivity of detection than G2 phase accumulation. Histone H3 is phosphorylated at Serine-10 (Histone H3 pS10) early in mitosis and therefore an antibody against phospho-histone H3 can be used to assess the IR-induced G2 checkpoint delay or entry into mitosis [147]. Histone-H3 pS10 staining is very specific for mitotic cells.

The experiment was performed with a clone bearing 8 pairs of I-*Sce*I sites in incompatible orientation (200SA549I8(16)) and A549 cells as a control. 24 hours post transfection with pEGFP-I-*Sce*I-GR, cells were collected at 0, 1 and 3h time points post addition of the drug TA and were processed for H3 pS10 stain. They were also simultaneously stained for DNA content with PI (multivariate FACS) (detailed description in Materials and Methods). Figure 34A depicts the results obtained. A decrease in Mitotic index was observed at all time points with the clone 200SA549I8(16), suggesting that the I-*Sce*I inducible system was leaky and lead to the reduction of MI even without the addition of TA.

Figure 34A shows a plot of mitotic index determination of a clone 200SA549I8(16) at 0, 1 and 3 hours either post irradiation with 0.5 Gy X-rays or after addition of TA 24 hours post transfection with pEGFP-I-*Sce*I-GR or untransfected both in the presence or absence of caffeine. Caffeine is known to abrogate G2 checkpoint. In this plot, caffeine completely abrogates the G2 checkpoint as seen by the maintenance of mitotic population moving through the cell cycle at all the observed time points with both irradiated and transfected cells, whereas MI drops to near zero for irradiated population. A drop is observed in MI as compared to untreated cells at all three time points of 0, 1

and 3 hr post addition of TA in caffeine untreated cells. In caffeine treated transfected cells, MI is observed to increase marginally.

Figure 34B shows a plot of mitotic index determination of A549 cells at 0, 1 and 3 hours either post irradiation with 0.5Gy X-rays or after addition of TA 24 hours post transfection with pEGFP-I-*Sce*I-GR and untransfected cells both in the presence or absence of caffeine. Although in the transfected cells, a drop in MI is witnessed as compared to the untreated cells, no difference in MI was observed in transfected cells whether in presence or absence of caffeine. Similar to results obtained with the clone 200SA549I8(16), Caffeine completely abrogated the G2 checkpoint leading to the restoration of normal MI in irradiated cells, whereas in absence of Caffeine MI drops to near zero for irradiated population.

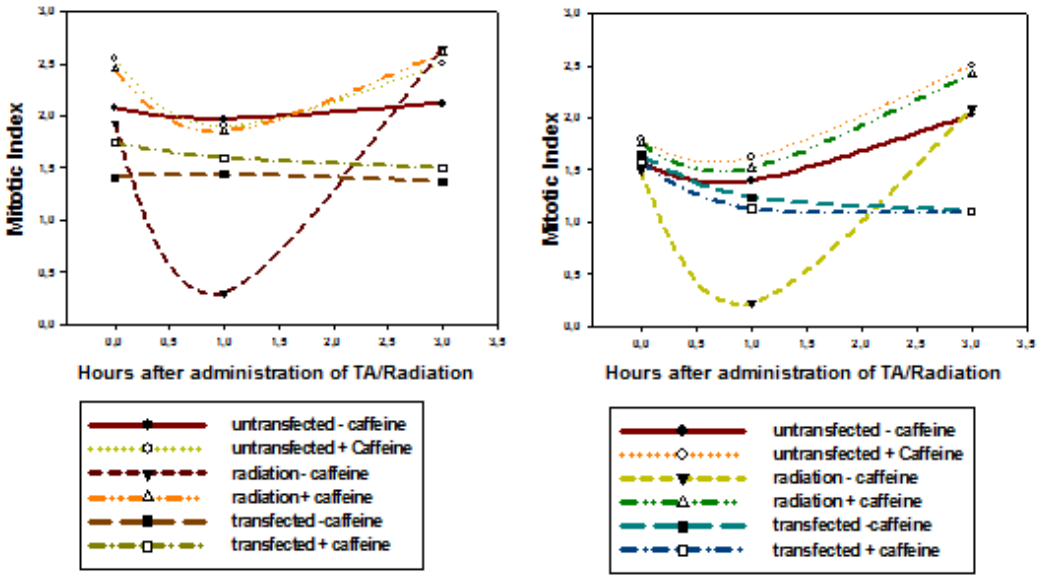

Fig. 34: Determination of Mitotic index by FACS using H3pS10 antibody. A. Plot representing the determination of MI in clone 200SA549I8(16) bearing 8 integrations of two I-SceI sites in incompatible orientations**. B**. Plot representing the determination of MI in wild type A549 cells. Cells were either treated with 0.5 Gy X-rays or transfected with pEGFP-I-*Sce*I-GR construct, or were untreated both in the presence and absence of Caffeine. MI was determined after 0, 1 and 3h post induction of damage.

3.2.10 Determination of induction of DSBs by I-*Sce*I using EGFP-tagged 53BP1 and live cell imaging

53BP1 was identified as a protein that interacts with p53 through its BRCT domain. BRCT domain, first described at the carboxyl terminus of the breast cancer protein BRCA1, occurs predominantly in proteins involved in cell cycle checkpoint functions responsive to DNA damage. Upon exposure to IR, 53BP1 is hyperphosphorylated in an ATM dependent manner and relocalizes rapidly to form discrete nuclear foci. These foci colocalize with Nbs1 and γ-H2AX foci, which have been shown to localize at sites of DNA DSBs. Furthermore, 53BP1 is required for the accumulation of p53 protein, G2-M checkpoint arrest and the intra-S-phase checkpoint in response to IR damage [37, 148]. We utilize here a construct expressing the EGFP-tagged version of 53BP1 protein (a kind gift from Prof. T. Halazonetis) for determination of induction of DSBs by I-*Sce*I utilizing live cell imaging.

Since live cells cannot be stained with protein labeling dyes or by fluorescence-tagged antibodies, constructs expressing fluorescence-tagged proteins are the reagents of choice. For example, fluorescence-tagged DNA repair proteins-expressing-constructs are transfected 24 hours prior to irradiating the cells. After induction of damage, these proteins may be recruited to the sites of DSBs and become visible as foci. The objective of our experiment was to detect the induction of DSBs by studying the formation of EGFP-tagged 53BP1 foci in cells transfected with the I-*Sce*I expression construct.

A clone bearing 8 pairs of I-*Sce*I sites in incompatible orientations (200SA549I8(16)) along with wild type A549 cells were used for the experiments. Results from live cell imaging have been plotted in Figure 36, which show the deployment and dissociation kinetics of EGFP-53BP1 foci tracked over a period of 24 hours. It was intriguing that most of the tracked green cells underwent apoptosis (as visualized by disruption of cell nucleus). This was observed for all of the three experiments performed, where both the EGFP-53BP1 and the I-*Sce*I expression construct were transfected. This phenomenon was seldom observed in cells where only the construct expressing EGFP-53BP1 was transfected. This suggests that cells receiving the I-*Sce*I expression construct may undergo apoptosis. Figure 36C represents foci kinetics of EGFP-53BP1 in wild type A549 cells irradiated with 1Gy X-rays which serves as a positive control. The cells were

nucleofected with the EGFP-53BP1 expressing construct 24 hours before irradiation. The cells were irradiated in 3-well live cell imaging chambers and immediately moved to a position under the microscope for capturing the images. The cells were maintained in Leibovitz media supplemented with 10% FBS. A number of cells were tracked over a period of approx. 2 hours post irradiation. The plotted graph shows the EGFP-53BP1 foci kinetics in a representative cell. The 53BP1 foci number reaches 28 within 5 min of 1Gy X-rays exposure and then falls to background levels at around 2 hours post irradiation.

Figure 36A and B represent the foci kinetics of EGFP-53BP1 in two cells of a clone with 8 pairs of I-SceI sites in incompatible orientations (200SA549I8(16)). In both plots, we observe the baseline foci of 2-3 in both cells which reaches a maximum of approximately 9 foci at 24 hours before reaching baseline levels again. Approximately 10 cells were tracked over a period of 20 hours after transfection of pCMV-I-*Sce*I-3xNLS construct, but as mentioned earlier; most of these cells underwent apoptosis midway through the 20 hour period where an increase in foci number was observed.

Figure 35 represents still images of cells with EGFP-53BP1 foci after transfection with pCMV-I-*Sce*I-3xNLS construct.

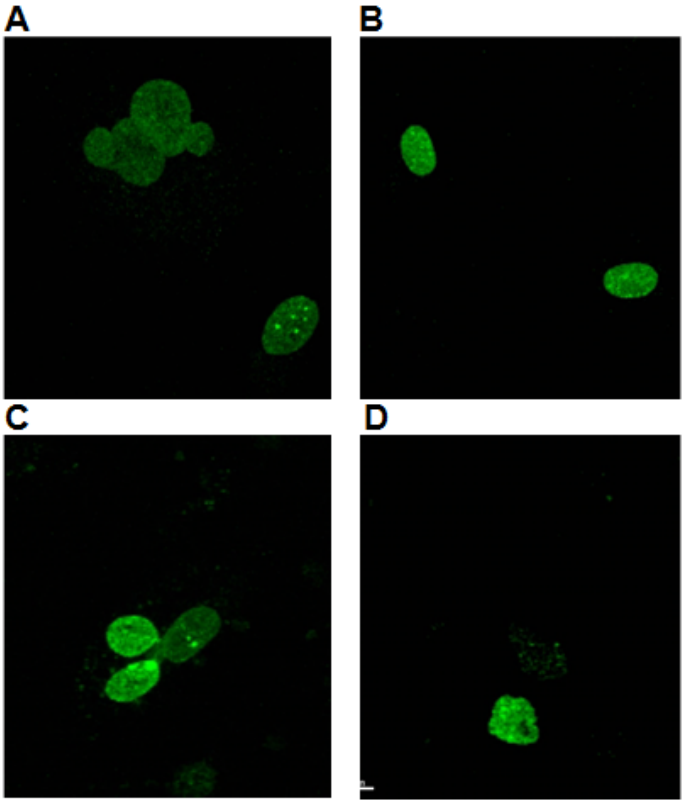

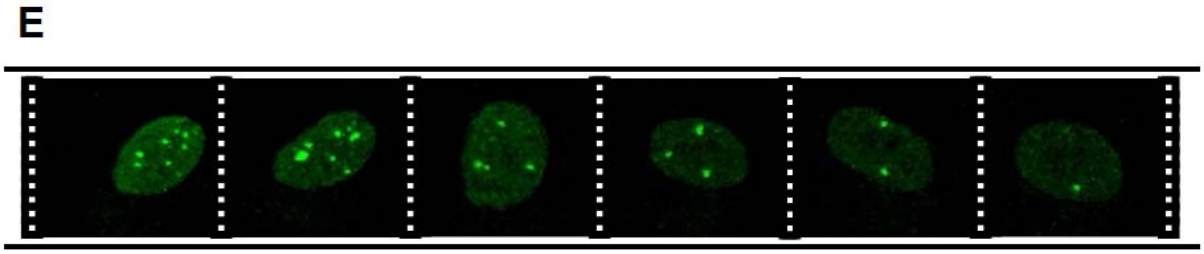

Fig. 35: A-C: Representative images of cells with EGFP-53BP1 foci. 200SA549I8(16) clone was transfected with a construct expressing EGFP-53BP1. 24 hours later, the cells were transfected with I-*Sce*I expression construct and the cells were tracked for a period of 20 hours.

E. Foci kinetics of EGFP-53BP1 after induction of DSBs by I-*Sce*I. The film strip shows still images of a single cell tracked over a period of 8 hours from the time of appearance of 53BP1 foci after transfection with pCMV-I-*Sce*I-3xNLS.

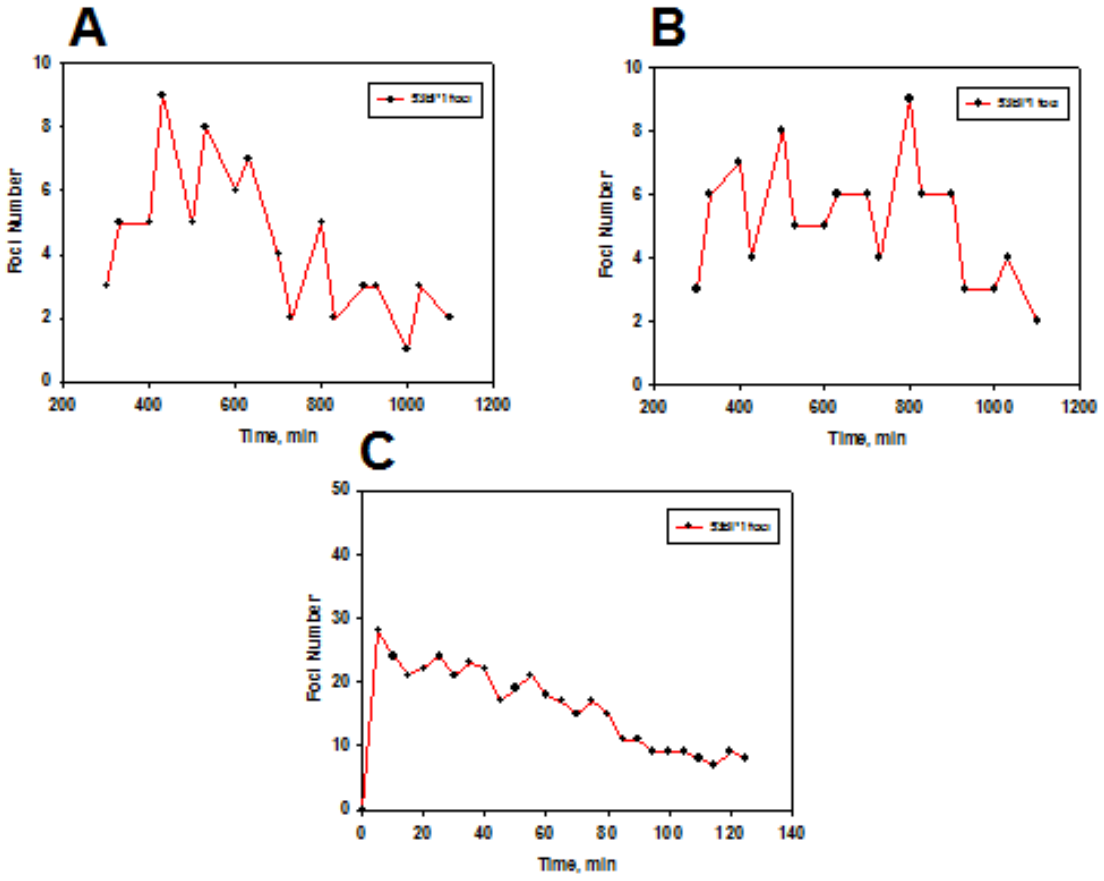

Figure 36 Figures representing the kinetics of induction and disappearance of EGFP-53BP1 foci in 1 Gy irradiated and I-*Sce*I expression construct transfected cells. A, B. Represents EGFP-53BP1 foci kinetics of two cells of a clone 200SA549I8(16) transfected with pCMV-I-*Sce*I-3xNLS and tracked over a period of 20 hours post transfection. **C.** Represents EGFP-53BP1 foci kinetics in wild type A549 cells irradiated with 1Gy of X-irradiation.

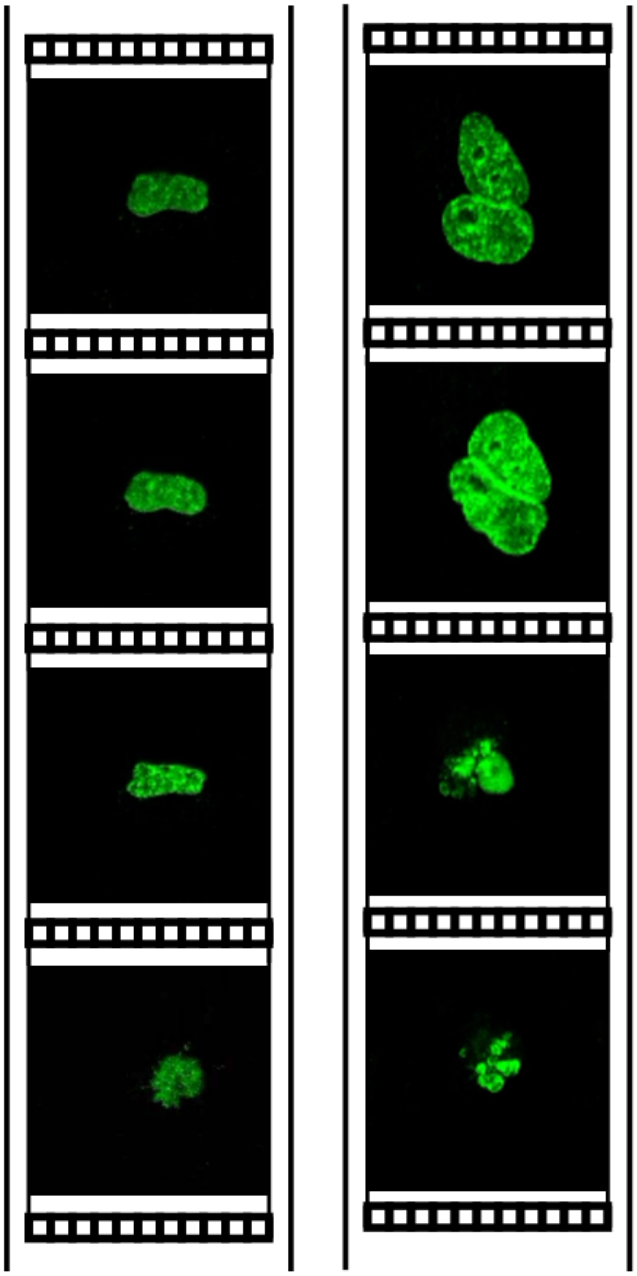

Fig. 37: Induction of apoptosis after induction of DSBs by I-*Sce*I. Live cell imaging film strips showing still images of cells undergoing apoptosis after transfection with pCMV-I-*Sce*I-3xNLS tracked over a period of 20h.

4 Discussion

4.1 Transfection approach versus repair pathway choice

Certain aspects of D-NHEJ are optimally studied using in vivo plasmid-based assays and standard cell transfection protocols. While these assays recapitulate important aspects of D-NHEJ, several reports show that they fail to reproduce the marked reduction in DNA end joining efficiency of genomic DSBs observed in a variety of D-NHEJ mutants. Here we report that much of this discrepancy derives from the transfection method used. We demonstrate that while plasmid electroporation generates plasmid end joining results in the different mutants closely reflecting rejoining of genomic DSBs, plasmid lipofection-generated results show a nearly wild type plasmid end joining efficiency in D-NHEJ mutants.

In experiments where transfections were performed with Lipofectamine™ reagent, the results exactly correspond to the earlier published results where not much variations or reductions were observed in the DNA end joining capacity of D-NHEJ deficient cells of Chinese hamster or rodent origin. We obtained, on the other hand, interesting results with the Nucleofector® technology, an electroporation method, where the manufacturer claims that conditions have been optimized for the DNA to be delivered directly into the nucleus, which seems to mimic the actual environment where DSBs occur. With this mode of transfection, we could demonstrate that the DNA end joining capability of D-NHEJ mutants was critically compromised in all of the *LIG4*$^{-/-}$, and *Ku80* and *DNA-PKcs*-mutants used.

We observed that the difference in rejoining efficiency of the *Ku80*-deficient *xrs-6* cells was not so pronounced between the two techniques as in the case of *LIG4* deficiency, and the *DNA-PKcs* mutant *XR-C1-3* cells, which show a large reduction in rejoining when tested with nucleofection, but only a marginal when tested with lipofection. The level of rejoining remained in *Ku80*-deficient cells low for both the techniques, although percent rejoining was nearly double to that seen after lipofection.

Although transfection and rejoining efficiencies varied from cell line to cell line and from experiment to experiment, when viewed from a wider perspective, the common interpretation that nucleofection provides a method better reflecting the response of the

mutants to genomic DSBs remains valid. To exclude that variations in the distribution of cells throughout the cell cycle caused the variations in rejoining efficiency observed with the different transfection methods, we checked in all individual experiments the cell cycle distribution by FACS analysis. In all experiments described here the amount of linear DNA transfected did not exceed 250ng, as higher amount caused saturation.

4.1.1 Determination of plasmid intracellular compartmentalization after lipofection and nucleofection

Careful analysis of results obtained from confocal imaging demonstrated that after lipofection, most of the transfected plasmid DNA fluorescence signal was localized in the cytoplasm in the form of aggregates with nuclear plasmid DNA aggregates present in some cells, which is in agreement with earlier reports that the transport of plasmid DNA into the nucleus in Lipofection depends on cell division. On the other hand, after nucleofection, no such inhibitions or demarcations were observed and DNA was localized randomly in the entire cell showing a markedly increased nuclear signal (See Fig. 17C).

To date, similar studies had not dealt with the analysis of the intracellular distribution of transfected plasmid, and confined themselves to the visualization of DNA aggregates inside the cell, often overlooking the high amount of diffuse signal in the nucleus or the cytoplasm. Hence, we decided to measure the distribution in the entire cell of CX-Rhodamine signal intensity, which would include both diffuse and aggregated DNA signals. Our intensity measurements data from in vivo DNA tracking experiments (Fig. 17C) were in agreement with earlier published results [149], but we observed that it was important to measure the signals (both diffuse and punctate) over the entire cell rather than focusing on the punctate DNA signals. We would conclude that the method of analysis employed in the present work provides a better basic mechanistic regarding the parameters determining the differences in NHEJ function observed between the two techniques.

On the basis of the above observation we hypothesize that the preferential delivery by nucleofection of plasmid DNA into the nucleus determines the fate of linearized plasmid DNA. One of the most prominent aspects of these experiments is that we always

observed higher transfection efficiencies for Nucleofection than for lipofection in all the cell lines tested. A word of caution here is that the transfection efficiencies are calculated with expression of GFP as an endpoint and not by the amount of DNA transported inside the cell. It is relevant that DNA tracking experiment show very similar intracellular transport of transfected plasmid after nucleofection and lipofection. This raises the question as to whether the intracellular plasmid localization also influences expression. According to a recent publication, where the authors trailed the microinjected DNA inside the nucleus and the cytoplasm, it was noted that plasmid in the cytoplasm is removed quickly and efficiently, whereas plasmid microinjected into the nucleus appears non motile [150].

It is possible that plasmid DNA transfected by lipid-based systems like Lipofectamine™ distribute mainly in the cytoplasm where it is acted upon by various cellular systems and be eventually discarded, damaged or degraded, reaching the nucleus with reduced efficiency and partially inactivated [150]. There is also a distinct possibility that improper compartmentalization of constructs remaining in cytoplasm may be acted upon by B-NHEJ generating thus the effects observed.

On the other hand, in Nucleofection, although the majority of the plasmid is transfected into the cytoplasm, a measurable amount is directly translocated into the nucleus. This extrachromosomal DNA may be compartmentalized and rendered non-motile by attachment to the nuclear matrix, thus protecting it somehow and making it available for processing by the nuclear DNA repair machinery. Thus, we speculate that when DNA is delivered quickly and efficiently into the nucleus, it remains in its original state without being acted upon by nucleases and that the DNA repair machinery can efficiently act upon in a manner similar to that of genomic DNA. The same may hold true for the subsequent expression. This may be the reason why D-NHEJ remains a key player, and why its deficiency is directly translated to major plasmid rejoining deficiencies in our nucleofection experiments.

4.1.2 Effect of nucleases on plasmid end joining assays performed using different transfection technologies

We further set out to examine whether the presence of nucleases in the cytoplasm or the nucleus of the cells had a role to play in the observed variations in NHEJ response. For this purpose, we treated cells with 100nM of the nuclease inhibitor ATA before transfection [151-154]. To our surprise, we could not reproduce the results published earlier with Lipofectamine^{TM} [151], as transfection with this reagent was close to completely inhibited after treatment of the cells with ATA. This may be due the inactivation by ATA of the reagent.

On the other hand, transfection was successful after nucleofection, but no significant differences were observed between the transfection efficiencies and percent rejoining in the presence or absence of ATA. Hence, these experiments failed to elucidate the possible role of nucleases in the effects under study. However, the results with ATA should be interpreted cautiously as ATA is not a very specific nuclease inhibitor and is also known to be a potent inhibitor of other cellular enzymes.

Another possibility worth introspecting and mentioning is that the plasmid system used here may be optimal for measuring DNA end joining in vivo, firstly, because the Pem-1 intron provides an excellent buffer region for normal DNA repair-associated deletion events without losing expression of EGFP. Secondly, the prospect that the construct harbors scaffold/matrix attachment sequences in the Pem1 intron may provide processing advantages and may generate a model system mimicking genomic DNA.

Thus, we conclude that proper compartmentalization of transfected plasmid in the cell nucleus is a prerequisite for assaying the function of D-NHEJ. In all other instances, the function of B-NHEJ is mainly assayed.

4.2 Models of complex lesions using special arrangements of I-*Sce*I recognition sites

4.2.1 Ionizing radiation induces clustered DNA damage

Energy deposition by ionizing radiation in the cell leads to several consequences, the most deleterious of which is its interaction with DNA, the basic unit of organization of a cell's genomic information. This energy deposition occurs within psec and leads to both direct and indirect interactions with DNA generating a vast array of damages. These damages include single strand breaks (SSBs), DSBs, sugar backbone and base damages along with other types of subtle damages like formation of heat labile sites[54] and probably other unknown types of damage. Due to this of induced damage, it is difficult to pin the type, which led to the observed effect. Whether the death of cells is due to additive effect from such damages, or whether only a certain forms of damage cause the cell mortality and other consequences is not known with certainty.

In addition, individual forms of damage, for example DSBs, can be of various configurations and can lead to deleterious effects not only depending on their location in the genome, but also their mutual spacing or their distance from other forms of damage. DNA lesions are not spread across the DNA molecule randomly, but they have a definite pattern that follows closely the pattern of energy deposition. As a result of this Multiple Damaged Sites (MDS) are generated. [14] Radiation physics clearly show that clustering of ionizations occurs with low LET radiation and predominates after high LET radiation. The consequences of this clustering are not yet known and are a topic of active investigation, but are thought to cause the higher efficacy of high LET radiation. Scientists have tried to model different kinds of lesions and their effects theoretically, but these models are conjectural and lack experimental base.

4.2.2 Designing an I-*Sce*I based model system to mimic clustered lesions

With this project, we set out to design and develop a model system for studying the ability of a cell to deal with simple and clustered DSBs.

We designed oligonucleotides with single I-*Sce*I sites along with oligos bearing pairs of I-*Sce*I sites placed either in direct or opposite orientation and separated by 200 bp. This distance was chosen because it represents the average amount of DNA accommodated

in one nucleosomal unit (including spacer region). We reasoned that when both sites are digested a situation destabilizing chromatin will be generated. It is known that DNA is wound in 1.7 turns around a nucleosome (see Figure 37). MDS clusters can spread across both strands of DNA, giving rise to damage separated by about 80-150 bp, which is nearly the length of DNA wrapped around the nucleosome.

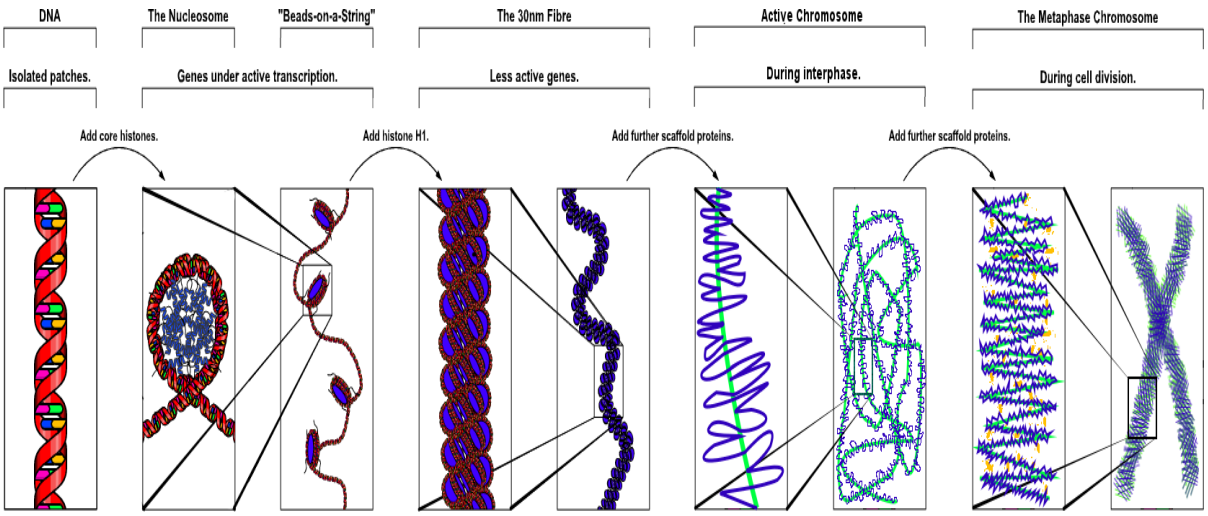

Fig. 37: Structure of Chromatin Organization. Courtesy www.molecularstation.com

For this study, we utilized homing endonucleases for induction of DSBs in the mammalian cell genome. There are numerous reports, which have either utilized random integration of the homing endonuclease site in the genome, or have performed targeted integration of such sites at specific chromosomal loci [155-159]. We differed from other studies by integrating a several pairs of I-*Sce*I sites in the cells and by employing different orientations and complexities. To maximize the number of integrations in the genome, we adapted the Sleeping Beauty Transposon system to our work.

4.2.3 Survival of clones bearing I-*Sce*I sites at different orientations

A goal of the project was to compare the biological effectiveness of single versus pairs of closely located DSBs. As is evident from the results, survival curves with clones

bearing single I-*Sce*I sites revealed that simple DSBs can be successfully handled by the cell showing no cell lethality even at relatively high numbers of integrations.

To increase the complexity of the damage and mimic the effects of high LET radiation, we designed oligonucleotides that sustain pairs of DSBs in close proximity (200bp). Assuming that both sites are cut at the same time and that the piece of DNA in between gets lost, a DSB will be generated that may pose greater problems to the cell than the single DSB. To further enhance the severity of the resulting DSB we varied the orientation of the I-*Sce*I sites to generate (after loss of the intervening piece of DNA) ends that were either compatible or incompatible to direct ligation.

Survival curves for clones with pairs of I-*Sce*I sites showed strong killing which appeared to increase with increasing number of integrations. Although it is tempting to speculate that DSBs with incompatible ends will have more severe biological effects than those with compatible ends, the results obtained thus far do allow such conclusion. Of course it is possible that DSBs with incompatible ends lead with a higher probability to deletions after repair, as our PCR indeed suggest, but more work will be need to arrive to more firm conclusions.

Damage caused by IR is thought to particularly complex within spurs and blobs leading to the formation of locally multiply damaged sites (LMDS). Increase in LET increases the number of spurs/blobs created at a given dose, which augments the severity of the inflicted damage to DNA. Spurs and blobs contain a number of ion pairs and have dimensions comparable to the DNA or even to small regions of chromatin. It is postulated that the average energy deposited in a spur is in the range of 100 eV. For low LET radiation, an average distance of 100 nm between two spurs is estimated, corresponding to a distance of approx. 300bp across a DNA molecule. This is similar to the 200bp of distance chosen in our work, vindicating thus our design. The distance of approximately 200 bps between the two DSBs may also prove to be more lethal than DSBs which are farther apart but this will need further experimentation. Nucleosome destabilization induced with this constellation of DSBs may result in local disruption of the nuclear architecture leading to disruption of various active processes like transcription, replication, etc. and may prove a hindrance to D-NHEJ or HRR.

Endonucleases are known to have preference for cutting at open chromatin sites like transcription start sites (TSS), and thus the chance of losing the intervening fragment becomes higher due to absence of nucleosomal arrangement at the site, leaving DNA sequences vulnerable to be lost in space. The scenarios originating from such breaks have not been investigated before and our study provides some tools in addressing such questions.

4.2.4 Correlation of G2-PCC results with colony formation assay

As observed in the colony formation experiments, extensive cell lethality is witnessed upon induction of DSBs by I-*Sce*I. Since classical cytogenetics did not allow the conclusive scoring of chromosomal aberrations at a number that would explain cell killing, we introduced the G2-PCC assay [143] with the objective of scoring aberrations in the G2 phase of the cell cycle before they get repaired, which would increase their number. Calyculin A induced G2-PCC was performed with various clones bearing I-*Sce*I sites in both compatible and incompatible orientations along with wild type A549 control. Although more chromosome damage was detected with this method, the breaks scored were present in low number in only few cells. The discrepancy between cell killing and formation of chromosome aberrations is puzzling and under investigation at present. As discussed below, we entertain the possibility that this is due to the loss to apoptosis of a large fraction of damaged cells.

4.2.4.1 β-AraA enhances G2-PCC breaks in clones bearing pairs of I-*Sce*I sites

As a further step, we used the known DNA synthesis inhibitor and potent radiosensitizer β-AraA [136, 137] in the G2-PCC assay[142]. We reasoned that treatment of cells with β-AraA would lead to inhibition of I-*Sce*I induced DSBs, which in turn would result in an increase in the number of G2-PCC breaks. Results obtained for G2-PCC after treatment with β-AraA showed increase in PCC breaks, but failed to reconciliate cell survival and chromosome aberration data. Similar conclusions could be drawn from the G2-PCC results obtained after treatment with hypertonic solution.

4.2.5 Closely spaced DSBs induced by I-*Sce*I lead to loss of the intervening sequence.

The results obtained by PCR on the fate of the intervening sequence between the two I-*Sce*I sites yielded very interesting results. The intervening sequence had not only been lost, but both I-*Sce*I sites were also lost along with some deletions both upstream and downstream of these sites. Other studies have reported loss of the intervening fragment between two homing endonuclease sites when excised simultaneously [91] [90]. In many model systems utilizing two I-*Sce*I sites for studying DSB repair, the loss of intervening sequence would restore a promoter or a fluorescence/antibiotic-resistance-conferring gene. The problem with such selection is that other events like end processing which disrupt completely the reporter genes go unnoticed, thus creating a bias on the outcome. It is likely that cells where end processing leads to larger deletions remain unreported.

We would like to hypothesize that loss of the fragment leads to a severe disruption of nuclear architecture, but it remains possible that cell with such deletion survive the insult. We do not know the frequency of such events, but it would be of interest to determine whether cell lethality depends on such events or whether it is induced by other more complex types of chromosome aberrations.

The results obtained with the PCR analysis of the ends after transfection with I-*Sce*I-expressing construct implicates error-prone canonical NHEJ in the repair of the induced DSBs, resulting in loss of nucleotides during the rejoining event as reported previously [91]. If the process of rejoining would have taken place by a pathway with unquestionable fidelity, the sites of I-*Sce*I would have been restored in case of non-simultaneous incision, or a single site of I-*Sce*I would have resulted in case of simultaneous cutting. It should be also kept in mind that the outcome of the rejoining event is dependent on the phase of the cell cycle where incision with I-*Sce*I takes place. Classical NHEJ is known to function predominantly in G1 phase of the cell cycle with HRR taking over in S and G2 phases [160]. It is possible that when these breaks are induced in G2 phase of the cell cycle, the outcome of simultaneous incision at the two sites and repair would yield a different configuration at the site, as HRR would strive to

restore the original sequence. This could explain our results of G2-PCC obtained with β-AraA, as some unpublished results from our group show that it inhibits HRR. Hence, treatment with β-AraA leads to inhibition of DSB processing, thus increasing G2-PCC breaks.

We speculate that cells may not be killed by the loss of the integral fragment as the lost sequence is a part of the integrated sequence and not part of their genome. However, disruption or destabilization of chromatin organization may be a reason for cell lethality.

4.2.6 No clear G2 checkpoint witnessed after I-*Sce*I-induced DSBs

Determination of G2-checkpoint activation by measuring the G2 phase content of cells over a period of 24 hours post transfection with the I-*Sce*I expression construct showed a slight increase in G2 content as compared to wild type A549 cells, but the increase was small and could not be interpreted on the basis of the potentially induced DSBs. This may be due to that fact that endonuclease-induced DSBs occur over a period of time (hours), depending on the expression of the construct and thus simultaneous presence of all DSBs is not possible. In this way the DSB threshold of approx. 20 DSBs [24, 161] required for the activation of the G2 checkpoint may not be reached. However, the possibility should also be entertained that most damage cells die of apoptosis and the observed accumulation of cells reflects a large proportion of untransfected cells.

4.2.7 No clear fluctuations in Mitotic Index after induction of I-*Sce*I DSBs

This method was employed to study the activation of G2 checkpoint on DSB induction, because the above described method is not sensitive enough for deciphering minor changes in checkpoint activation. Histone H3 phospho-Serine 10 staining is a sensitive assay for the determination of MI, which is an indirect indication of G2 checkpoint function. Results with this assay, although they occasionally showed a decrease in MI, the difference was not significant enough to draw any definitive conclusions. This result may arise due to the reasons discussed above.

4.2.8 Live cell imaging shows apoptosis in a majority of cells after expression of I-*Sce*I

Live cell imaging experiments performed with a construct expressing EGFP-53BP1 in clones bearing 8 pairs of I-*Sce*I sites showed an increase in EGFP-53BP1 foci when tracked over a period of 16-24 hours after transfection. An interesting phenomenon was witnessed in this experiment that may have important ramifications for the interpretation of many of the results presented above. We observed that the majority of cells which showed appearance of EGFP-53BP1 foci underwent apoptosis with only a few cells showing kinetics of appearance and disappearance of 53BP1 foci over a period of 24 hours. The tendency for apoptosis could explain the results with the colony and chromosome aberration formation, where extensive cell lethality is observed but chromosomal aberrations cannot be seen. Thus, effectively transfected cells may activate apoptotic signals and may not attempt repair. In any event, analysis of chromosome aberrations in an apoptotic cell is not possible.

Our work tests and partially confirms the hypothesis that clustering of DSBs at distances affecting nucleosomal stability may be highly lethal for the cell. With these results, it is clear that our attempt to model simple and complex lesions has achieved its share of success but would require further refinement to be able to answer some intriguing questions arising out of this study. The most important challenge is to confirm that apoptosis confounds the results obtained and to develop ways and means to overcome this limitation.

5 Conclusions

In our pursuit to decode and understand radiation induced damage response in mammalian cells without actually utilizing radiation, we designed the two studies, one involving linearized plasmids mimicking broken DNA whose rejoining can be quantified by fluorescent proteins in cells deficient in D-NHEJ pathway; the second on developing homing endonuclease-based model systems utilizing Sleeping Beauty Transposition for the study of simple and complex DNA lesions.

In our *in vivo* plasmid assay, end joining of lipofected DNA showed only a small dependence on *LIG4*, *DNA-PKcs* or *Ku* than in end joining of genomic DNA, whereas, end joining of nucleofected DNA showed a strong dependence on above mentioned D-NHEJ components. The preferential delivery by nucleofection of plasmid DNA into the nucleus probably determines the fate of linearized plasmid. Thus, proper compartmentalization of transfected plasmid in the cell nucleus is a prerequisite for assaying the function of D-NHEJ. On the other hand, in lipofection, where the plasmid DNA remains in the cytoplasm until the cell divides, the function of B-NHEJ is mainly assayed.

The results prove that nucleofection provides a method better reflecting the response of the mutants to genomic DSBs and hence is a technique of choice for studying DSB repair by plasmid rejoining *in vivo.*

Results from our second study show conclusively that increasing lesion complexity leads to increased cell lethality as cells with simple DSBs (single I-*Sce*I sites) showed no cell killing in complete contrast to the cells inflicted with complex DSBs (2 closely spaced I-*Sce*I sites). We also observed dose dependent effect of killing by I-*Sce*I-induced DSBs, i.e. clones with increasing numbers of integrations showed increased cell lethality in cell survival assays. We conclude that the breaks induced by I-*Sce*I probably led to nucleosome loss resulting in local disruption of chromatin, thus driving the cell to undergo apoptosis

Overall, the findings validate our model system for the study of the biological effects of complex DNA lesions and suggest a substantially enhanced killing potential for DSB pairs as compared to single DSBs, which are a hallmark of high LET radiation.

6 Future Strategies

Although results from our plasmid tracking experiment showed that plasmid localization after transfection is the key factor in determining the outcome of plasmid based DNA repair assays, mechanistic studies for determining whether the plasmid DNA is acted upon by different repair pathways when compartmentalized in different locations in the cell need to be carried out.

For the study of simple and complex lesions, initial designs of constructs included oligonucleotides with a single (simple lesions) or two I-*Sce*I sites (complex lesions) in different orientations separated by 200bp. Due to the clear difference observed between clones bearing single and pairs of DSBs, it would be interesting to vary the distances between the two I-*Sce*I sites to span two to four nucleosomes and determine the cellular response to such lesions. To add another degree of lesion complexity to the system, constructs can be designed bearing four or more I-*Sce*I sites separated by varied distances and orientations and integrating them in the genome using SB transposase. These lesions would in principle mimic clustered type of damage, which is a hallmark of high LET radiation. A targeted approach can also be adopted for integrating these constructs bearing varied lesion complexities in specific loci of chromosomes with fluorescence or antibiotic-based reporter assays to signal the induction of I-*Sce*I induced DSBs.

As extensively discussed in the thesis, the percentage of killing observed with clones bearing two sites in cell survival assay does not correlate to our G2-PCC data, which is surprising as it is known that cell lethality has a one to one correlation with asymmetrical chromosomal aberrations. It is imperative to determine the possible reasons for this effect. Live cell imaging experiments with EGFP-tagged 53BP1 gave some hints to the possibility of apoptosis playing a role in the extensive cell killing observed. For taking it to the next step, experiments would have to be performed to determine the extent of apoptosis and devise ways to prevent it. Experiments also need to be performed to rule

out the possibility that plasmid toxicity of the I-*Sce*I expression constructs is responsible for some of the effects observed on cell lethality and chromosomal aberration formation.

7 References

1. Khanna, K.K. and S.P. Jackson, *DNA double-strand breaks: signaling, repair and the cancer connection.* Nature Genetics, 2001. **27**: p. 247-254.
2. Ward, J.F., *DNA damage produced by ionizing radiation in mammalian cells: Identities, mechanisms of formation, and reparability.* Progress in Nucleic Acid Research, 1988. **35**: p. 95-125.
3. Ackland, S.P., et al., *Synergistic cytoxicity and DNA strand break formation by bromodeoxyuridine and bleomycin in human tumor cells.* Cancer Research, 1988. **48**: p. 4244-4249.
4. Povirk, L.F., et al., *Processing of 3'-Phosphoglycolate-terminated DNA Double Strand Breaks by Artemis Nuclease.* Journal of Biological Chemistry, 2007. **282**(6): p. 3547-3558.
5. Elmroth, K., et al., *Cleavage of cellular DNA by calicheamicin γI.* DNA Repair, 2003. **2**: p. 363-374.
6. Sato, K., N. Hieda-Shiomi, and H. Hama-Inaba, *X-ray-sensitive mutant mouse cells with various sensitivities to chemical mutagens.* Mutation Research, 1983. **121**: p. 281-285.
7. Mattern, M.R., et al., *Relationship between the intracellular effects of camptothecin and the inhibition of DNA topoisomerase I in cultured L1210 cells.* Cancer Research, 1987. **47**: p. 1793-1798.
8. Riches, L.C., A.M. Lynch, and N.J. Gooderham, *Early Events in the Mammalian Response to DNA Double-Strand Breaks.* Mutagenesis, 2008. **23**(5): p. 331-339.
9. Smart, D.J., et al., *Assessment of DNA double-strand breaks and [gamma]H2AX induced by the topoisomerase II poisons etoposide and mitoxantrone.* Mutation Research/Fundamental and Molecular Mechanisms of Mutagenesis, 2008. **641**(1-2): p. 43-47.
10. Richardson, C., N. Horikoshi, and T.K. Pandita, *The role of the DNA double-strand break response network in meiosis.* DNA Repair, 2004. **3**: p. 1149-1164.
11. Weaver, D.T., *V(D)J recombination and double-strand break repair.* Advances in Immunology, 1995. **58**: p. 29-85.
12. Bassing, C.H., W. Swat, and F.W. Alt, *The Mechanism and Regulation of Chromosomal V(D)J Recombination.* Cell, 2002. **109**: p. S45-S55.
13. Jackson, S.P. and J. Bartek, *The DNA-damage response in human biology and disease.* Nature, 2009. **461**(7267): p. 1071-1078.
14. Rydberg, B., *Radiation-induced DNA Damage and Chromatin Structure.* Acta Oncologica, 2001. **40**: p. 682-685.
15. Kanaar, R., J.H.J. Hoeijmakers, and D.C. van Gent, *Molecular mechanisms of DNA double-strand break repair.* Journal of Cell Biology, 1998. **8**: p. 483-489.
16. Paques, F. and J.E. Haber, *Multiple pathways of recombination induced by double-strand breaks in Saccharomyces cerevisiae.* Microbiology and Molecular Biology Reviews, 1999. **63**: p. 349-404.
17. Valerie, K. and L.F. Povirk, *Regulation and mechanisms of mammalian double-strand break repair.* Oncogene, 2003. **22**: p. 5792-5812.
18. Iliakis, G., *Backup pathways of NHEJ in cells of higher eukaryotes: Cell cycle dependence.* Radiotherapy and Oncology, 2009. **92**: p. 310-315.

19. Wang, H., et al., *DNA Ligase III as a Candidate Component of Backup Pathways of Nonhomologous End Joining.* Cancer Research, 2005. **65**(10): p. 4020-4030.
20. Audebert, M., B. Salles, and P. Calsou, *Involvement of Poly(ADP-ribose) Polymerase-1 and XRCC1/DNA Ligase III in an Alternative Route for DNA Double-strand Breaks Rejoining.* Journal of Biological Chemistry, 2004. **279**: p. 55117-55126.
21. You, Z. and J.M. Bailis, *DNA damage and decisions: CtIP coordinates DNA repair and cell cycle checkpoints.* Trends in Cell Biology, 2010. **20**(7): p. 402-409.
22. Sartori, A.A., et al., *Human CtIP promotes DNA end resection.* Nature, 2007. **450**: p. 509-514.
23. Takeda, S., et al., *Ctp1/CtIP and the MRN Complex Collaborate in the Initial Steps of Homologous Recombination.* Molecular Cell, 2007. **28**(3): p. 351-352.
24. Löbrich, M. and P.A. Jeggo, *The impact of a negligent G2/M checkpoint on genomic instability and cancer induction.* Nature Reviews. Cancer, 2007. **7**(11): p. 861-869.
25. Williams, R.S., et al., *Mre11 Dimers Coordinate DNA End Bridging and Nuclease Processing in Double-Strand-Break Repair.* Cell, 2008. **135**(1): p. 97-109.
26. Dupre, A., L. Boyer-Chatenet, and J. Gautier, *Two-step activation of ATM by DNA and the Mre11-Rad50-Nbs1 complex.* Nature Structural & Molecular Biology, 2006. **13**(5): p. 451-457.
27. Horejsi, Z., et al., *Distinct functional domains of Nbs1 modulate the timing and magnitude of ATM activation after low doses of ionizing radiation.* Oncogene, 2004. **23**: p. 3122-3127.
28. Paull, T.T. and J.-H. Lee, *The Mre11/Rad50/Nbs1 Complex and Its Role as a DNA Double-Strand Break Sensor for ATM.* Cell Cycle, 2005. **4**(6): p. e55-e58.
29. Zhang, X. and T.T. Paull, *The Mre11/Rad50/Xrs2 complex and non-homologous end-joining of incompatible ends in S. cerevisiae.* DNA Repair, 2005. **4**(11): p. 1281-1294.
30. Williams, R.S., J.S. Williams, and J.A. Tainer, *Mre11-Rad50-Nbs1 is a keystone complex connecting DNA repair machinery, double-strand break signaling, and the chromatin template.* Biochemistry and Cell Biology, 2007. **85**: p. 509-520.
31. Cherry, S.M., et al., *The Mre11 Complex Influences DNA Repair, Synapsis, and Crossing Over in Murine Meiosis.* Current Biology, 2007. **17**: p. 373-378.
32. Downs, J.A. and S.P. Jackson, *A means to a DNA end: The many roles of Ku.* Nature Reviews. Molecular Cell Biology, 2004. **5**: p. 367-378.
33. Morio, T. and H. Kim, *Ku, Artemis, and ataxia-telangiectasia-mutated: Signalling networks in DNA damage.* International Journal of Biochemistry & Cell Biology, 2008. **40**(4): p. 598-603.
34. Kinner, A., et al., *γ-H2AX in recognition and signaling of DNA double-strand breaks in the context of chromatin.* Nucleic Acids Research, 2008. **36**(17): p. 5678-5694.
35. Stiff, T., et al., *ATM and DNA-PK function redundantly to phosphorylate H2AX after exposure to ionizing radiation.* Cancer Research, 2004. **64**: p. 2390-2396.
36. Rogakou, E.P., et al., *DNA double-stranded breaks induce histone H2AX phosphorylation on serine 139.* Journal of Biological Chemistry, 1998. **273**: p. 5858-5868.
37. Zgheib, O., et al., *An Oligomerized 53BP1 Tudor Domain Suffices for Recognition of DNA Double-Strand Breaks.* Molecular and Cellular Biology, 2009. **29**(4): p. 1050-1058.
38. Schultz, L.B., et al., *p53 binding protein 1 (53BP1) is an early participant in the cellular response to DNA double-strand breaks.* Journal of Cell Biology, 2000. **151**: p. 1381-1390.
39. Mochan, T.A., et al., *53BP1, an activator of ATM in response to DNA damage.* DNA Repair, 2004. **3**: p. 945-952.
40. Costanzo, V., et al., *Mre11 Assembles Linear DNA Fragments into DNA Damage Signaling Complexes.* PLoS Biology, 2004. **2**: p. 600-609.

41. Callebaut, I., et al., *Cernunnos Interacts with the XRCC4{middle dot}DNA-ligase IV Complex and Is Homologous to the Yeast Nonhomologous End-joining Factor Nej1.* Journal of Biological Chemistry, 2006. **281**(20): p. 13857-13860.
42. Wang, H., et al., *Genetic evidence for the involvement of DNA ligase IV in the DNA-PK-dependent pathway of non-homologous end joining in mammalian cells.* Nucleic Acids Research, 2001. **29**: p. 1653-1660.
43. Grawunder, U., et al., *Activity of DNA ligase IV stimulated by complex formation with XRCC4 protein in mammalian cells.* Nature, 1997. **388**: p. 492-495.
44. Ahnesorg, P., P. Smith, and S.P. Jackson, *XLF Interacts with the XRCC4-DNA Ligase IV Complex to Promote DNA Nonhomologous End-Joining.* Cell, 2006. **124**(2): p. 301-313.
45. Yano, K.-i., K. Morotomi-Yano, and H. Akiyama, *Cernunnos/XLF: A new player in DNA double-strand break repair.* International Journal of Biochemistry & Cell Biology, 2009. **41**(6): p. 1237-1240.
46. Malivert, L., et al., *The C-Terminal Domain of Cernunnos/XLF Is Dispensable for DNA Repair In Vivo.* Molecular and Cellular Biology, 2009. **29**(5): p. 1116-1122.
47. Audebert, M., et al., *Involvement of Polynucleotide Kinase in a Poly(ADP-ribose) Polymerase-1-dependent DNA Double-strand Breaks Rejoining Pathway.* Journal of Molecular Biology, 2006. **356**: p. 257-265.
48. Goodhead, D.T., *Initial events in the cellular effects of ionizing radiations: clustered damage in DNA.* International Journal of Radiation Biology, 1994. **65**(1): p. 7-17.
49. Goodhead, D.T., *Molecular and cell models of biological effects of heavy ion radiation.* Radiation and Environmental Biophysics, 1995. **34**: p. 67-72.
50. Nikjoo, H., D.E. Charlton, and D.T. Goodhead, *Monte Carlo Track Structure Studies of Energy Deposition and Calculation of Initial DSB and RBE.* Advances in Space Research, 1994. **14**(10): p. 10161-10180.
51. Goodhead, D.T., et al. *Current Biophysical Approaches to the Understanding of Biological Effects of Radiation in Terms of Local Energy Deposition.* in *Fifth Symposium on Neutron Dosimetry*. 1985: European Commission.
52. Lafleur, M.V.M., J. Woldhuis, and H. Loman, *Alkali-labile sites and post-irradiation effects in gamma-irradiated biologically active double-stranded DNA in aqueous solution.* International Journal of Radiation Biology 1979. **36**(3): p. 241-247.
53. Karlsson, K.H., et al., *Repair of Radiation-Induced Heat-Labile Sites is Independent of DNA-PKcs, XRCC1 and PARP.* Radiation Research, 2008. **169**: p. 506-512.
54. Singh, S.K., et al., *Extensive Repair of DNA Double-Strand Breaks in Cells Deficient in the DNA-PK Dependent Pathway of NHEJ after Exclusion of Heat-Labile Sites.* Radiation Research, 2009. **172**: p. 152-164.
55. Sutherland, R.M., et al., *Clustered DNA Damages Induced by X Rays in Human Cells.* Radiation Research, 2002. **157**: p. 611-616.
56. Sutherland, B.M., et al., *Clustered DNA damages induced in isolated DNA and in human cells by low doses of ionizing radiation.* Proceedings of the National Academy of Sciences of the United States of America, 2000. **97**: p. 103-108.
57. Paap, B., D.M. Wilson III, and B.M. Sutherland, *Human abasic endonuclease action on multilesion abasic clusters: implications for radaition-induced biological damage.* Nucleic Acids Research, 2008. **36**(8): p. 2717-2727.
58. Hada, M. and A.G. Georgakilas, *Formation of Clustered DNA Damage after High-LET Irradiation: A Review.* Journal of Radiation Research, 2008. **49**(3): p. 203-210.
59. Hagen, U., *Biochemical aspects of radiation biology.* Experientia, 1989. **45**: p. 7-12.

60. Anderson, R.M., et al., *Effect of Linear Energy Transfer (LET) on the Complexity of α-Particle-Induced Chromosome Aberrations in Human CD34^{+} Cells.* Radiation Research, 2007. **167**: p. 541-550.
61. Kadhim, M.A., M.A. Hill, and S.R. Moore, *Genomic instability and the role of radiation quality.* Radiation Protection Dosimetry, 2006. **122**(1-4): p. 221-227.
62. Goodhead, D.T. and H. Nikjoo, *Track structure analysis of ultrasoft X-rays compared to high- and low-LET radiations.* International Journal of Radiation Biology 1989. **55**(4): p. 513-529.
63. Nikjoo, H., et al., *Quantitative modelling of DNA damage using Monte Carlo track structure method.* Radiation and Environmental Biophysics, 1999. **38**: p. 31-38.
64. Goodhead, D.T., *Energy deposition stochastics and track structure: what about the target?* Radiation Protection Dosimetry, 2006. **122**(1-4): p. 3-15.
65. Goodhead, D., *Radiation Tracks in Biological Materials: Initial Damage in Cells, DNA and Associated Structures*, in *Genes, Cancer and Radiation Protection*, M.L. Mendelsohn, Editor. 1992, National Council of Radiation Protection and Measurements: Bethesda, MD, USA. p. 25-37.
66. Nikjoo, H. and D.T. Goodhead, *Track structure analysis illustrating the prominent role of low-energy electrons in radiobiological effects of low-LET radiations.* Physics in Medicine and Biology, 1991. **36**(2): p. 229-238.
67. Cucinotta, F.A., H. Nikjoo, and D.T. Goodhead, *Applications of amorphous track models in radiation biology.* Radiation and Environmental Biophysics, 1999. **38**: p. 81-92.
68. Tsao, D., et al., *Induction and Processing of Oxidative Clustered DNA Lesions in ^{56}Fe-Ion-Irradiated Human Monocytes.* Radiation Research, 2007. **168**: p. 87-97.
69. Ward, J.F., *Biochemistry of DNA lesions.* Radiation Research, 1985. **104**: p. S103-S111.
70. Rydberg, B., *Clusters of DNA damage induced by ionizing radiation: Formation of short DNA fragments. 11. Experimental detection.* Radiation Research, 1996. **145**: p. 200-209.
71. Barendsen, G.W., *RBE-LET relationships for different types of lethal radiation damage in mammalian cells: comparison with DNA dsb and an interpretation of differences in radiosensitivity.* International Journal of Radiation Biology, 1994. **66**: p. 433-436.
72. Charlton, D.E., H. Nikjoo, and J.L. Humm, *Calculation of initial yields of single- and double-strand breaks in cell nuclei from electrons, protons and alpha particles.* International Journal of Radiation Biology 1989. **56**(1): p. 1-19.
73. Holley, W.R. and A. Chatterjee, *Clusters of DNA damage induced by ionizing radiation: Formation of short DNA fragments. 1. Theoretical modeling.* Radiation Research, 1996. **145**: p. 188-199.
74. Pomplun, E. and M. Terrissol, *Low-energy electrons inside active DNA models: a tool to elucidate the radiation action mechanisms.* Radiation and Environmental Biophysics, 1994. **33**: p. 279-292.
75. Johnston, P.J. and P.E. Bryant, *A component of DNA double-strand break repair is dependent on the spatial orientation of the lesions within the higher-order structures of chromatin.* International Journal of Radiation Biology, 1994. **66**: p. 531-536.
76. Johnston, P.J., et al., *Higher-Order Chromatin Structure-Dependent Repair of DNA Double-Strand Breaks: Involvement of the V(D)J Recombination Double-Strand Break Repair Pathway.* Radiation Research, 1998. **149**: p. 455-462.
77. Bryant, P.E. and P.J. Johnston, *Restriction-endonuclease-induced DNA double-strand breaks and chromosomal aberrations in mammalian cells.* Mutation Research, 1993. **299**: p. 289-296.

78. Johnston, P.J., P.L. Olive, and P.E. Bryant, *Higher-Order Chromatin Structure-Dependent Repair of DNA Double-Strand Breaks: Modeling the Elution of DNA from Nucleoids.* Radiation Research, 1997. **148**: p. 561-567.
79. Rouet, P., F. Smih, and M. Jasin, *Expression of a site-specific endonuclease stimulates homologous recombination in mammalian cells.* Proceedings of the National Academy of Sciences of the United States of America, 1994. **91**: p. 6064-6068.
80. Jasin, M., *Genetic manipulation of genomes with rare-cutting endonucleases.* Trends in Genetics, 1996. **12**: p. 224-228.
81. Jasin, M., M.E. Moynahan, and C. Richardson, *Targeted transgenesis.* Proceedings of the National Academy of Sciences of the United States of America, 1996. **93**: p. 8804-8808.
82. Soutoglou, E., et al., *Positional stability of single double-strand breaks in mammalian cells.* Nature Cell Biology, 2007. **9**(6): p. 675-682.
83. Berkovich, E., R.J. Monnat Jr., and M.B. Kastan, *Roles of ATM and NBS1 in chromatin structure modulation and DNA double-strand break repair.* Nature Cell Biology, 2007. **9**(6): p. 683-690.
84. Guirouilh-Barbat, J., et al., *Defects in XRCC4 and KU80 differentially affect the joining of distal nonhomologous ends.* Proceedings of the National Academy of Sciences of the United States of America, 2007. **104**(52): p. 20902-20907.
85. Schulte-Uentrop, L., et al., *Distinct roles of XRCC4 and Ku80 in non-homologous end-joining of endonuclease- and ionizing radiation-induced DNA double-strand breaks.* Nucleic Acids Research, 2008. **36**(8): p. 2561-2569.
86. Bennardo, N., et al., *Alternative-NHEJ Is a Mechanistically Distinct Pathway of Mammalian Chromosome Break Repair.* PLoS Genetics, 2008. **4**(6): p. e1000110.
87. Bennardo, N., et al., *Limiting the Persistence of a Chromosome Break Diminishes Its Mutagenic Potential.* PLoS Genet, 2009. **5**(10): p. e1000683.
88. Cui, X. and K. Meek, *Linking double-stranded DNA breaks to the recombination activating gene complex directs repair to the nonhomologous end-joining pathway.* Proceedings of the National Academy of Sciences of the United States of America, 2007. **104**(43): p. 17046-17051.
89. Dodson, H. and C.G. Morrison, *Increased sister chromatid cohesion and DNA damage response factor localization at an enzyme-induced DNA double-strand break in vertebrate cells.* Nucleic Acids Research, 2009. **37**(18): p. 6054-6063.
90. Boubakour-Azzouz, I. and M. Ricchetti, *Low joining efficiency and non-conservative repair of two distant double-strand breaks in mouse embryonic stem cells.* DNA Repair, 2008. **7**(2): p. 149-161.
91. Honma, M., et al., *Non-homologous end-joining for repairing I-SceI-induced DNA double strand breaks in human cells.* DNA Repair, 2007. **6**(6): p. 781-788.
92. Wang, H., et al., *Caffeine inhibits homology-directed repair of I-SceI-induced DNA double-strand breaks.* Oncogene, 2004. **23**: p. 824-834.
93. Rouet, P., F. Smih, and M. Jasin, *Introduction of double-strand breaks into the genome of mouse cells by expression of a rare-cutting endonuclease.* Molecular and Cellular Biology, 1994. **14**: p. 8096-8106.
94. Donoho, G., M. Jasin, and P. Berg, *Analysis of gene targeting and intrachromosomal homologous recombination stimulated by genomic double-strand breaks in mouse embryonic stem cells.* Molecular and Cellular Biology, 1998. **18**: p. 4070-4078.
95. Chevalier, B.S. and B.L. Stoddard, *Homing endonucleases: structural and functional insight into the catalysts of intron/intein mobility.* Nucleic Acids Research, 2001. **29**(18): p. 3757-3774.

96. Perrin, A., M. Buckle, and B. Dujon, *Asymmetrical recognition and activity of the I-SceI endonuclease on its site and on intron - exon junctions.* EMBO Journal, 1993. **12**: p. 2939-2947.
97. Arnould, S., et al., *Engineered I-CreI Derivatives Cleaving Sequences from the Human XPC Gene can Induce Highly Efficient Gene Correction in Mammalian Cells.* Journal of Molecular Biology, 2007. **371**(1): p. 49-65.
98. Choulika, A., et al., *Induction of homologous recombination in mammalian chromosomes by using the I-SceI system of Saccharomyces cerevisiae.* Molecular and Cellular Biology, 1995. **15**(4): p. 1968-73.
99. Sargent, R.G., M.A. Brenneman, and J.H. Wilson, *Repair of site-specific double-strand breaks in a mammalian chromosome by homologous and illegitimate recombination.* Molecular and Cellular Biology, 1997. **17**(1): p. 267-77.
100. Bellaiche, Y., V. Mogila, and N. Perrimon, *I-SceI Endonuclease, a New Tool for Studying DNA Double-Strand Breaks Repair Mechanisms in Drosophila.* Genetics, 1999. **152**: p. 1037-1044.
101. Brenneman, M., F.S. Gimble, and J.H. Wilson, *Stimulation of intrachromosomal homologous recombination in human cells by electroporation with site-specific endonucleases.* Proceedings of the National Academy of Sciences of the United States of America, 1996. **93**: p. 3608-3612.
102. Liang, F., et al., *Homology-directed repair is a major double-strand break repair pathway in mammalian cells.* Proceedings of the National Academy of Sciences of the United States of America, 1998. **95**: p. 5172-5177.
103. Rebuzzini, P., et al., *New mammalian cellular systems to study mutations introduced at the break site by non-homologous end-joining.* DNA Repair, 2005. **4**(5): p. 546-555.
104. Ivics, Z. and Z. Izsvak, *Transposable Elements for Transgenesis and Insertional Mutagenesis in Vertebrates.* Methods in Molecular Biology, 2004. **260**: p. 255-276.
105. Ivics, Z., et al., *The Sleeping Beauty Transposable Element: Evolution, Regulation and Genetic Applications.* Current Issues in Molecular Biology, 2004. **6**: p. 43-56.
106. Flavell, A.J., *Long terminal repeat retrotransposons jump between species.* Proceedings of the National Academy of Sciences of the United States of America, 1999. **96**(22): p. 12211-12212.
107. Matsutani, S., *Links Between Repeated Sequences.* Journal of Biomedicine and Biotechnology, 2006. **2006**: p. 1-3.
108. Yang, G., et al., *Tuned for Transposition: Molecular Determinants Underlying the Hyperactivity of a Stowaway MITE.* Science, 2009. **325**(5946): p. 1391-1394.
109. Wicker, T., et al., *A unified classification system for eukaryotic transposable elements.* Nature Reviews. Genetics, 2007. **8**(12): p. 973-982.
110. Ivics, Z., et al., *Molecular Recontruction of Sleeping Beauty, a Tc1-like Transposon from Fish, and Its Transposition in Human Cells.* Cell, 1997. **91**: p. 501-510.
111. Zayed, H., et al., *Development of Hyperactive Sleeping Beauty Transposon Vectors by Mutational Analysis.* Molecular Therapy, 2004. **9**: p. 292-304.
112. Izsvak, Z. and Z. Ivics, *Sleeping Beauty Transposition: Biology and Applications for Molecular Therapy.* Molecular Therapy, 2004. **9**: p. 147-156.
113. Vigdal, T.J., et al., *Common Physical Properties of DNA Affecting Target Site Selection of Sleeping Beauty and other Tc1/mariner Transposable Elements.* Journal of Molecular Biology, 2002. **323**(3): p. 441-452.
114. Izsvak, Z., et al., *Healing the Wounds Inflicted by Sleeping Beauty Transposition by Double-Strand Break Repair in Mammalian Somatic Cells.* Molecular Cell, 2004. **13**: p. 279-290.

115. Verkaik, N.S., et al., *Different types of V(D)J recombination and end-joining defects in DNA double-strand break repair mutant mammalian cells.* European Journal of Immunology, 2002. **32**: p. 701-709.
116. Secretan, M.B., et al., *Effect of Ku86 and DNA-PKcs deficiency on non-homologous end-joining and homologous recombination using a transient transfection assay.* Mutation Research, 2004. **554**: p. 351-364.
117. Roth, D.B. and J.H. Wilson, *Relative rates of homologous and nonhomologous recombination in transfected DNA.* Proceedings of the National Academy of Sciences of the United States of America, 1985. **82**: p. 3355-3359.
118. Roth, D.B. and J.H. Wilson, *Nonhomologous recombination in mammalian cells: Role for short sequence homologies in the joining reaction.* Molecular and Cellular Biology, 1986. **6**: p. 4295-4304.
119. Kabotyanski, E.B., et al., *Double-strand break repair in Ku86- and XRCC4-deficient cells.* Nucleic Acids Research, 1998. **26**: p. 5333-5342.
120. Liang, F. and M. Jasin, *Ku80-deficient cells exhibit excess degradation of extrachromosomal DNA.* Journal of Biological Chemistry, 1996. **271**(24): p. 14405-14411.
121. Smith-Ravin, J. and P.A. Jeggo, *Use of damaged plasmid to study DNA repair in X-ray sensitive (xrs) strains of Chinese hamster ovary (CHO) cells.* International Journal of Radiation Biology, 1989. **56**: p. 951-961.
122. Bühler, B., G. Köhler, and P.J. Nielsen, *Efficient nonhomologous and homologous recombination in scid cells.* Immunogenetics, 1995. **42**: p. 181-187.
123. Morrison, C. and E. Wagner, *Extrachromosomal recombination occurs efficiently in cells defective in various DNA repair systems.* Nucleic Acids Research, 1996. **24**(11): p. 2053-2058.
124. North, P., A. Ganesh, and J. Thacker, *The rejoining of double-strand breaks in DNA by human cell extracts.* Nucleic Acids Research, 1990. **18**: p. 6205-6210.
125. Baekelandt, V., et al., *DNA-Dependent Protein Kinase Is Not Required for Efficient Lentivirus Integration.* Journal of Virology, 2000. **74**(23): p. 11278-11285.
126. Tzung, T.-Y. and T.M. Rünger, *Reduced joining of DNA double strand breaks with an abnormal mutation spectrum in rodent mutants of DNA-PKcs and Ku80.* International Journal of Radiation Biology, 1998. **73**: p. 469-474.
127. Collis, S.J., et al., *Development of a novel rapid assay to assess the fidelity of DNA double-strand-break repair in human tumour cells.* Nucleic Acids Research, 2002. **30**(2).
128. Daniel, R., R.A. Katz, and A.M. Skalka, *A Role for DNA-PK in Retroviral DNA Integration.* Science, 1999. **284**: p. 644-647.
129. Felgner, P.L., et al., *Lipofection: A highly efficient, lipid-mediated DNA-transfection procedure.* Proceedings of the National Academy of Sciences of the United States of America, 1987. **84**: p. 7413-7417.
130. Seluanov, A., et al., *DNA end joining becomes less efficient and more error-prone during cellular senescence.* Proceedings of the National Academy of Sciences of the United States of America, 2004. **101**: p. 7624-7629.
131. Miskey, C., et al., *DNA transposons in vertebrate functional genomics.* Cellular and Molecular Life Sciences, 2005. **62**: p. 629-641.
132. Izsvak, Z. and Z. Ivics, *Sleeping Beaty hits them all: transposon-mediated saturation mutagenesis in the mouse germline.* Nature Methods, 2005. **2**(10): p. 735-736.
133. Frank, K.M., et al., *DNA ligase IV deficiency in mice leads to defective neurogenesis and embryonic lethality via the p53 pathway.* Molecular Cell, 2000. **5**: p. 993-1002.

134. Jeggo, P.A. and L.M. Kemp, *X-ray-sensitive mutants of Chinese hamster ovary cell line. Isolation and cross-sensitivity to other DNA-damaging agents.* Mutation Research, 1983. **112**: p. 313-327.
135. Ross, G.M., et al., *DNA strand break rejoining defect in xrs-6 is complemented by transfection with the human Ku80 gene.* Cancer Research, 1995. **55**: p. 1235-1238.
136. Iliakis, G. and P.E. Bryant, *Effects of the nucleoside analogues α-araA, β-araA and β-araC on cell growth and repair of both potentially lethal damage and DNA double strand breaks in mammalian cells in culture.* Anticancer Research, 1983. **3**: p. 143-150.
137. Iliakis, G., et al., *Comparative studies on repair inhibition by AraA, AraC and aphidicolin of radiation induced DNA and chromosome damage in rodent cells: Comparison with fixation of PLD.* International Journal of Radiation Oncology Biology Physics, 1989. **16**.
138. Stenerlöw, B., et al., *Clonogenic cell survival and rejoining of DNA double-strand breaks: comparisons between three cell lines after photon or He ion irraditaion.* International Journal of Radiation Biology, 1994. **65**: p. 631-639.
139. Bryant, P.E., *9-ß-D-arabinofuranosyladenine increases the frequency of x-ray induced chromosome abnormalities in mammalian cells.* International Journal of Radiation Biology, 1983. **43, No. 4**: p. 459-464.
140. Iliakis, G., et al., *Hypertonic treatment during premature chromosome condensation allows visualization of interphase chromosome breaks repaired with fast kinetics in irradiated CHO cells.* Radiation Research, 1993. **135**: p. 160-170.
141. Okayasu, R., J. Varlotto, and G. Iliakis, *Hypertonic treatment does not affect the radiation yield of interphase chromosome breaks in DNA double-strand break repair deficient xrs-5 cells.* Radiation Research, 1993. **135**: p. 171-177.
142. Tosuji, H., N. Fusetani, and Y. Seki, *Calyculin A causes the activation of histone H_1 kinase and condensation of chromosomes in unfertilized sea urchin eggs independently of the maturation-promoting factor.* Comparative Biochemistry and Physiology. C: Comparative Pharmacology, 2003. **135**: p. 415-424.
143. Terzoudi, G.I., et al., *Premature chromosome condensation reveals DNA-PK independent pathways of chromosome break repair.* International Journal of Oncology, 2008. **31**(1): p. 145-152.
144. Canman, C.E., et al., *The p53-dependent G1 cell cycle checkpoint pathway and ataxia-telangiectasia.* Cancer Research, 1994. **54**: p. 5054-5058.
145. Krohn, M., et al., *The G1-S checkpoint in fission yeast is not a general DNA damage checkpoint.* J Cell Sci, 2008. **121**(24): p. 4047-4054.
146. Barratt, R.A., et al., *The G_2 block induced by DNA damage: a caffeine-resistant component independent of Cdc25C, MPM-2 phosphorylation, and H1 kinase activity.* Cancer Research, 1998. **58**: p. 2639-2645.
147. Juan, G., et al., *Histone H3 Phosphorylation and Expression of Cyclins A and B1 Measured in Individual Cells During Their Progression Through G_2 and Mitosis.* Cytometry, 1998. **32**: p. 71-77.
148. Halazonetis, T.D., V.G. Gorgoulis, and J. Bartek, *An Oncogene-Induced DNA Damage Model for Cancer Development.* Science, 2008. **319**(5868): p. 1352-1355.
149. Pastwa, E., et al., *DNA uptake and repair enzyme access to transfected DNA is under reported by gene expression.* Biochemical and Biophysical Research Communications, 2003. **306**: p. 421-429.
150. Shimizu, N., F. Kamezaki, and S. Shigematsu, *Tracking of microinjected DNA in live cells reveals the intracellular behavior and elimination of extrachromosomal genetic material.* Nucleic Acids Research, 2005. **33**(19): p. 6296-6307.

151. Hoffman, E.A., et al., *Barriers to productive transfection of trabecular meshwork cells.* Molecular Vision, 2005. **11**: p. 869-875.
152. Glasspool-Malone, J., et al., *DNA transfection of macaque and murine respiratory tissue is greatly enhanced by use of a nuclease inhibitor.* Journal of Gene Medicine, 2002. **4**: p. 323-332.
153. Walther, W., et al., *Use of the nuclease inhibitor aurintricarboxylic acid (ATA) for improved non-viral intratumoral in vivo gene transfer by jet-injection.* Journal of Gene Medicine, 2005. **7**: p. 477-485.
154. Hallick, R.B., et al., *Use of aurintricarboxylic acid as an inhibitor of nucleases during nucleic acid isolation.* Nucleic Acids Research, 1977. **4**(9): p. 3055-3064.
155. Simsek, D. and M. Jasin, *Alternative end-joining is suppressed by the canonical NHEJ component Xrcc4-ligase IV during chromosomal translocation formation.* Nature Structural & Molecular Biology, 2010. **17**(4): p. 410-416.
156. Weinstock, D.M., E. Brunet, and M. Jasin, *Formation of NHEJ-derived reciprocal chromosomal translocations does not require Ku70.* Nature Cell Biology, 2007. **9**(8): p. 978-981.
157. Weinstock, D.M., et al., *Assaying Double-Strand Break Repair Pathway Choice in Mammalian Cells Using a Targeted Endonuclease or the RAG Recombinase.* Methods in Enzymology, 2006. **409**: p. 524-540.
158. Weinstock, D.M., et al., *Modeling oncogenic translocations: Distinct roles for double-strand break repair pathways in translocation formation in mammalian cells.* DNA Repair, 2006. **5**(9-10): p. 1065-1074.
159. Coquelle, A., et al., *Induction of multiple double-strand breaks within an hsr by meganuclease I-SceI expression or fragile site activation leads to formation of double minutes and other chromosomal rearrangements.* Oncogene, 2002. **21**: p. 7671-7679.
160. Tamulevicius, P., M. Wang, and G. Iliakis, *Homology-Directed Repair is Required for the Development of Radioresistance during S Phase: Interplay between Double-Strand Break Repair and Checkpoint Response.* Radiation Research, 2007. **167**: p. 1-11.
161. Deckbar, D., et al., *Chromosome breakage after G2 checkpoint release.* Journal of Cell Biology, 2007. **176**(6): p. 749-755.
162. Tanaka, T., et al., *ATM activation accompanies histone H2AX phosphorylation in A549 cells upon exposure to tobacco smoke.* BMC Cell Biology, 2007. **8**: p. 26.

8 Appendix

Appendix 1: Settings for bivariate flow cytometry

Flow cytometry: COULTER EPICS XL
Sheath Speed: middle
Total cells sampled: 20000
Maximal running duration: 900 seconds
Working mode: Manual

Program/Parameter	DNA-PI H3-pS10-FITC
FS-PMT (volt)	55
FS-Gain	2
SS-PMT (volt)	400
SS-Gain	1
AUX-PMT (volt)	300
AUX-Gain	2
Excitation of PI	488 nm
PI-Filter spectrum	655-735 nm
PI-PMT (volt)	520
PI-Gain	2
PI-Signal	Linear
PI-GATE	Single cell
Discriminator	PI>3
Excitation of FITC	488 nm
FITC Filter	490-550 nm
FITC-PMT (volt)	520
FITC-Gain	2
FITC-Signal	Linear
FITC-GATE	FITC positive

Appendix 2: Antibody dilution for bivariate flow cytometry

Protein Name	Primary Antibody	Secondary Antibody
H3-pS10	mAb 1:200	FITC 1:300

Appendix 3: Settings for Confocal microscope and Imaris® software

Settings for Leica TCS SP5 Confocal microscope

Instrument Parameter Setting: Confocal LDM
Argon laser intensity: 50%
Objective: HCX PL APO lambda blue 63.0x1.40 OIL UV
Speed: 400Hz
Image size: 246.03 µm x 246.03 µm

Pixel size: 481.46 nm x 481.47nm

Sequential Scan: Between stacks
Scan direction: Bidirectional
.
Step size: 0.5 µm
Resolution: 512x512

Program/Parameter	DAPI	γ-H2AX Alexa 568
Excitation	405 nm	488 nm
Laser Intensity	16%	23%
Filter Range	410-550 nm	495-550 nm
PMT	850 V	540 V
Smart Gain Offset	-2%	-5%
Minimal Foci Size (Imaris®)		0.5 µm
Threshold setting for Imaris®		17

Buffers and Solutions

Appendix 4: Tissue culture and flow cytometry

1x Phosphate Buffered Saline (PBS)

Dissolve the following in 800ml Double distilled water (ddH_2O).

8 g of NaCl

0.2 g of KCl

1.44 g of Na_2HPO_4

0.24 g of KH_2PO_4

Adjust pH to 7.4. Adjust volume to 1L with additional ddH_2O. Sterilize by autoclaving and store at 4°C.

Trypsin-EDTA (Trypsin 0.05%, EDTA 0.02%)

0.5 g of Trypsin

0.2 g of EDTA

Adjust the volume to 1L with 1x PBS.

Sterilize by passing through 0.22 µm filter and store at -20 °C.

Sodium azide (NaN_3 0.02%)

10 g of NaN_3

Adjust the volume to 100 ml with ddH_2O.

Store at RT.

Freezing Solution A

5mM KH_2PO_4

25mM KOH

30mM NaCl

20mM L (+) lactic acid

5mM Dextrose

0.5mM $MgCl_2$

200mM Sorbitol in Milli-Q

Freezing Solution B

5mM KH_2PO_4

25mM KOH

30mM NaCl

20mM L (+) lactic acid

5mM Dextrose

0.5mM $MgCl_2$

200mM Sorbitol in 80% Milli-Q and 20% DMSO

BrdU stock solution (10mM)

0.307 g of BrdU.

Adjust the volume to 100 ml with 1x PBS.

Sterilize by passing through 0.22 µm filter and store at -20°C in dark.

100X Propidium iodide (4 mg/ml) solution

400 mg of PI.

Adjust the volume to 100 ml with ddH2O.

Store at -20°C in dark.

100X RNase (6.2 mg/ml) solution

620 mg of RNase

Adjust the volume to 100 ml with MQ

Store at -20°C in dark.

1M HCl

Add 10 ml 12M HCl to 50 ml ddH2O.

Adjust the volume to 120ml with ddH_2O.

Store at RT.

FACS Permeabilization solution

PBS + 0.25% Triton X-100

2.5 ml Triton X-100

Adjust the volume to 1000 ml with PBS.

Store the solution at RT in dark.

FACS blocking buffer

PBS + 0.05% Tween-20 + 1% BSA

10 g BSA

2.5 ml 20% Tween-20

Adjust the volume to 1000 ml with PBS.

Store at -20°C.

Appendix 5: Electrophoresis

Electrode buffer (4X)

0.1M Tris

0.768M Glycine, pH 8.3

4x Tris/SDS pH 6.8, stacking gel buffer

Dissolve 6.05 g Tris-base in 40ml ddH_2O.

Adjust pH to 6.8 with 1N HCl.

Add H_20 to 100 ml.

Add 0.4 g SDS.

Store at 4°C.

4x Tris/SDS pH 8.8, resolving gel buffer

Dissolve 91 g Tris-base in 300 ml ddH_2O.

Adjust to pH 8.8 with 1 N HCl.

Add H_2O to 500 ml.

Add 2 g SDS.

Store at room temperature.

5x SDS electrophoresis buffer

15.1 g Tris-base.

72.0 g Glycine

5.0 g SDS

Add ddH_2O to 1000 ml.

Store at room temperature.

TBE (0.5X)

45mM Tris.

45mM Boric acid.

1mM EDTA.

6x SDS sample buffer

7 ml 4x Tris/SDS pH 6.8 stacking gel buffer

3.0 ml glycerol

1 g SDS

0.93 g DTT

1.2 mg Bromophenol blue

Add ddH_2O to 10 ml.

Store in 1 ml aliquots at -20 °C.

1X Transfer Buffer (Western blot transfer buffer)

Dissolve the following in 1600ml ddH_2O.

28.8 g of Glycine

6.04 g Tris base

Add 200 ml methanol.

Adjust the volume to 2000 ml with ddH_2O.

Store at 4°C.

Tween-20 20%

200 ml Tween-20

Adjust the volume to 1000ml with ddH_2O.

Store the solution at RT in dark.

TBST (PBS-0.05% Tween-20, washing buffer)

2.5 ml 20% Tween-20

Adjust the volume to 1000 ml with PBS.

Store the solution at RT in dark.

PBST-milk (PBST-5% ,Tween-20, washing buffer)

5g of milk (blot grade)

Adjust the volume to 1000 ml with ddH_2O.

Store the solution at 4°C in dark.

Coommassie Staining Solution

0.02% Coommassie Brilliant Blue G250

2% (w/v) Phosphoric acid

5% Aluminium sulphate

10% Ethanol

Appendix 6: Cell Fractionation

Hypotonic Buffer

10mM HEPES, pH 7.5

1.5mM $MgCl_2$

5mM KCl

0.2 mM PMSF

0.5mM DTT

Low Salt Buffer

20mM HEPES, pH 7.9 at 4°C

1.5mM $MgCl_2$

0.02M KCl

0.2mM EDTA

0.2mM PMSF

0.5mM DTT

High Salt Buffer

10mM HEPES, pH 7.9 at 4°C

1.6 M KCl

1.5 mM $MgCl_2$

Dialysis Buffer

25mM Tris/HCl pH 7.5 at 4°C

10% Glycerol

50mM EDTA

1mM EDTA

0.5 mM DTT

0.2mM PMSF

DAPI solution

2µg/ml DAPI

0.1M Tris

0.1M NaCl

5mM $MgCl_2$

0.05% TritonX-100

Appendix 7. Buffers for Cytogenetics

Hypotonic solution

0.56 g KCl.

Adjust the volume to 100ml with ddH_2O.

Prepare fresh at the time of experiment.

Carnoy's fixative

3 parts Methanol + 1 part acetic acid.

75 ml methanol

25 ml acetic acid

Prepare fresh at the time of experiment.

Appendix 8: Buffers for Southern Blotting

20x SSPE (pH7.4)

3M NaCl

0.2M $NaH_2PO_4.H_2O$

0.02M EDTA

Depurination Solution (500 ml)

0.2NHCl

Mix 10 ml of fuming HCl with 490 ml of ddH_2O

Denaturation Solution

1.5M NaCl

0.5M NaOH

Neutralization Solution

1M Tris (pH7.4)

1.5 M NaCl

Washing Solution I

2x SSPE

0.5% SDS

Washing Solution II

2x SSPE

0.1% SDS

Washing Solution III

0.1x SSPE

0.1% SDS

Washing Solution IV

0.1x SSPE

Table 1: Cell lines used in *in vivo* experiments.

Name	Description	Culture Medium	References
A549	Human alveolar basal cell carcinoma of epithelial origin	McCoy's 5A + 10% FBS	[162]
xrs-6	Chinese hamster ovary	MEM + 10% FBS	[134]
XR-C1-3	Chinese hamster ovary	MEM + 10% FBS	
CHO9	Chinese hamster ovary	MEM + 10% FBS	
$p53^{-/-}$ $LIG4^{+/+}$ (WT)	Mouse Embryonic Fibroblast	DMEM + 10% FBS	[133]
$Lig4^{-/-}$ $p53^{-/-}$	Mouse Embryonic Fibroblast	DMEM + 10% FBS	[133]

Table 2: Oligonucleotide Sequences

Oligonucleotides	Sequence
Fwnest/O/SB	5' GACTGTGCCTTTAAACAGC 3'
Rev460/SB	5' ACTTTCCACACCCTAACT 3'
1SB1NS	CCCGAGCTCGAATTCTACCCGCGGAGATCTCCCAACC CTGAA**TAGGGATAACAGGGTAAT**AACCCTGAACCCCT CGAGTCTA GACCCGAATTCGGTACCGGG
200A	CCCGAGCTCGAATTCTACCCGCGGAGATCTCCCAACC CTGAA**TAGGGATAACAGGGTAAT**ATCATTTTCGGTAG CAAGTTTAAGCATCAATTCTAGGATGAAGGAGGGAATT TGTAAATCTTCAGCCCATTGCAGATGACGCGGCCGCG ATACTAGTGACAAGCTTGATGGATCCTGAGATATCTAC GGCAGACCGCAATTAAAGACCTTGCTGTGTCTTCCTGA TTGTAAGGAGTCCACATACGATGGTGCTTGTCTA**TAGG GATAACAGGGTAAT**AACCCTGAACCCCTCGAGTCTAG ACCCGAATTCGGTACCGGG
200B	CCCGAGCTCGAATTCTACCCGCGGAGATCTCCCAACC CTGAA**TAGGGATAACAGGGTAAT**ATCATTTTCGGTAG CAAGTTTAAGCATCAATTCTAGGATGAAGGAGGGAATT TGTAAATCTTCAGCCCATTGCAGATGACGCGGCCGCG ATACTAGTGACAAGCTTGATGGATCCTGAGATATCTAC GGCAGACCGCAATTAAAGACCTTGCTGTGTCTTCCTGA CTTGTAAGGAGTCCACATACGATGGTGCTTGTCTA**ATT ACCCTGTTATCCCTA**AACCCTGAACCCCTCGAGTCTAG ACCCGAATTCGGTACCGGG

NB: Text in RED is the I-*Sce*I sites in compatible and incompatible orientations.

Table 3: Antibodies

Antibodies	MW(kDa)	Type	Manufacture	Cat. number	Dilution
Primary Ab					
γ-H2AX	14	mAb	Abcam	Ab22551	1:200
Secondary Ab					
Mouse IgG-Alexa 568		pAb	Molecular Probes, Invitrogen	A11004	1:400

Table 4: Software used for quantification of results

Program	Software
Image Quant	Molecular Dynamics (Invitrogen), USA
Quantity One	Bio-Rad, USA
Adobe Illustrator	Adobe Systems Inc. USA
SigmaPlot 10	Systat Software Inc. USA
MS Office	Microsoft, USA
Unicorn	Aekta (GE Healthcare)
Wincycle®	Beckman Coulter, USA
Imaris®	Bitplane AG; Switzerland

9 Acknowledgements

I submit the present endeavor with utmost gratitude for all those whose contribution and company made me to learn the things sincerely and whole heartedly.

While writing this acknowledgement, I take the opportunity to bestow the crown upon all those who were instrumental in the successful completion of this work. The present thesis is the direct or indirect contribution of these people, whom with great pleasure I mention here.

Firstly, my supervisor, Prof. Dr. George Iliakis, who provided me the chance to perform my Ph.D. work in this institute. His enthusiastic and untiring pursuit of perfectionism forced me to look into the finer details of whatever he entrusted me – his unquenchable curiosity and love for the subject are probably the most valuable lessons I have learned from him, and his continual support and encouragement has kept me going through the rough and the smooth.

I am in dilemma to choose the words to thank my moral support, Dr. H. K. Pradhan, without whose blessings and guidance I may never have reached where I am today.

I would also like to thank Prof. Dr. Wolfgang-Ulrich Müller and Dr. Peter Tamulevicius for giving me insights into radiation protection, dosimetry and laboratory safety. I am also extremely thankful to Frau Müller for her excellent and extremely efficient administrative assistance during my stay in the institute.

It is next to impossible to produce results without a conducive environment in the lab. A lively ambience and cooperation was what I got here, and is what I aspire wherever I am in the future. I would take this opportunity to convey my special thanks to Agnes, Andrea, Alena, Bustanur, Christian, Emil, Fan, Katja, Minli, Mario, Maria, Radi, Li-hua, Swetlana, Sascha, Simon, and Theresa. I am also indebted to Agnes for her inputs for the thesis and contribution to this work,

without which the project would not have reached thus far. Thank you guys for being such great contemporaries.

In prosperity our friends know us; in adversity we know our friends. Aparna deserves a special mention here for her ever-present smile and support. I am also extremely thankful to Satyendra and Aashish for being there always.

I would also like to thank to all my Indian friends who made my stay congenial here. I extend my special acknowledgements to Aruna, Hemant, Kunal, Manoj, Meenakshi, Nisha, Pratima, Pankaj, Preet, Pooja, Savita and Shreenath.

I would be failing in my duties without acknowledging the efforts of Anita, Malihe, Tamara, and also Frau Lander, without whose lab skills and organization, the work in the lab would come to a stand still. Anita and Malihe deserve a special mention here as they always made me felt at home here. Thank you all for everything.

I dedicate my thesis to my parents who are more important to me than mere words can describe. They have always been my guiding light and their unfading encouragement and trust in me helped me stand firm and face the world with confidence. I would also like to thank Kakuli, Rahul, Rohan and Joyanta for their unfailing support.

At last but not the least, the financial support from BMBF is gratefully acknowledged for the smooth completion of this work.

"The biography is not included in the online version for reasons of data protection"

"The biography is not included in the online version for reasons of data protection"

"The biography is not included in the online version for reasons of data protection"

"The biography is not included in the online version for reasons of data protection"

"The biography is not included in the online version for reasons of data protection"

"The biography is not included in the online version for reasons of data protection"

12 Erklärung

Hiermit erkläre ich, gem. § 6 Abs. 2, Nr. 7 der Promotionsordnung der Math.-Nat.- Fachbereiche zur Erlangung der Dr. rer. nat., dass ich das Arbeitgebiet, dem das Thema *„Development of Defined Biological Models for Complex Radiation-Induced DNA Lesions Using Homing Endonucleases and Transposon Technology: Feasibility and Initial Characterization“* zuzuordnen ist, in Forschung und Lehre vertrete und den Antrag von Herr Janapriya Saha befürworte.

Essen, den _____ _____ _____

Name des wissenschaftl. Betreuers/Mitglieds der Universität Duisburg-Essen	Unterschrift d. wissenschaftl. Betreuers/Mitglieds Universität Duisburg-Essen

Erklärung:

Hiermit erkläre ich, gem. § 6 Abs. 2, Nr. 6 der Promotionsordnung der Math.-Nat.- Fachbereiche zur Erlangung des Dr. rer. nat., dass ich die vorliegende Dissertation selbständig verfasst und mich keiner anderen als der angegebenen Hilfsmittel bedient habe.

Essen, den _____ _____

Unterschrift des/r Doktoranden/in

Erklärung:

Hiermit erkläre ich, gem. § 6 Abs. 2, Nr. 8 der Promotionsordnung der Math.-Nat.- Fachbereiche zur Erlangung des Dr. rer. nat., dass ich keine anderen Promotionen bzw. Promotionsversuche in der Vergangenheit durchgeführt habe und dass diese Arbeit von keiner anderen Fakultät abgelehnt worden ist.

Essen, den _____ _____

Unterschrift des Doktoranden